

An Approach to “Quantumness” in Coherent Control

Torsten Scholak* and Paul Brumer†

*Chemical Physics Theory Group, Department of Chemistry, and
Center for Quantum Information and Quantum Control,
University of Toronto, Toronto, Ontario, Canada, M5S 3H6*

Dated: March 30, 2018

Abstract

Developments in the foundations of quantum mechanics have identified several attributes and tests associated with the “quantumness” of systems, including entanglement, nonlocality, quantum erasure, Bell test, etc.. Here we introduce and utilize these tools to examine the role of quantum coherence and nonclassical effects in 1 vs. N photon coherent phase control, a paradigm for an all-optical method for manipulating molecular dynamics. In addition, truly quantum control scenarios are introduced and examined. The approach adopted here serves as a template for studies of the role of quantum mechanics in other coherent control and optimal control scenarios.

Contents

1	Introduction	3
1.1	A General Overview of This Article	5
1.2	Quantum-Classical Correspondence in Coherent Phase Control	7
1.3	The Nonlinear Response Perspective	8
1.4	Is There Quantum Mechanics in 1 vs. N Coherent Phase Control?	9
2	The Coherent Control Interferometer (CCI)	10
2.1	A General Theory of Two-Color Weak-Field Coherent Phase Control	11
2.2	Dichotomous Material Observables	16
2.3	The Coherent Control Interferometer for 1 vs. N	17

*Electronic address: tscholak@chem.utoronto.ca

†Electronic address: pbrumer@chem.utoronto.ca

3	Path Distinguishability	21
3.1	The Open Interferometer Configuration	21
3.2	The Closed Interferometer Configuration	25
4	Quantum Erasure Coherent Control	30
4.1	Welcher-Weg Marking And Nontrivial CCI Configurations .	30
4.1.1	Welcher-Weg Measurements	32
4.1.2	Quantum Erasure	33
4.2	The Special Case of Symmetric CCIs	34
4.2.1	An Optimum Welcher-Weg Measurement	37
4.2.2	An Optimum What-Phase Measurement	37
4.3	Quantum Erasure with Displaced Photon Threshold Measurements	39
4.4	Can Welcher-Weg Or What-Phase Measurements Probe Non-classicality?	42
5	Delayed Choice Coherent Control	45
5.1	The Simultaneously Both Open And Closed Configuration .	46
5.2	Quantum Delayed Choice	48
5.3	A Comparison between Quantum Erasure And Quantum Delayed Choice	49
6	Towards Rigorous Experimental Certification of The Non-classicality of Coherent Phase Control	51
6.1	A Bell Inequality Test for Coherent Control	51
6.2	The Case of Quantum Erasure Coherent Control	52
6.3	The Case of Quantum Delayed Choice Coherent Control . .	54
7	Application To Photoelectron Spin Polarization Control in Alkali Photoionization	58
7.1	A Model for The Material Degrees of Freedom	58
7.2	The Proposed Experiment	59
7.3	Implementation of The Open And The Closed CCI Configurations	63
8	Facing the Loopholes	71
9	Conclusions	73
	Acknowledgments	76
	Appendix A: The Longtime Limit of The Total Density Operator	76

1 Introduction

The goal of coherent control is to manipulate the dynamics of matter at the molecular, atomic, and even subatomic level. The methodology, which has been extensively reviewed [1, 2] relies on an external driving field, the characteristics of the material target system, and the coupling between them. For example, in two-color phase control [3], control over the material system is achieved by irradiating the system with a field of the form:

$$E(t) = \varepsilon_1 \cos(\omega t + \phi_1) + \varepsilon_2 \cos(N\omega t + \phi_2) , \quad (1)$$

and then varying the relative phase $\phi = N\phi_1 - \phi_2$ between the two incident weak laser fields of frequencies ω and $N\omega$, with $N = 2, 3, \dots$. This particular control scenario has proven of interest in applications ranging from control of electric currents [4–7] to the control of laser phase envelopes in precision measurements [8, 9], and is the primary scenario upon which we focus in this Advances.

Two-color phase control has repeatedly [3, 5, 10–30] been explained as a quantum analog of Young’s double slit experiment [31], with the slits replaced by two independent and mutually exclusive dynamical pathways, A and B, both leading from an initial material state $|\psi(t = -\infty)\rangle$ to a final state $|\psi(t = \infty)\rangle$. In this picture, path A is given by a 1-photon transition induced by the laser field of frequency $N\omega$, and path B by an N -photon transition caused by the second field of frequency ω . In accord with the standard quantum description, the probability of excitation at long times $P(\infty)$ is then obtained by adding the transition amplitudes $a_A(\infty)$ and $a_B(\infty)$ for the pathways and taking the square of the absolute value to give:

$$\begin{aligned} P(\infty) &= |a_A(\infty)|^2 + |a_B(\infty)|^2 + a_A(\infty)a_B^*(\infty) + a_B(\infty)a_A^*(\infty) \\ &= P_A(\infty) + P_B(\infty) + 2\sqrt{P_A(\infty)P_B(\infty)}\cos(\phi - \theta), \end{aligned}$$

where θ denotes a material phase. Phase control, a subset of coherent control effects, is manifest only in the latter term, which depends on the external control phase ϕ . This interference term can contribute either constructively or destructively, resulting in nonadditive probabilities, so that $P(\infty) \neq P_A(\infty) + P_B(\infty)$.

Arguments for the validity and applicability of coherent phase control have primarily relied upon formulations of this kind, which emphasize the importance of quantum interference in control. In particular, they rely on the functional form of this equation, which is reminiscent of double slit interference, the phase sensitivity of the control, and the display of nonadditivity of the contributions. Early two-color photoionization experiments with alkali atoms, [14, 15, 32, 33], serve as seminal examples of this scenario, as do experiments on current directionality in quantum wells [5] and semiconductors [20]. However, phase sensitivity and nonadditivity can also be of classical origin arising, for example, in transport processes[34]. Hence,

one can ask [35, 36] whether 1 vs. N phase control can also be viewed as a classical interference phenomenon or, for example, as a system’s collective response to shaped incident laser fields [37, 38]. Related concerns are raised by a number of additional studies [39–41] that consider 1 vs. 2 photon phase control as an intrinsically classical phenomenon.

In this article, we justify this concern and then provide a formal approach to addressing this issue. Specifically, we examine quantum control from a *foundational perspective*, relying upon modern concepts in quantum mechanics, such as entanglement, quantum erasure, nonlocality, and Bell tests (for an introduction, see [42]) to see how a truly quantum phase control scenario can be tested and built. Although this article focuses explicitly on the 1 vs. N photon weak-field phase control, our goal is to provide a detailed approach to examining the role of quantum mechanics in control scenarios that is applicable to other coherent control, and to optimal control scenarios. In the case of coherent control, such a degree of foundational rigor has so far not been considered necessary. Rather, one has been satisfied with “bona fide nonclassicality”, i.e., the expectation that a classical theory can not be written down that also conforms to what one believes to be the physics of the observed phenomenon. From a foundational perspective, this approach is problematic [43, 44], as discussed below.

Hence, the central focus of this Advances is the use of modern foundational ideas in quantum mechanics to explore “quantumness” in coherent control. In our examination of the 1 vs. N scenario, we begin by noting that no features of interference are displayed that go beyond the nonadditivity and the phase sensitivity of nonlinear response to the incident laser field. Indeed, if nonclassical effects play a role in this coherent control scenario, then it is by virtue of the fact that the material upon which the lasers are incident display quantum features. This is, of course, distinct from saying that the *control scenario* itself reflects principles that are non-classical. This distinction requires clarification through two significant comments.

- (i) There is absolutely no question that quantum mechanics is necessary to *quantitatively* describe the outcome of coherent control scenarios. For example, a classical computation gives products of HD^+ dissociation in a 1 vs. 2 photon experiment that are antiparallel to the correct quantum result [45]. Indeed, even the absorption of light by matter requires quantum mechanics to obtain quantitatively accurate results, although, a classical description is often qualitatively satisfactory [46–48]. Here, however, our focus is on the *conceptual* relationship between the quantum and classical perspectives.
- (ii) From a *formal foundational perspective*, in both dynamics and control, quantitative agreement with quantum theory does not provide a *proof* of nonclassicality. Rather, formally, proving the role of quantum mechanics requires that all classical descriptions and explanations be falsified, i.e., all classical models must be unable to reproduce

the phenomenon. As a consequence, the rigorous certification of nonclassicality is a challenging task which has, for example, been the subject of intense efforts in quantum optics [49–51], quantum information [52–58], and, most notably, quantum foundations [59–64]. Studies of this type take the form of carefully crafted experimental protocols that close all loopholes that would prevent rigorous assertions about the degree to which quantum mechanics is necessary to describe the phenomenon—called here, and below, “quantumness”.

If conventional 1 vs. N phase control, at its core, conceptually admits a classical description, and thus does not show nontrivial aspects of quantum mechanics, what new, extended verifiably quantum coherent phase control scenarios can be designed? Here, we introduce tools to answer these questions in any coherent control scenario and apply them specifically to the 1 vs. N photon case. Finally, we note that understanding the nonclassicality of coherent control has practical applications that arise from a recognition that decoherence effects [65] often bring a system to the classical limit. Hence, if control is indeed (at least partially) classical, then it may well survive in the often unavoidable decohering environments associated with realistic molecular processes.

1.1 A General Overview of This Article

Sections 1.2 to 1.4 review arguments that standard two-color weak-field phase control is, conceptually, an analog of a purely classical control phenomenon in which quantum interference and the double-slit analogy play no role. As noted below, quantum physics only influences the material component of the system, expressed by response functions to the external field. These quantities contain the complete information that is necessary to calculate the perturbation of a system property in response to classical driving radiation, particularly weak two-color fields.

In the main body of this article, we address the question of how and when nontrivial aspects of *quantum interference* affect phase control. Note that by “quantum interference” we do not just mean that interference is observed, but rather that the interference is verifiably quantum, as described below. Indeed, in this context quantum interference and quantum mechanics are essentially synonymous. Since these aspects will be seen to be absent in conventional phase control, we extend our search to unconventional scenarios. To do so, we introduce, in Sec. 2, a novel type of two-path interferometer, the “coherent control interferometer” (the CCI). As in a Mach-Zehnder interferometer (MZI), the CCI will be seen to have two input ports, two output ports, and two path alternatives. Each port is identified with one of two possible outcomes in the measurement of a matter observable that is diagonal in the material eigenbasis, e.g., spin, parity, etc. For example, the path alternatives are given by the two excitation processes in a 1 vs. N coherent control scenario. The resultant CCI framework is general and

applicable to many systems, from atoms [15, 66] to molecules [27, 45, 67–69] to bulk solids [4, 5, 20, 30, 70–75]. Further, the control field can be in a semiclassical coherent or in a quantum state of light, such as a multimode Fock state or a squeezed state.

The CCI will prove central to the study of nontrivial quantum interference effects in phase control, insofar as it formalizes the relationship between coherent phase control and quantum interference phenomena. With it, we are able to study the fundamental complementarity of wave- and particle-like behavior in the context of coherent control (Sec. 3). Further, the trade-off between these two behaviors is quantified via duality relations of the form $\mathfrak{V}^2 + \mathfrak{K}^2 \leq 1$ that provide upper bounds on the interference fringe contrast \mathfrak{V} , a wave property, and the simultaneously acquirable amount of path knowledge \mathfrak{K} , a particle property. Relations of this type are not only conducive to an experimental demonstration of complementarity and thus one of the hallmarks of quantum interference, but they are of immediate practical significance in coherent phase control. This is because these relations show the maximum amount of control achievable through “quantum erasure”, a measurement strategy by which path knowledge can be “erased” and interference restored (Sec. 4) and that there is a strict equivalence between controllability and interference contrast in the CCI that can be indicative of nonclassical correlations and entanglement.

Another hallmark of quantum interference is “delayed choice” [76]. In the context of quantum erasure, delayed choice refers to the fact that the time at which the experimenter decides to restore wave-like interference (naturally, at the expense of any particle-like path knowledge) is of no consequence to the measurement results. The choice can be made even well after detecting the output from the CCI. Below, we exploit the CCI to design a novel coherent control implementation of “quantum delayed choice” [77] that has thus far only been observed in experiments with photons [51, 78, 79] and nuclear spins [80, 81] (Sec. 5). Note that quantum delayed choice will be seen to differ from delayed choice in that the system is in a quantum superposition of both particle- and wavelike behaviors that, in the CCI, are controlled by the incident light field. As such, prior to the measurement it can be physically unknowable whether control is achieved or not.

Rigorous experimental proofs for the nonclassicality of our proposed quantum erasure and quantum delayed choice coherent phase control scenarios are discussed in Sec. 6. These verifications are made possible with the Bell-CHSH inequality tests introduced below. If these inequalities are unambiguously violated in an experiment, it would guarantee that the observed measurement statistics cannot be described by *any* classical theory. But even without these tests, these new scenarios come significantly closer to demonstrating quantum coherence and nonclassical interference effects in a 1 vs. N coherent phase control experiment.

Section 7 applies the CCI formalism to an example of control over the spin polarization of the ejected photoelectron in the photoionization of

an alkali atom by a 1 vs. 2 control field. We derive explicit settings that facilitate the implementation of the new control scenarios and, in particular, we design control fields for wave- and particle-like CCI output statistics.

Loopholes are discussed in Sec. 8, and conclusions are provided in Sec. 9.

1.2 Quantum-Classical Correspondence in Coherent Phase Control

The issue of classical vs. nonclassical effects in coherent control has been recently addressed for a number of control scenarios. For example [6, 35, 82], a classical, two-color cw driving field with frequency components ω and 2ω of the form $E(t) = E_1(t) + E_2(t) = \varepsilon_1 \cos(\omega t + \phi_1) + \varepsilon_2 \cos(2\omega t + \phi_2)$ can induce an asymmetry in the position or momentum distribution of a single charged particle trapped in a symmetric potential with quartic anharmonicity. The asymmetry is controllable by changing the relative phase $\phi = 2\phi_1 - \phi_2$ of the two field components. In the quantum case, the time-averaged position \bar{x}_q is given by [6]

$$\bar{x}_q = \chi_q^{(3)} \frac{3}{4} \varepsilon_1^2 \varepsilon_2 \cos \phi, \quad (2)$$

where the average position \bar{x}_q is seen to be proportional to $\cos \phi$ and to the field amplitudes $\varepsilon_1, \varepsilon_2$, with a coefficient given by the quantum susceptibility $\chi_q^{(3)}$. The quantum-mechanical description of control was found [6] to cross over smoothly to the classical limit,

$$\lim_{\hbar \rightarrow 0} \bar{x}_c = \chi_c^{(3)} \frac{3}{4} \varepsilon_1^2 \varepsilon_2 \cos \phi. \quad (3)$$

Here the quantum and classical results are seen to be of exactly the same form, albeit with a *quantitatively* different susceptibilities $\chi_c^{(3)}$ and $\chi_q^{(3)}$. In particular, the quantum result adds a series of correction terms, $\Delta\chi = (\chi_q^{(3)} - \chi_c^{(3)})$, that describe the \hbar -dependent resonance structure of the system. Further, in the specific example discussed above, both quantum and classical control can be explained by solely considering classical arguments based on reflection symmetry, in contrast to earlier explanations [1] that attributed control to the breaking of parity, an inherently quantum effect. In addition, consider uncoupled, charged, massive particles in static, symmetric, one-dimensional potentials subject to external driving fields in the dipole approximation. In these general cases, the necessary conditions for the creation of net dipoles or currents is identical in the quantum and the classical regime if the driving fields are time-periodic and have vanishing temporal average [82]—a standard case in scenarios of coherent phase control. That is, both quantum and classical control rely on the same temporal asymmetries in the driving field and on the presence of anharmonicities in the static potential. All of these results suggest that, conceptually, the phase control is consistent with classical mechanics.

The quantitative quantum-classical correspondence breaks down when the initial state becomes semi-classically inadmissible or when the driving frequencies approach the quantum resonances. In such cases, classical and quantum control can be wildly different and may not necessarily correspond to the same physical phenomenon. Such a conclusion has been reached in a particular case of two-color strong-field photodissociation of a diatomic molecule modeled as a Morse oscillator [39, 40]. Away from the resonances, however, the classical and quantum calculations have been found to agree and further to reproduce the control achieved in a related photoionization experiment [22, 83].

Notwithstanding, the case of the quartic oscillator discussed above illustrates that quantum-classical correspondence is not restricted to weak-field coherent control (i.e., the perturbative limit), but can also occur for intense driving. The results make clear that a general approach to the role of quantum mechanics in control is necessary.

1.3 The Nonlinear Response Perspective

Such an approach to analyzing quantum control scenarios and their possible classical analog, formulates the issue in terms of nonlinear perturbative response [35, 41]. Non-linear response provides an infinite series expansion for the time-dependent ensemble average of the outcome of a measurement performed on a material system that is subject to an external (and here for simplicity, scalar-valued) driving signal $E(t)$. If $O(t)$ is the response signal, then [84]

$$\begin{aligned}
 O(t) = & R^{(0)} \\
 & + \sum_{n=1}^{\infty} \int_{-\infty}^t d\tau_n \int_{-\infty}^{\tau_n} d\tau_{n-1} \cdots \int_{-\infty}^{\tau_2} d\tau_1 R^{(n)}(\tau_2 - \tau_1, \tau_3 - \tau_2, \dots, t - \tau_n) \\
 & \times E(\tau_n)E(\tau_{n-1}) \cdots E(\tau_1). \quad (4)
 \end{aligned}$$

If all response functions $R^{(n)}$ are known, $O(t)$ can be obtained to arbitrary precision for virtually any $E(t)$. Eq. (4) is completely general and applicable in both quantum and classical mechanics, where the response functions $R^{(n)}$ are obtainable from time-dependent perturbation theory in the coupling between $E(t)$ and the material system.

Perturbation theory also suggests criteria for truncating the series [Eq. (4)]. For weak two-color phase control, the input signal $E(t)$ is a small parameter and, typically, only low orders n are relevant. Further, in this case, the signal separates into two components, $E = E_1 + E_2$, according to their frequencies. Hence, by suppressing one component, the contribution of each input component to the response O can be assessed. If O_1 and O_2 are the individual responses to E_1 and E_2 , then, in general, if the response is nonlinear in the field amplitude, the collective response O will differ from

the sum $O_1 + O_2$. With $\hat{R}^{(n)}$, \hat{E}_1 and \hat{E}_2 as the Fourier transforms of the response functions and the field components, the difference

$$\begin{aligned}
O(t) - O_1(t) - O_2(t) &= \int d\omega_1 \int d\omega_2 e^{i(\omega_1 + \omega_2)t} \hat{R}^{(2)}(\omega_1, \omega_1 + \omega_2) \\
&\quad \times \left[\hat{E}_2(\omega_1) \hat{E}_1(\omega_2) + \hat{E}_1(\omega_1) \hat{E}_2(\omega_2) \right] \\
&\quad + \int d\omega_1 \int d\omega_2 \int d\omega_3 e^{i(\omega_1 + \omega_2 + \omega_3)t} \hat{R}^{(3)}(\omega_1, \omega_1 + \omega_2, \omega_1 + \omega_2 + \omega_3) \\
&\quad \times \left[\hat{E}_2(\omega_1) \hat{E}_1(\omega_2) \hat{E}_1(\omega_3) + 5 \text{ permutations} \right] + \text{higher orders (neglected)}
\end{aligned} \tag{5}$$

quantifies the contribution to the response due to the simultaneous presence of both fields.

The primary control parameter in two-color control scenarios is the relative phase between two frequencies. The direct terms O_1 and O_2 are typically not phase controllable [85] and the only way a phase shift ϕ_1 of, e.g., the component E_1 can affect the response is by means of the mixed cross terms given by Eq. (5). Consider, specifically, the effect of the phase change:

$$\hat{E}_i(\omega) \mapsto \hat{E}_i(\omega) e^{i \operatorname{sgn}(\omega) \phi_i} \tag{6}$$

The right-hand side of Eq. (6) is the Fourier transform of $a_i(t) \cos[\varphi_i(t) + \phi_i]$, if $\hat{E}_i(\omega)$ is the Fourier transform of $E_i(t) = a_i(t) \cos[\varphi_i(t)]$. The functions a_i and φ_i are, respectively, the instantaneous amplitude and phase of the field E_i before shifting its phase by ϕ_i . Equation (5) shows explicitly that the phases ϕ_i affect the field terms, but not the response functions, which depend on the field frequencies, but not on the field phases ϕ_i . This feature is common to both the classical and the quantum descriptions of conventional two-color weak-field control, and generalizes the case of the quartic oscillator [6] reviewed in Sec. 1.2. This approach shows that the difference between the classical and quantum 1 vs. N response can only result from quantitative differences in the response functions obtained in either regime. Phenomena like quantum resonances, tunneling, broken parity, etc. only contribute to the response functions, but not to the fundamental structure of phase control, i.e., the dependence on the phase of the incident field.

The discussion above would apply to any coherent control scheme for which the nonlinear response is valid; those that do not fit into this category merit additional consideration.

1.4 Is There Quantum Mechanics in 1 vs. N Coherent Phase Control?

Section 1.3, makes no reference to either “interference” or to “quantum interference”. That is, neither of these concepts is necessary to understand

the coherent phase control scenario. Hence, the idea that coherent phase control results from the quantum-coherent interference of mutually exclusive excitation pathways is challenged by the above treatment. Furthermore, even if quantum interference were involved, none of its hallmark features, discussed below, would be displayed; rather one only finds the nonadditivity and phase sensitivity of the nonlinear response. At this trivial level, quantum interference and the double-slit analogy are of questionable relevance.

Moreover, the double-slit analogy can, at times, even be misleading. This is demonstrated in the example of the bichromatically driven quartic oscillator (see Refs. 6, 35, and Sec. 1.2 above), a system that admits a description in terms of quantum-coherently interfering dynamic pathways that is formally analogous to single-particle interference in the Young double-slit (YDS). However, and significantly, single-particle YDS interference does not survive in the classical limit; rather, one obtains an average over ballistic particle trajectories that alternate probabilistically between the two slits. This is not the case for the 1 vs. 2 control process, which retains its wavelike interference behavior in the classical limit. Indeed, as we have explained elsewhere [35], the primary difference between the YDS and coherent phase control is that the latter occurs due to *external driving*, i.e., $E(t)$, whereas the former requires no such external influence. This result is in full agreement with the nonlinear response description in Sec. 1.3, but it is at odds with the double-slit analogy.

We have to conclude that, for standard scenarios of 1 vs. 2 coherent phase control, the double-slit analogy should be avoided, and 1 vs. 2 phase control should not be advertised conceptually as a quantum interference effect. The result motivates our efforts below, in which we seek to develop and test a genuinely and verifiable quantum mechanical phase control scenario.

2 The Coherent Control Interferometer

To address this issue, we focus on the quantum mechanical principle of complementarity, and its role in coherent control. This principle addresses a fundamental qualitative property of quantum mechanics: the violation of realism. Realism is central to classical physics, stating that the properties and configurations of classical systems are independent of their observation, and exist prior to their measurement. In quantum physics, however, this concept is no longer expected. Rather, quantum mechanics describes systems and measurements probabilistically. A globally consistent classical picture of a quantum system is impossible because sequential measurements give evidence for properties that classically would be regarded as contradictory, but are in fact equally valid. One therefore cannot regard a system as having "intrinsic" properties, i.e., properties that exist independent of measurement. Rather, since Bohr, it is known that the true nature of a quantum phenomenon can only be understood by obtaining evidence

through complementary measurements. In practical terms, this means that if some measurement is absolutely predictable and its *a priori* outcome certain, then there is a complementary measurement whose outcome will be completely uncertain [86].

In the context of interference, Bohr’s principle refers to the complementarity of waves and particles. According to the laws of classical physics, these are intrinsic properties: particles never interfere in an interferometer, and, for waves, passage through slits is not mutually exclusive. In quantum mechanics, however, the notions of wave and particle exist only as concepts that are borrowed from classical physics. The chances of a system displaying wave- or particle-like behavior are intrinsic to the mathematical framework of quantum superpositions that, formally, ascribes these properties to a quantum system simultaneously. It is the choice of the experiment that determines what property the system displays. These properties are thus not intrinsic: it is not just the ignorance of the measurement that prevents an observer from knowing if something is a wave or a particle.

The focus of the remaining part of this chapter discusses ways to demonstrate complementarity in new, unconventional scenarios of true quantum coherent phase control, scenarios in which nonlinear response theory cannot be applied. In contrast to previous coherent phase control experiments, the scenarios proposed below strongly support an analogy between coherent phase control and the single-particle interference in the Young double-slit. Further, the central hallmarks of quantum interference—complementarity and the violation of realism in particular—are displayed prominently and unambiguously. Essential to this approach is the framework of the CCI that is introduced in this section. This CCI is inspired by the optical MZI, a standard two-path interferometer that, like the Young double-slit (YDS), can demonstrate complementarity and the probabilistic nature of quantum mechanics. Introducing the CCI will, however, necessitate the introduction of a general structure for the phase control scenario under consideration.

2.1 A General Theory of Two-Color Weak-Field Coherent Phase Control

Here we introduce a fully general quantum-mechanical description of the two-color weak-field 1 vs. N coherent control scheme, where $N = 2, 3$, etc. The treatment allows for realistic pulse profiles that are compact in space and thus have a spread in frequency. Furthermore, the full quantum treatment accounts for the radiation field as an additional quantum degree of freedom \mathcal{R} [87] that can be in a nonclassical state and that can exhibit correlations with the material degrees of freedom \mathcal{M} . Here, the field will be subject to feedback and change due to its interaction with the matter, an extension of the coherent control approach described above, where the driving field is external and predetermined.

Consider now a material system \mathcal{M} upon excitation by light. The

material Hamiltonian $H_{\mathcal{M}}$ is assumed to be time-independent with a bound and continuum spectrum E_{μ} with eigenstates $\{|\mu\rangle\}$. That is,

$$H_{\mathcal{M}}|\mu\rangle = E_{\mu}|\mu\rangle. \quad (7)$$

Initially, in the distant past, the material system is its ground state,

$$\varrho_{\mathcal{M}}(-\infty) = \sum_{\nu \in \mathcal{D}_-} p_{\nu} |\nu\rangle \langle \nu| \quad (8)$$

where $\sum_{\nu \in \mathcal{D}_-} p_{\nu} = 1$ with $p_{\nu} \geq 0$, and the quantum numbers ν from the set \mathcal{D}_- count over any ground state degeneracies.

The material system then interacts with the quantized radiation field, which is described via continuous multimode Fock space, where the vacuum $|\text{vac}\rangle$ and all n -photon states of the form $|\mathbf{k}_1\lambda_1, \dots, \mathbf{k}_n\lambda_n\rangle$ are the preferred basis states. Here the indices $\lambda_i = 1, 2$ label two unit polarization vectors $\hat{\boldsymbol{\epsilon}}(\mathbf{k}_i, \lambda_i)$ that are each perpendicular to the corresponding wave vector $\mathbf{k}_i = \omega(k_i) \hat{\mathbf{k}}_i/c$ and to one another. The field Hamiltonian is

$$H_{\mathcal{R}} = \int d\mathbf{k} \sum_{\lambda} \hbar\omega(k) a^{\dagger}(\mathbf{k}, \lambda) a(\mathbf{k}, \lambda), \quad (9)$$

where the vacuum radiation field energy is ignored, and $a^{\dagger}(\mathbf{k}, \lambda)$ and $a(\mathbf{k}, \lambda)$ are the photon creation,

$$a^{\dagger}(\mathbf{k}, \lambda)|\text{vac}\rangle = |\mathbf{k}\lambda\rangle, \quad (10a)$$

$$a^{\dagger}(\mathbf{k}, \lambda)|\mathbf{k}_1\lambda_1, \dots, \mathbf{k}_n\lambda_n\rangle = \sqrt{n+1} |\mathbf{k}\lambda, \mathbf{k}_1\lambda_1, \dots, \mathbf{k}_n\lambda_n\rangle, \quad (10b)$$

and annihilation operators,

$$a(\mathbf{k}, \lambda)|\mathbf{k}_1\lambda_1, \dots, \mathbf{k}_n\lambda_n\rangle = \frac{1}{\sqrt{n}} \sum_{i=1}^n \delta(\mathbf{k} - \mathbf{k}_i) \delta_{\lambda\lambda_i} \times |\dots, \mathbf{k}_{i-1}\lambda_{i-1}, \mathbf{k}_{i+1}\lambda_{i+1}, \dots\rangle, \quad (10c)$$

$$a(\mathbf{k}, \lambda)|\text{vac}\rangle = 0, \quad (10d)$$

respectively. In this continuous Fock space, wave vectors can take any value and we have

$$\langle \mathbf{k}'_1\lambda'_1, \dots, \mathbf{k}'_m\lambda'_m | \mathbf{k}_1\lambda_1, \dots, \mathbf{k}_n\lambda_n \rangle = \delta_{nm} \frac{1}{n!} \sum_{\sigma \in S_n} \delta(\mathbf{k}_1 - \mathbf{k}'_{\sigma(1)}) \delta_{\lambda_1\lambda'_{\sigma(1)}} \cdots \delta(\mathbf{k}_n - \mathbf{k}'_{\sigma(n)}) \delta_{\lambda_n\lambda'_{\sigma(n)}}, \quad (11)$$

where the sum runs over all $n!$ permutations σ in the symmetric group S_n . The creation and annihilation operators obey the standard commutation relations [87], i.e.,

$$[a(\mathbf{k}, \lambda), a(\mathbf{k}', \lambda')] = [a^{\dagger}(\mathbf{k}, \lambda), a^{\dagger}(\mathbf{k}', \lambda')] = 0, \quad (12)$$

and

$$[a(\mathbf{k}, \lambda), a^\dagger(\mathbf{k}', \lambda')] = \delta(\mathbf{k} - \mathbf{k}') \delta_{\lambda\lambda'}. \quad (13)$$

The total Hamiltonian is

$$H = H_{\mathcal{M}} + H_{\mathcal{R}} + V, \quad (14)$$

with the light-matter interaction V , treated here within the electric dipole approximation. In the length gauge, and when the material part is modeled as a point scatterer, the interaction is given by

$$V = -\mathbf{d} \cdot \int d\mathbf{k} \sum_{\lambda} i\hbar\mathcal{E}(k) [a(\mathbf{k}, \lambda)\hat{\boldsymbol{\epsilon}}(\mathbf{k}, \lambda) - \text{h.c.}], \quad (15)$$

where \mathbf{d} is the material dipole operator, $\mathcal{E}(k) = \sqrt{\hbar\omega(k)/\epsilon_0(2\pi)^3}/\hbar$ is the vacuum field strength, and h.c. denotes the Hermitian conjugate of the preceding expression.

At time $t = -\infty$, the total system with density matrix $\rho(-\infty)$ assumes an uncorrelated, separable state,

$$\varrho(-\infty) = \varrho_{\mathcal{M}}(-\infty) \otimes \varrho_{\mathcal{R}}(-\infty), \quad (16)$$

where \mathcal{M} and \mathcal{R} subscripts denote the material and radiative subsystems. Subsequently, the light and the matter interact, and finally ($t = \infty$) totally separate from one another. The resultant final state $\varrho(\infty)$ of the total system will in general be correlated and inseparable, $\varrho(\infty) \neq \varrho_{\mathcal{M}}(\infty) \otimes \varrho_{\mathcal{R}}(\infty)$. Interest is then in a small fraction of the final states, denoted $\tilde{\varrho}(\infty)$ that culminate with matter in specific states $|\mu\rangle$ at particular energies E_μ , with $\mu \in \mathcal{D}_+$:

$$\varrho(\infty) \mapsto \tilde{\varrho}(\infty). \quad (17)$$

[See also Eq. (150) in App. A.] Here \mathcal{D}_+ denotes the set of quantum numbers that characterizes all interesting scattering events. For example, in the case of molecular photodissociation, a scattering event is interesting if enough energy is absorbed from the field to drive the material to the continuum. The set \mathcal{D}_+ and the state $\tilde{\varrho}(\infty)$ are then associated with that particular energy range. We assume that \mathcal{D}_- and \mathcal{D}_+ do not overlap.

Scattering into $|\mu\rangle$ requires fields with frequencies whose integer multiples are equal to $\Delta_{\mu\nu}/\hbar = (E_\mu - E_\nu)/\hbar$, where E_ν with $\nu \in \mathcal{D}_-$ refers to the ground state energy. We focus attention on the case where the energy range of $\Delta_{\mu\mu'}$ is sufficiently narrow so that the resonance conditions are approximately the same for all states associated with \mathcal{D}_+ , greatly reducing the number of possible optical excitation routes from \mathcal{D}_- to \mathcal{D}_+ .

In the 1 vs. N control scheme, one irradiates the system with two coherent wavepackets that are well monochromatized, have nonoverlapping frequency

spectra, and are initially localized far away from the material system. To account for these features, we use multimode creation operators $a^\dagger[f]$ to describe the initial state $\varrho_{\mathcal{R}}(-\infty)$ of the radiation field. In particular, we focus on pure states of light and define $\varrho_{\mathcal{R}}(-\infty) = |\chi\rangle\langle\chi|$ with

$$|\chi\rangle = g_1(a^\dagger[\hat{f}_1]) g_2(a^\dagger[\hat{f}_2]) |\text{vac}\rangle. \quad (18)$$

Here g_1, g_2 are two smooth functions that characterize the photon statistics of the wavepackets. The operator $a^\dagger[f]$ differs from the photon creation operator $a^\dagger(\mathbf{k}, \lambda)$ insofar as the photon is not created exactly with wavevector \mathbf{k} and polarization λ , but with a spread in frequency, orientation and polarization defined by a complex-valued photonic amplitude function f :

$$a^\dagger[f] = \int d\mathbf{k} \sum_\lambda f(\mathbf{k}, \lambda) a^\dagger(\mathbf{k}, \lambda). \quad (19)$$

The operator $a^\dagger[f]$ and its hermitian adjoint, $a[f]$, allow for an elegant description of pulses with realistic spectral profiles. The amplitude functions f_1 and f_2 in Eq. (18) have disjoint supports, and thus the multimode operators $a[f_1]$ and $a^\dagger[f_2]$ commute. Specifically,

$$[a[f_1], a^\dagger[f_2]] = (f_1, f_2) = 0, \quad (20)$$

where (f_1, f_2) is a scalar product,

$$(f_1, f_2) = \int d\mathbf{k} \sum_\lambda f_1^*(\mathbf{k}, \lambda) f_2(\mathbf{k}, \lambda). \quad (21)$$

In Eq. (18), the g_i are functions of $a^\dagger[\hat{f}_i]$, where $\hat{f}_i = f_i/\|f_i\|$ with $\|f_i\| = \sqrt{(f_i, f_i)}$. Normalization of $|\chi\rangle$ requires

$$\sum_{n=0}^{\infty} \frac{1}{n!} |g_i^{(n)}(0)|^2 = 1, \quad (22)$$

where $g_i^{(n)}(0)$ denotes the n^{th} derivative of $g_i(x)$ evaluated at $x = 0$. The introduction of the functions g_i allows for a solution of the scattering problem that is universal with respect to the photon statistics of the initial wavepackets. For example, to obtain the result for an initially sharply defined number of photons n_i , we set $g_i(x) = x^{n_i}/\sqrt{n_i!}$. Alternatively, for coherent states of light, we choose $g_i(x) = \exp(\|f_i\|x - \|f_i\|^2/2)$, where $\|f_i\|$ is the absolute value of the amplitude of the coherent state. Analogously, setting $g_i(x) = \exp[-\tanh(\rho_i)x^2/2]/\sqrt{\cosh \rho_i}$ gives a squeezed vacuum state with quadrature fluctuations $\exp(-2\rho_i)$ and $\exp(2\rho_i)$ for arbitrary ρ_i [88].

As noted above, we assume that the energies of the incoming wavepackets are narrowly clustered around integer multiples of $\Delta_{\mu\nu}$ in energy between the material asymptotic in- ($|\nu\rangle$, $\nu \in \mathcal{D}_-$) and the asymptotic out-states ($|\mu\rangle$, $\mu \in \mathcal{D}_+$). In particular, f_1 is concentrated around $\Delta_{\mu\nu}/(N\hbar)$, whereas

f_2 is concentrated around $\Delta_{\mu\nu}/\hbar$. For this scenario, we show in Appendix A that within perturbation theory the longtime limit of the total density operator projected on the sector \mathcal{D}_+ of interesting scattering outcomes is

$$\begin{aligned} \tilde{\varrho}(\infty) = \frac{1}{\tilde{p}} \sum_{\mathcal{D}_+}^{\mathcal{F}} d\mu \sum_{\mathcal{D}_+}^{\mathcal{F}} d\mu' |\mu\rangle\langle\mu'| \otimes \sum_{\nu \in \mathcal{D}_-} p_\nu \\ \times \left\{ T_1[\hat{f}_2](\mu, \nu) T_1^*[\hat{f}_2](\mu', \nu) |\tilde{\chi}^1\rangle\langle\tilde{\chi}^1| \right. \\ + T_1[\hat{f}_2](\mu, \nu) T_N^*[\hat{f}_1](\mu', \nu) |\tilde{\chi}^1\rangle\langle\tilde{\chi}^N| \\ + T_N[\hat{f}_1](\mu, \nu) T_1^*[\hat{f}_2](\mu', \nu) |\tilde{\chi}^N\rangle\langle\tilde{\chi}^1| \\ \left. + T_N[\hat{f}_1](\mu, \nu) T_N^*[\hat{f}_1](\mu', \nu) |\tilde{\chi}^N\rangle\langle\tilde{\chi}^N| \right\}, \quad (23) \end{aligned}$$

where

$$|\tilde{\chi}^1\rangle = g_1(a^\dagger[\hat{f}_1]) g_2^{(1)}(a^\dagger[\hat{f}_2])|\text{vac}\rangle, \quad (24a)$$

$$|\tilde{\chi}^N\rangle = g_1^{(N)}(a^\dagger[\hat{f}_1]) g_2(a^\dagger[\hat{f}_2])|\text{vac}\rangle \quad (24b)$$

are the final (nonnormalized) states of radiation and

$$\tilde{p} = \sum_{\mathcal{D}_+}^{\mathcal{F}} d\mu \text{Tr}[(|\mu\rangle\langle\mu| \otimes \mathbb{1}_{\mathcal{R}})\varrho(\infty)] \quad (25)$$

is the probability of any interesting scattering event to occur. The identity operator $\mathbb{1}_{\mathcal{R}}$ on the continuous multimode Fock space is

$$\begin{aligned} \mathbb{1}_{\mathcal{R}} = \sum_{n=0}^{\infty} \frac{1}{n!} \int d\mathbf{k}_1 \sum_{\lambda_1} \cdots \int d\mathbf{k}_n \sum_{\lambda_n} a^\dagger(\mathbf{k}_1, \lambda_1) \cdots a^\dagger(\mathbf{k}_n, \lambda_n) |\text{vac}\rangle \\ \times \langle \text{vac} | a(\mathbf{k}_1, \lambda_1) \cdots a(\mathbf{k}_n, \lambda_n). \quad (26) \end{aligned}$$

The symbol $\sum_{\mathcal{D}_+}^{\mathcal{F}}$ denotes summation over all discrete states and integration over all continuum states associated with \mathcal{D}_+ .

The 1- and the N -photon transition amplitudes are shown in App. A to be given by

$$\begin{aligned} T_1[\hat{f}_2](\mu, \nu) = -2\pi i \int d\mathbf{k} \sum_{\lambda} \delta[\Delta_{\nu\mu} + \hbar\omega(k)] \hat{f}_2(\mathbf{k}, \lambda) (-i)\hbar\mathcal{E}(k) \\ \times \langle \mu | \mathbf{d} | \nu \rangle \cdot \hat{\mathbf{e}}(\mathbf{k}, \lambda) \quad (27a) \end{aligned}$$

and

$$\begin{aligned}
T_N[\hat{f}_1](\mu, \nu) &= -2\pi i \int d\mathbf{k}_1 \sum_{\lambda_1} \cdots \int d\mathbf{k}_N \sum_{\lambda_N} \delta[\Delta_{\nu\mu} + \sum_{i=1}^N \hbar\omega(k_i)] \\
&\times \hat{f}_1(\mathbf{k}_1, \lambda_1) (-i)\hbar\mathcal{E}(k_1) \cdots \hat{f}_1(\mathbf{k}_N, \lambda_N) (-i)\hbar\mathcal{E}(k_N) \prod_{\mathcal{D}_+} d\xi_1 \cdots \prod_{\mathcal{D}_+} d\xi_{N-1} \\
&\times \frac{\langle \mu | \mathbf{d} | \xi_1 \rangle \cdot \hat{\mathbf{e}}(\mathbf{k}_1, \lambda_1) \langle \xi_1 | \mathbf{d} | \xi_2 \rangle \cdot \hat{\mathbf{e}}(\mathbf{k}_2, \lambda_2) \cdots \langle \xi_{N-1} | \mathbf{d} | \nu \rangle \cdot \hat{\mathbf{e}}(\mathbf{k}_N, \lambda_N)}{(\Delta_{\xi_2\xi_1} + \hbar\omega(k_2) + i0) \cdots (\Delta_{\nu\xi_{N-1}} + \hbar\omega(k_N) + i0)},
\end{aligned} \tag{27b}$$

respectively, where the transition amplitudes are complex-valued functionals of the photonic amplitude functions \hat{f}_i . The quantum resonance condition is contained within T_1 and T_N through the δ -kernels. Specifically, for T_1 , the kernel extracts a single frequency component from the amplitude function \hat{f}_2 . For T_N , the kernel is nonzero for \hat{f}_1 sharply peaked on the wave number shell with radius $\Delta_{\nu\mu}/\hbar cN$.

Note first that the first and the last term in the braces, $\{\cdots\}$, in Eq. (23) describes excitation processes caused by either of the two incoming wavepackets, contributions corresponding to the individual nonlinear responses O_1 and O_2 discussed in Sec. 1.3. Second, the terms in the second line of Eq. (23) are ‘‘cross contributions’’, containing both the single-photon transition amplitude T_1 and the N -photon transition amplitude T_N . They are contributions that contain coherences between the two possible final states of the radiation field $|\tilde{\chi}^1\rangle$ and $|\tilde{\chi}^N\rangle$, which arise when the material target state is reached via either a 1- or N -photon process. For the focus on coherent control, these cross terms are the more relevant, having been interpreted as occurring due to the *interference* between the processes described by the ladder contributions. It is usually argued that these processes interfere because they simultaneously couple the same initial and final states [1, 3], a role analogous to the one played by the joint contributions term $O - O_1 - O_2$ [cf. Eq. (5), Sec. 1.3]. Finally, note that Eq. (23) can take the form of an entangled state of the radiation field and the matter, an issue discussed below.

2.2 Dichotomous Material Observables

In general, the objective is to control population transfer to a final region \mathcal{D}_+ so that material eigenstates with a desired property are populated in preference to other undesired states. Here we define a material observable, M , that labels material eigenstates as either desired (with label +1) or undesired (with label -1). The role of control is then to maximize the expectation value $\langle M \rangle = \text{Tr}[(M \otimes \mathbf{1}_{\mathcal{R}})\tilde{\rho}(\infty)]$ of M . We define M in the

following general but implicit way:

$$M = \sum_{\eta=\pm 1} \eta \frac{1}{2}(\mathbb{1} + \eta M) = \sum_{\eta=\pm 1} \eta \int d\mu |\eta\mu\rangle\langle\eta\mu|. \quad (28)$$

The states $|\eta\mu\rangle$ are defined in terms of both M and the eigenstates $|\mu\rangle$ of the material Hamiltonian $H_{\mathcal{M}}$,

$$|\eta\mu\rangle = \frac{1}{2}(\mathbb{1} + \eta M)|\mu\rangle = \frac{1}{2}(1 + \eta M_{\mu})|\mu\rangle = \delta_{\eta M_{\mu}}|\mu\rangle \quad (29)$$

with $M_{\mu} = \pm 1$ fixed and $\langle\eta\mu|\eta'\mu'\rangle = \delta_{\eta\eta'}\delta_{\mu\mu'}\delta_{\eta M_{\mu}}$. Since M has only two eigenvalues $M_{\mu} = \pm 1$, it is termed a ‘‘dichotomous’’ observable. In particular, M is sensitive only to whether a state is desired or undesired; it remains completely ignorant about all other properties of the material system.

The above definition of M conveniently assures that (i) M is dichotomous, i.e., measuring M (on a single realization of the system) yields one of two possible outcomes: either $+1$ or -1 ; (ii) M is diagonal in the basis $\{|\mu\rangle\}$ and thus commutes with the Hamiltonian $H_{\mathcal{M}}$, $\langle\mu|M|\mu'\rangle = M_{\mu}\delta_{\mu\mu'}$ with $M_{\mu} = \pm 1$; and (iii) M is its own inverse, $M^2 = \mathbb{1}$. Effectively, in defining M , we assign a pseudospin label, $M_{\mu} = +1$ or -1 , to every material eigenstate $|\mu\rangle$. Hence, the pseudospin label admits a decomposition of the material Hilbert space $\mathcal{H}_{\mathcal{M}}$ into two subspaces: the subspace of states that are superpositions of material eigenstates with label $+1$ and those states that are linear combinations of eigenstates labelled -1 , and $\mathcal{H}_{\mathcal{M}} = \mathcal{H}_{\mathcal{M},+1} \oplus \mathcal{H}_{\mathcal{M},-1}$. In the case of control, this will divide the product space into states associated with desired properties, and those which are not.

The definition of M is more intuitive when the controlled physical property can only have one of two possible outcomes. An example is the coherent control of a single-electron spin, whose polarization against any chosen observation axis can have only two values, a case focussed upon in Sec. 7. In the absence of spin-orbit interaction, the spin observable commutes with $H_{\mathcal{M}}$, and the system is described by a two-dimensional Hilbert space. Therefore, the direct sum decomposition into subspaces $\mathcal{H}_{\mathcal{M},+1}$, $\mathcal{H}_{\mathcal{M},-1}$ of positive and negative spin is equivalent to a direct product of the two-dimensional spin Hilbert space and the Hilbert space of the remainder of the material system.

Below, we use these dichotomous labels to define both initial and final states of the scattering problem.

2.3 The Coherent Control Interferometer for 1 vs. N

Given this formalism, we are ready to define the coherent control interferometer (CCI). Conceptually, it is borrowed from the optical MZI, shown schematically in Fig. 1, and the approach constitutes a significant reformulation of multichannel scattering theory [89]. Like an MZI, the CCI has two input ports, two output ports, and two path alternatives.

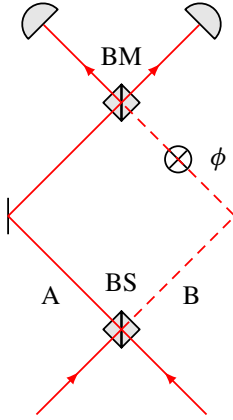


Figure 1: (color online) In an optical MZI, two incoming beams of light are first split at a half-transparent mirror, BS, into two spatially well-separated daughter beams, A and B, then allowed to accumulate a mutual phase shift ϕ , and eventually recombined by another half-transparent mirror, BM. At the two output ports of the MZI, detectors measure the intensity of the outgoing light. Observed is an oscillation of the intensity with the phase shift ϕ . In units of the background intensity, this ‘fringe pattern’ is, ideally, equal to $(1 \pm \cos \phi)/2$.

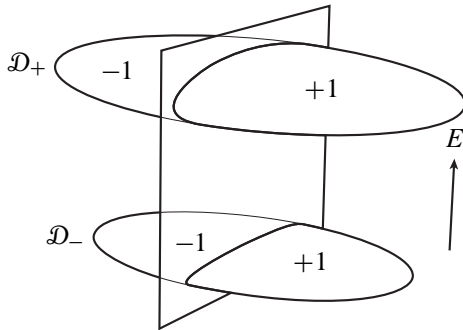


Figure 2: Schematic of the proposed coherent control interferometer (CCI). Shown are the sets \mathcal{D}_- and \mathcal{D}_+ as well as the CCI’s input and output ports. The hyperplane separates the regions $\mathcal{H}_{\mathcal{M},+1}$ and $\mathcal{H}_{\mathcal{M},-1}$.

The dichotomous observable M allows us to directly define the *input ports* of the CCI, identified with labels ± 1 , cf. Fig. 2. The input port σ is said to be occupied if the material system is prepared with population in the state $|\sigma\nu\rangle$. To formalize this, we redefine the initial state $\varrho_{\mathcal{M}}(-\infty)$ [originally introduced in Eq. (8) on page 12] as

$$\varrho_{\mathcal{M}}(-\infty) = \sum_{\sigma=\pm 1} \frac{p_{\sigma}}{\sum_{\nu \in \mathcal{D}_-} \delta_{M_{\nu}\sigma}} \sum_{\nu \in \mathcal{D}_-} |\sigma\nu\rangle\langle\sigma\nu| \quad (30)$$

with $p_{+1}+p_{-1} = 1$. The normalization factor in the denominator, $\sum_{\nu \in \mathcal{D}_-} \delta_{M_{\nu}\sigma}$, counts the number of states $|\nu\rangle$ with quantum numbers $\nu \in \mathcal{D}_-$ that are labeled with σ . If, for instance, the ground state is spin- $\frac{1}{2}$, and M measures ($2/\hbar$ times the) spin quantum-number, then that count is 1 for each of $\sigma = +1$ and -1 . Accordingly, Eq. (30) reduces to an incoherent sum of the two ground state spin orientations. This leaves us with an initial state $\varrho_{\mathcal{M}}(-\infty)$ far simpler than our original definition (8). In cases with a larger count, $\sum_{\nu \in \mathcal{D}_-} \delta_{M_{\nu}\sigma} > 1$, our new initial state (30) is still simpler than the original (8), since the populations $p_{\sigma\nu}$ of all states $|\sigma\nu\rangle$ with $\nu \in \mathcal{D}_-$ and fixed σ will be the same, i.e.

$$p_{\sigma\nu} = \frac{p_{\sigma}}{\sum_{\nu' \in \mathcal{D}_-} \delta_{M_{\nu'}\sigma}} \quad (31)$$

is independent of ν .

Turning now to the *output ports* of the CCI, and incorporating the changes made to the initial state $\varrho_{\mathcal{M}}(-\infty)$, the state $\tilde{\varrho}(\infty)$ is given by

$$\begin{aligned} \tilde{\varrho}(\infty) &= \tilde{p}^{-1} \sum_{\eta, \eta'=\pm 1} \sum_{\sigma=\pm 1} \frac{p_{\sigma}}{\sum_{\nu \in \mathcal{D}_-} \delta_{M_{\nu}\sigma}} \\ &\times \sum_{\nu \in \mathcal{D}_-} \left(|\tilde{\psi}_{\eta, \sigma\nu}^1\rangle |\tilde{\chi}^1\rangle + |\tilde{\psi}_{\eta, \sigma\nu}^N\rangle |\tilde{\chi}^N\rangle \right) \left(\langle \tilde{\psi}_{\eta', \sigma\nu}^1 | \langle \tilde{\chi}^1 | + \langle \tilde{\psi}_{\eta', \sigma\nu}^N | \langle \tilde{\chi}^N | \right), \end{aligned} \quad (32)$$

where

$$|\tilde{\psi}_{\eta, \sigma\nu}^1\rangle = \int_{\mathcal{D}_+} d\mu T_1[\hat{f}_2](\eta\mu, \sigma\nu)|\eta\mu\rangle \quad (33a)$$

$$= \int_{\mathcal{D}_+} d\mu \delta_{M_{\mu}\eta} \delta_{M_{\nu}\sigma} T_1[\hat{f}_2](\mu, \nu)|\eta\mu\rangle \quad (33b)$$

and

$$|\tilde{\psi}_{\eta, \sigma\nu}^N\rangle = \int_{\mathcal{D}_+} d\mu T_N[\hat{f}_1](\eta\mu, \sigma\nu)|\eta\mu\rangle \quad (33c)$$

$$= \int_{\mathcal{D}_+} d\mu \delta_{M_{\mu}\eta} \delta_{M_{\nu}\sigma} T_N[\hat{f}_1](\mu, \nu)|\eta\mu\rangle \quad (33d)$$

where both $|\tilde{\psi}_{\eta,\sigma\nu}^1\rangle$ and $|\tilde{\psi}_{\eta,\sigma\nu}^N\rangle$ are not normalized. Here the subscript $\eta = \pm 1$ denotes the value of M of the final state, and the $\sigma = \pm 1$ subscript denotes the M value of the initial state ν . Below, we only refer to the labeled transition amplitudes $T_i[\hat{f}_j](\eta\mu, \sigma\nu)$ defined in Eq. (33d). The definition of the CCI is completed by the following identifications. First, the final labels $\eta = \pm 1$ are the *output ports* and, second, the population statistics in these product channels are *interference patterns*. Specifically, if we measure the observable M and sort the measurement events into two subensembles according to the measurement outcome η , then, following our convention, the interference pattern of the output port η is encoded in the expectation value

$$\begin{aligned} \langle \tfrac{1}{2}(\mathbf{1} + \eta M) \rangle &= \tilde{p}^{-1} \sum_{\sigma=\pm 1} \frac{p_\sigma}{\sum_{\nu \in \mathcal{D}_-} \delta_{M\nu\sigma}} \sum_{\nu \in \mathcal{D}_-} \left(\langle \tilde{\psi}_{\eta,\sigma\nu}^1 | \tilde{\psi}_{\eta,\sigma\nu}^1 \rangle \langle \tilde{\chi}^1 | \tilde{\chi}^1 \rangle \right. \\ &+ \langle \tilde{\psi}_{\eta,\sigma\nu}^1 | \tilde{\psi}_{\eta,\sigma\nu}^N \rangle \langle \tilde{\chi}^1 | \tilde{\chi}^N \rangle + \langle \tilde{\psi}_{\eta,\sigma\nu}^N | \tilde{\psi}_{\eta,\sigma\nu}^1 \rangle \langle \tilde{\chi}^N | \tilde{\chi}^1 \rangle + \langle \tilde{\psi}_{\eta,\sigma\nu}^N | \tilde{\psi}_{\eta,\sigma\nu}^N \rangle \langle \tilde{\chi}^N | \tilde{\chi}^N \rangle \Big), \end{aligned} \quad (34)$$

where

$$\begin{aligned} \tilde{p} &= \sum_{\eta=\pm 1} \sum_{\sigma=\pm 1} \frac{p_\sigma}{\sum_{\nu \in \mathcal{D}_-} \delta_{M\nu\sigma}} \sum_{\nu \in \mathcal{D}_-} \left(\langle \tilde{\psi}_{\eta,\sigma\nu}^1 | \tilde{\psi}_{\eta,\sigma\nu}^1 \rangle \langle \tilde{\chi}^1 | \tilde{\chi}^1 \rangle \right. \\ &+ \langle \tilde{\psi}_{\eta,\sigma\nu}^1 | \tilde{\psi}_{\eta,\sigma\nu}^N \rangle \langle \tilde{\chi}^1 | \tilde{\chi}^N \rangle + \langle \tilde{\psi}_{\eta,\sigma\nu}^N | \tilde{\psi}_{\eta,\sigma\nu}^1 \rangle \langle \tilde{\chi}^N | \tilde{\chi}^1 \rangle + \langle \tilde{\psi}_{\eta,\sigma\nu}^N | \tilde{\psi}_{\eta,\sigma\nu}^N \rangle \langle \tilde{\chi}^N | \tilde{\chi}^N \rangle \Big) \end{aligned} \quad (35)$$

is the total probability of detection. Note that we can only speak of an interference, or fringe pattern, if this expectation value is nonadditively dependent on the phase of the field components. In turn, non-additivity and phase-dependency can only originate from the cross terms, which depend on both transition amplitudes (T_1 and T_N) contained in the respective final material states ($|\tilde{\psi}_{\eta,\sigma\nu}^1\rangle$ and $|\tilde{\psi}_{\eta,\sigma\nu}^N\rangle$), as well as the overlaps of both final radiation states ($|\tilde{\chi}^1\rangle$ and $|\tilde{\chi}^N\rangle$). If these states are perfectly distinguishable, i.e. $\langle \tilde{\psi}_{\eta,\sigma\nu}^1 | \tilde{\psi}_{\eta,\sigma\nu}^N \rangle$ or $\langle \tilde{\chi}^1 | \tilde{\chi}^N \rangle = 0$, the cross terms vanish and the output statistics are additive and phase-independent. If, on the contrary, these overlaps are both finite, then the coherences $\langle \tilde{\psi}_{\eta,\sigma\nu}^1 | \tilde{\psi}_{\eta,\sigma\nu}^N \rangle$ and $\langle \tilde{\chi}^1 | \tilde{\chi}^N \rangle$ impart the phase difference of the excitation pathways on the expectation value $\langle \tfrac{1}{2}(\mathbf{1} + \eta M) \rangle$. In the CCI, this phenomenon is akin to interference and is synonymous with phase control. These observations will be useful in the next section, where we define the particle and the wave property in the context of the CCI, a prerequisite for studying wave-particle complementarity.

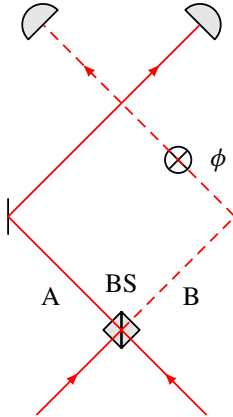


Figure 3: (color online) Mach-Zehnder interferometer in the open configuration with missing beam merger. The beams are mapped one-to-one into the detector ports. No interference pattern is measured.

3 Path Distinguishability

Central to quantum interference is the complementarity of particles and waves. In both, the Young double-slit (YDS) experiment and the MZI, the distinction between a wave and a particle is intuitive and elementary. Moreover, in these standard devices, interference is tangible in that it is macroscopic and occurs in free space. By contrast, it is by no means obvious how waves and particles manifest in the abstract context of the CCI. In order to show that wave- and particle-like behavior can be demonstrated in the CCI, as in a YDS or an MZI, it is necessary to clarify the notion of each such behavior. To this end we consider two particular CCI configurations, the *closed* and the *open configuration*, that allow an explicit identification of wave- and particle-like features.

3.1 The Open Interferometer Configuration: Particle-like Statistics

There exist versions of every two-path interference experiment in which it is possible to obtain “welcher-weg” (i.e., which-way or which-path) information about the object in the interferometer. By definition, complete welcher-weg information (WWI) allows us to unambiguously predict or trace the path of the object from input to output. For example, in the single-photon YDS experiment, it is possible to determine which slit a photon has passed through by replacing the screen with a pair of telescopes that focus on each slit [90]. Similarly, in a YDS experiment with single electrons, WWI is obtainable by placing the electron counter close to one of the slits [91]. Further, WWI is

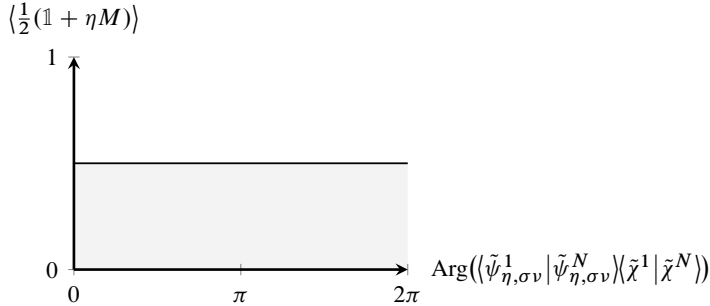


Figure 4: Sketch of the output port populations $\langle \frac{1}{2}(\mathbb{1} + \eta M) \rangle$, $\eta = \pm 1$, of the coherent control interferometer (CCI) in the open configuration o . Interference is absent. An identical pattern is produced by the open Mach-Zehnder interferometer (MZI) shown in Fig. 3.

trivially available for an MZI with the beam merger removed [77] as depicted in Fig. 3. In these alternative experimental arrangements, interference is absent. Rather, the welcher-weg measurement assigns classical alternatives to the object in the interferometer and the resultant classical alternatives do not interfere. Interference occurs only if the path of the object through the interferometer cannot be fully inferred, even in principle.

According to the definition of the CCI, interference fringes are manifest in the phase sensitivity of the population statistics of material eigenstates $|\eta\mu\rangle$ that carry a particular label, $\eta = M_\mu = \pm 1$. By convention, the statistical fringe pattern emerges from counting the fraction of measurement events with outcome $+1$ or -1 in many repeated measurements, and by varying the phase relationship of the two incoming wavepackets. The analysis of the preceding Sec. 2.3 shows that the fringe pattern can only be observed if the states $|\tilde{\psi}_{\eta,\sigma\nu}^1\rangle|\tilde{\chi}^1\rangle$ and $|\tilde{\psi}_{\eta,\sigma\nu}^N\rangle|\tilde{\chi}^N\rangle$ are not orthogonal. Individually, these quantum states describe the final state of the system reaching the output port η from the input port σ in one of the following two photoexcitation events:

- A, a first-order transition process fed by the second field component, (f_2, g_2) , that is concentrated around the frequencies $\Delta_{\mu\nu}/\hbar$, where μ is in the domain \mathcal{D}_+ and ν in \mathcal{D}_- , or
- B, an N^{th} -order transition driven by the first field component, (f_1, g_1) , with central frequency approximating $\Delta_{\mu\nu}/\hbar N$, where $N = 2, 3, \dots$

Therefore, according to this quantum description, distinguishing the final states $|\tilde{\psi}_{\eta,\sigma\nu}^1\rangle|\tilde{\chi}^1\rangle$ and $|\tilde{\psi}_{\eta,\sigma\nu}^N\rangle|\tilde{\chi}^N\rangle$ is equivalent to distinguishing the excitation processes, the consequence of which is then the absence of interference, Fig. 4. This conclusion is in full agreement with the ‘general principle of coherent control’ as originally stated [1]:

“The general principle of coherent control is to coherently drive a state with phase coherence through multiple, coherent, *indistinguishable*, optical excitation routes to the same final state in order to allow for the possibility of control.”

However, for this procedure to be rigorously analogous to the interference between binary paths in a YDS, it is necessary that these excitation routes constitute genuine binary path alternatives. To show that this is the case, we first have to verify that, *classically*, the excitation processes are mutually exclusive. In the case of the YDS, the mutual exclusivity of a classical particle passing through the first or the second slit is obvious. Further, if we took an electron—a quantum particle—and let it pass through a YDS, we could first make, and then falsify, the classical proposition that the electron is either going through one or the other slit [91]. In the case of the CCI this is much less clear. First, the processes A and B do not constitute a *path qubit*, i.e., a two-state quantum path degree of freedom with a mathematical structure of a spin- $\frac{1}{2}$. This is different for the YDS and most other two-path interferometers in use, since these have a path qubit [92]. For instance, in order to model the kinematics of interference in a YDS, the path alternatives can be described by two orthonormal state vectors, $|A\rangle$ and $|B\rangle$, that symbolize the amplitudes of slit A and slit B [93, 94]. However, such a description does not lend itself immediately to the case of the CCI. We address this issue in greater detail in the next section (Sec. 3.2).

The second complication of the CCI is that, due to the finite nature of \hbar , the material system may evolve on paths for which a classical analog does not exist. If this is the case, then there is no classical concept of what one should expect to occur. In order to mitigate this latter issue, we can invoke the principle of complementarity that gives meaning to “classical mutual exclusivity”. According to the principle, every measurement outcome must be interpreted in classical terms. Thus, classical mutual exclusivity means that there has to be a measurement that distinguishes the photoexcitation processes and guarantees that only one process is executed. Such measurements indeed exist. As a trivial example (non-trivial examples are discussed in Sec. 4) consider a scenario in which, starting from the input port $\sigma = +1$, the output port $\eta = +1$ can only be reached by process A and the port $\eta = -1$ only by B (and vice versa for $\sigma = -1$) i.e.

$$T_1[\hat{f}_2](\eta\mu, \sigma\nu) \propto \delta_{\eta, -\sigma}, \quad (36a)$$

$$T_N[\hat{f}_1](\eta\mu, \sigma\nu) \propto \delta_{\eta, \sigma} \quad (36b)$$

This is the case shown in Fig. 5. It is analogous to the MZI configuration shown in Fig. 3. In this highly simplified scenario, measuring the observable M amounts to discriminating between the transition processes A and B. Moreover, one would always find that only one of them is chosen, since measurements on quantum systems always have a single outcome. Classically,

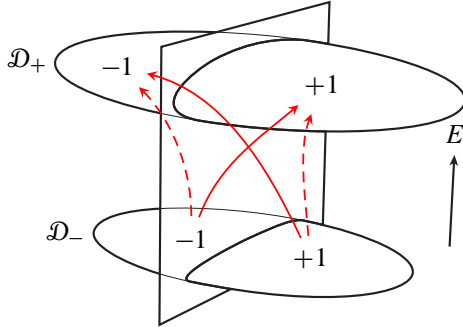


Figure 5: (color online) A trivially open CCI. Solid: process A. Dashed: process B.

it would then only be conceivable that the state $\tilde{\varrho}(\infty)$ is reached by one process at a time, not by both. By this paradigm, A and B are indeed mutually exclusive.

Second, we also have to verify the completeness (i.e., there are only these two paths) as well as the unidirectionality of the processes. In the cases of the YDS and the MZI, we have a clear and strict order of events: there are only two pathways from injection to detection, and these are traversed exactly once. In the CCI, a violation of unidirectionality can come about through higher order effects such as multiphoton processes. However, these are typically orders of magnitude smaller than processes A and B. By neglecting such higher order effects, the conditions of completeness and unidirectionality are met.

The conclusion is that, from a classical perspective, processes A and B are indeed binary path alternatives. Furthermore, there is only one relevant phase that occurs between the pathways: the phase of the coherence $\langle \tilde{\psi}_{\eta,\sigma\nu}^1 | \tilde{\psi}_{\eta,\sigma\nu}^N \rangle \langle \tilde{\chi}^1 | \tilde{\chi}^N \rangle$. If the photoexcitation pathways are fully distinguishable, then the principle of complementarity dictates that the controllability of η (i.e. the contrast of the statistical fringe pattern in the output port η) is zero. This is the same interpretation that is used to understand similar circumstances with photons in the YDS or an MZI. If the configuration of the interferometer is such that it is possible to say with certainty on which spatial path—upper or lower slit, left or right arm—the photon wavepacket reaches the detector, then a fringe pattern does not appear. Hence, the output port statistics from repeated measurements would indicate a particle-like character of the photon. Indeed, like a particle, the photon is traveling only on one path instead of two. Similarly, in the absence of interference fringes in the CCI, we speak of particle-like statistics of the output port populations. That does not imply that we regard a

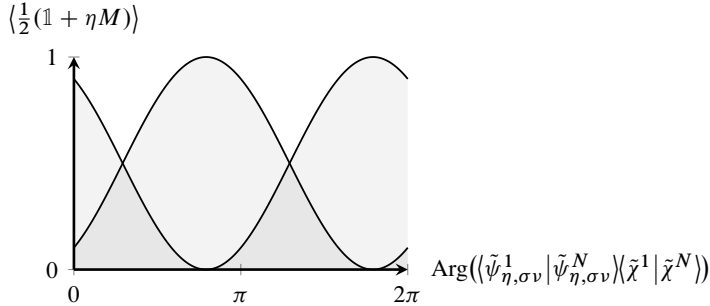


Figure 6: Sketch of the output port populations $\langle \frac{1}{2}(\mathbb{1} + \eta M) \rangle$, $\eta = \pm 1$, of the coherent control interferometer (CCI) in the closed configuration c . The interference contrast is maximal on both ports. An analogous pattern is produced by the closed Mach-Zehnder interferometer (MZI) shown in Fig. 1.

particle as being responsible for the statistics; rather, the conclusion is that the statistics are akin to those of a classical particle traversing a YDS. This is the case since, in a nondeterministic and probabilistic theory such as quantum mechanics, it is only meaningful to base the notion of a particle on observed statistics.

Particle-like statistics can have a number of different causes, not all of which are profound. For example, an interference pattern could simply be washed out due to imperfections in the measurement. It is also easily possible to falsely identify particle behavior, since an interference pattern requires a statistically large number of measurements. However, of the physical causes of particle-like statistics, the most fundamental one is the distinguishability of path alternatives, the WWI. In general, it is enough that WWI can be acquired *in principle* for a quantum system to display particle-like statistics; it is of no consequence if this measurement cannot be done in practice.

We call an interferometer “open” when it is possible to trace paths, and use the symbol o to denote the open interferometer configuration.

3.2 The Closed Interferometer Configuration: Wave-like Statistics

In quantum mechanics, wave and particle behavior are classical alternatives that are realized in complementary measurements; they are not intrinsic properties of a system. The measurement scheme that demonstrates the wave property of a quantum system is provided by the closed interferometer configuration, denoted c . It is characterized by a complete absence of WWI; it is the standard configuration of any two-path interferometer, and it maximizes the amount of observed interference. It is also the the

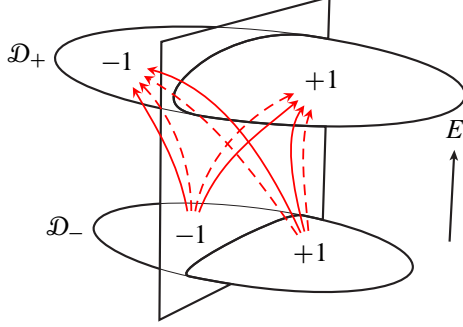


Figure 7: A closed CCI. Solid: process A. Dashed: process B.

configuration that adheres most to the general principle of coherent control, as stated on page 23. That is, in a closed CCI it is impossible to identify the excitation process by which the output port η was reached and, as such, it displays maximal controllability over η .

To illustrate, consider the model case in which the transition amplitudes of the processes A and B are each unbiased with respect to the label η , that is where

$$T_1[\hat{f}_2](+1\mu, \sigma\nu) = T_1[\hat{f}_2](-1\mu, \sigma\nu), \quad (37a)$$

$$T_N[\hat{f}_1](+1\mu, \sigma\nu) = -T_N[\hat{f}_1](-1\mu, \sigma\nu) \quad (37b)$$

for all $\mu \in \mathcal{D}_+$, $\nu \in \mathcal{D}_-$, and $\sigma = \pm 1$. If Eqs. (37) hold, then it is straightforward to show that the final state $\tilde{\varrho}(\infty)$ can be written as

$$\begin{aligned} \tilde{\varrho}(\infty) &= 2\tilde{p}^{-1} \sum_{\sigma=\pm 1} \frac{p_\sigma}{\sum_{\nu \in \mathcal{D}_-} \delta_{M_\nu \sigma}} \\ &\times \sum_{\nu \in \mathcal{D}_-} R\left(\frac{\pi}{4}\right)^\dagger \left(|\tilde{\psi}_{+1, \sigma\nu}^1\rangle |\tilde{\chi}^1\rangle + |\tilde{\psi}_{-1, \sigma\nu}^N\rangle |\tilde{\chi}^N\rangle \right) \\ &\times \left(\langle \tilde{\psi}_{+1, \sigma\nu}^1 | \langle \tilde{\chi}^1 | + \langle \tilde{\psi}_{-1, \sigma\nu}^N | \langle \tilde{\chi}^N | \right) R\left(\frac{\pi}{4}\right) \end{aligned} \quad (38a)$$

with

$$\begin{aligned} \tilde{p} &= 2 \sum_{\sigma=\pm 1} \frac{p_\sigma}{\sum_{\nu \in \mathcal{D}_-} \delta_{M_\nu \sigma}} \sum_{\nu \in \mathcal{D}_-} \left(\langle \tilde{\psi}_{+1, \sigma\nu}^1 | \tilde{\psi}_{+1, \sigma\nu}^1 \rangle \langle \tilde{\chi}^1 | \tilde{\chi}^1 \rangle \right. \\ &\quad \left. + \langle \tilde{\psi}_{-1, \sigma\nu}^N | \tilde{\psi}_{-1, \sigma\nu}^N \rangle \langle \tilde{\chi}^N | \tilde{\chi}^N \rangle \right), \end{aligned} \quad (38b)$$

and where $R(\zeta)$ denotes the unitary transformation

$$R(\zeta) = \exp\left[\int \mathfrak{f} d\mu(\zeta) | +1\mu \rangle \langle -1\mu | - \zeta^* | -1\mu \rangle \langle +1\mu | \right]. \quad (39)$$

Consider, in Eq. (38a), the terms bracketed by the rotations R . Interestingly, they take a form analogous to the superposition $(|A\rangle + |B\rangle)/\sqrt{2}$ of *path states* $|A\rangle$ and $|B\rangle$ that corresponds to the intermediate stage of a two-path interferometer [92, 93], e.g., the stage between the beam splitter and the beam merger in a MZI, as shown in Fig. 1. In fact, from this perspective the states $|\tilde{\psi}_{+1,\sigma\nu}^1\rangle$ and $|\tilde{\psi}_{-1,\sigma\nu}^N\rangle$ assume the role of path states for the CCI. To make the argument clearer, we temporarily assume that $|\tilde{\chi}^1\rangle$ and $|\tilde{\chi}^N\rangle$ are proportional to one another, i.e. that

$$\alpha^{-1}|\tilde{\chi}^1\rangle = \beta^{-1}|\tilde{\chi}^N\rangle = |\tilde{\chi}\rangle \quad (40)$$

with some $\alpha, \beta \in \mathbb{C}$ and the state $|\tilde{\chi}\rangle$ for which $\langle\tilde{\chi}|\tilde{\chi}\rangle = 1$. We can then say that an intermediate effect of the light-matter interaction is to transform the initial state $|\sigma\nu\rangle|\chi\rangle$ (with $|\chi\rangle$ from Eq. (18) on page 14) into the superposition

$$\left(\alpha\left|\tilde{\psi}_{+1,\sigma\nu}^1\right\rangle + \beta\left|\tilde{\psi}_{-1,\sigma\nu}^N\right\rangle\right)|\tilde{\chi}\rangle. \quad (41)$$

This state factorizes into a material and a radiative component. Here we are particularly interested in the material component. Looking at the above equation it appears that, as with common two-path interferometers, the routes through the CCI are characterized by the state of the system at the intermediate stage, cf. Fig. 7. In the positively labeled way, characterized by $|\tilde{\psi}_{+1,\sigma\nu}^1\rangle$, the excitation happens through process A, whereas, in the negatively labeled way, characterized by $|\tilde{\psi}_{-1,\sigma\nu}^N\rangle$, the excitation occurs through process B. Since $\langle\tilde{\psi}_{+1,\sigma\nu}^1|\tilde{\psi}_{-1,\sigma\nu}^N\rangle = 0$, these are the binary alternatives in all CCIs that fulfill Eqs. (37). According to Eq. (38a), these alternatives are subsequently brought into interference by the rotation R —that is the effect of the light-matter interaction. In this view, this operation plays a role analogous to the beam merger in a MZI. In fact, for

$$R\left(\frac{\pi}{4}\right) = \frac{1}{\sqrt{2}} \sum_{\mu} d\mu (|+1\mu\rangle\langle+1\mu| + |+1\mu\rangle\langle-1\mu| - |-1\mu\rangle\langle+1\mu| + |-1\mu\rangle\langle-1\mu|), \quad (42)$$

the action of the operator $R(\frac{\pi}{4})$ is equivalent, barring phase shifts introduced by reflections at the mirror, to the transformation between the single-photon input and output modes of a half-transparent mirror comprising the MZI's beam merger (BM in Fig. 1).

In the perfectly symmetric interferometer [i.e., given by Eq. (37) above], one cannot make an educated guess about which of the processes, A or B, will be realized. Such a prediction would be correct in only half of the cases. By contrast, in asymmetric interferometers, where there is a bias with respect to the label η , the accuracy of a welcher-weg guess depends on the amount of a *a priori* WWI. In the following, we assume that only one CCI input port is populated, i.e., we fix σ and set $p_{\sigma} = 1$, $p_{-\sigma} = 0$. In this

case,

$$w_{+1} = \int d\mu \langle +1\mu | R(\frac{\pi}{4}) \tilde{\rho}_{\mathcal{M}}(\infty) R(\frac{\pi}{4})^\dagger | +1\mu \rangle \quad (43)$$

$$= \frac{\sum_{\nu \in \mathcal{D}_-} |\alpha|^2 \langle \tilde{\psi}_{+1,\sigma\nu}^1 | \tilde{\psi}_{+1,\sigma\nu}^1 \rangle}{\sum_{\nu \in \mathcal{D}_-} (|\alpha|^2 \langle \tilde{\psi}_{+1,\sigma\nu}^1 | \tilde{\psi}_{+1,\sigma\nu}^1 \rangle + |\beta|^2 \langle \tilde{\psi}_{-1,\sigma\nu}^N | \tilde{\psi}_{-1,\sigma\nu}^N \rangle)} \quad (44)$$

is the *a priori* probability that the CCI executes process A, and $w_{-1} = 1 - w_{+1}$ is the *a priori* probability of process B. In Eq. (43), $\tilde{\rho}_{\mathcal{M}}(\infty)$ is the reduced density matrix of the material system, $\tilde{\rho}_{\mathcal{M}}(\infty) = \text{Tr}_{\mathcal{R}} \tilde{\rho}(\infty)$. The amount of *a priori* WWI is given by the *predictability* \mathfrak{P} of the alternatives:

$$\mathfrak{P} = |w_{+1} - w_{-1}|. \quad (45)$$

It states that, of all educated guesses made, (at least) the fraction $(1 + \mathfrak{P})/2$ will be correct. If the CCI is biased completely towards one excitation process—as it is the case in the open configuration discussed above—, then $\mathfrak{P} = 1$, and all educated guesses will be 100% accurate.

Maximum interference contrast requires a symmetric CCI with $\mathfrak{P} = 0$, i.e. a CCI with equally likely *a priori* path alternatives. To see this, we compute the output port statistics, which reduce to

$$\langle \frac{1}{2}(\mathbb{1} + \eta M) \rangle = \frac{1}{2} + \frac{\eta \sum_{\nu \in \mathcal{D}_-} \text{Re}[\alpha\beta^* \langle \tilde{\psi}_{+1,\sigma\nu}^1 | \tilde{\psi}_{+1,\sigma\nu}^N \rangle]}{\sum_{\nu \in \mathcal{D}_-} (|\alpha|^2 \langle \tilde{\psi}_{+1,\sigma\nu}^1 | \tilde{\psi}_{+1,\sigma\nu}^1 \rangle + |\beta|^2 \langle \tilde{\psi}_{-1,\sigma\nu}^N | \tilde{\psi}_{-1,\sigma\nu}^N \rangle)}. \quad (46)$$

If we additionally examine the case in which

$$|\alpha| T_1[\hat{f}_2](+1\mu, \sigma\nu) = \exp\{-i\gamma[\hat{f}_1, \hat{f}_2](+1, \sigma)\} |\beta| T_N[\hat{f}_1](+1\mu, \sigma\nu) \quad (47a)$$

and

$$\alpha |T_1[\hat{f}_2](+1\mu, \sigma\nu)| = e^{-i\phi} \beta |T_N[\hat{f}_1](+1\mu, \sigma\nu)| \quad (47b)$$

for all $\mu \in \mathcal{D}_+$ and $\nu \in \mathcal{D}_-$, then the predictability vanishes, $\mathfrak{P} = 0$, and Eq. (46) becomes

$$\langle \frac{1}{2}(\mathbb{1} + \eta M) \rangle = \frac{1}{2}[1 + \eta \cos(\phi + \gamma)]. \quad (48)$$

This simplification results because, by assumption, Eqs. (47) hold for all transition amplitudes, regardless of the values of μ and ν . This allows us in Eq. (48) to eliminate the incoherent sum over ν .

The phases γ and ϕ in Eq. (48) are assumed to be independent of both μ and ν . Indeed, γ and ϕ are the primary control parameters of the CCI and, in the following, are assumed to be arbitrarily variable.

The first phase,

$$\gamma = \gamma[\hat{f}_1, \hat{f}_2](+1, \sigma), \quad (49)$$

is sensitive to both material and radiative properties. For example, if the amplitude functions of the incident radiation were to gain additional phase factors, i.e., if we applied the map

$$\Phi_i: \hat{f}_i \mapsto e^{i\varphi_i} \hat{f}_i \quad (50)$$

with $-\pi < \varphi_i \leq \pi$, then γ would transform as $\gamma \mapsto \gamma + N\varphi_1 - \varphi_2$.

On the other hand, the second phase, ϕ , is sensitive only to the properties of the radiation field. It characterizes the phase relationship between the two outgoing radiation states $|\tilde{\chi}^1\rangle$ and $|\tilde{\chi}^N\rangle$,

$$\phi = \text{Arg}\langle \tilde{\chi}^1 | \tilde{\chi}^N \rangle \quad (51a)$$

$$= \text{Arg} \left\{ \sum_{n=0}^{\infty} \frac{1}{n!} [g_1^{(n)}(0)]^* g_1^{(N+n)}(0) \sum_{m=0}^{\infty} \frac{1}{m!} [g_2^{(1+m)}(0)]^* g_2^{(m)}(0) \right\} \quad (51b)$$

$$= \phi[g_1, g_2]. \quad (51c)$$

Thus ϕ can have a value different from 0 or π only if g_1 or g_2 are complex. For example, for given real g_i , we can make the transformation $g_i \mapsto g_i \circ \Phi_i$. Then ϕ transforms according to $\phi \mapsto \phi + N\varphi_1 - \varphi_2$.

Let us now go back to Eq. (48). This expectation value describes interference fringes with maximum contrast, as can be seen from the value of the fringe visibility \mathfrak{V} , that, following Michelson's definition [88], is

$$\mathfrak{V} = \frac{\max_{\gamma, \phi} \langle \frac{1}{2}(\mathbf{1} + \eta M) \rangle - \min_{\gamma, \phi} \langle \frac{1}{2}(\mathbf{1} + \eta M) \rangle}{\max_{\gamma, \phi} \langle \frac{1}{2}(\mathbf{1} + \eta M) \rangle + \min_{\gamma, \phi} \langle \frac{1}{2}(\mathbf{1} + \eta M) \rangle} = 1. \quad (52)$$

For general, unbiased CCIs [those for which Eqs. (37) hold], the fringe visibility can also be computed directly from Eq. (38a) by using

$$\mathfrak{V} = 2 \left| \int \! \! \int d\mu \langle +1\mu | R(\frac{\pi}{4}) \tilde{\rho}_{\mathcal{M}}(\infty) R(\frac{\pi}{4})^\dagger | -1\mu \rangle \right|. \quad (53)$$

For any two-path interferometer, it can further be shown [95–99] that the complementarity between wave and particle behavior is quantitatively manifest in the *duality relation*

$$\mathfrak{V}^2 + \mathfrak{P}^2 \leq 1. \quad (54)$$

That is, the contrast of the interference pattern (given by \mathfrak{V}) is bounded by the amount of WWI (given by \mathfrak{P}) that is *a priori* available, and solely due to the asymmetry of the interferometer. The inequality also states that full particle statistics with absolute welcher-weg knowledge (as in the open configuration *o*) as well as wavelike statistics with truly indistinguishable path alternatives (as in the closed configuration *c*) are idealized cases. Quantum mechanics allows a system to display either one of those ideal properties; however, the standard case is a blend of the two that fits into

neither classical concept of wave or particle [93]. Hence, as quantified in the duality relation, it is possible to have limited *a priori* WWI (increasing the accuracy of welcher-weg predictions) and simultaneously observe interference with a reduced contrast.

This concludes the introduction of the closed CCI configuration, in which we can fully control the population of the CCI's output ports. It is the control scheme that allows one to demonstrate wavelike behavior of the output statistics; they are fully analogous to the measurement statistics of a classical wave passing through a YDS.

One comment is in order. The open and the closed configuration (and thus the wave and the particle property) are defined here with respect to measurements in the eigenbasis of the material Hamiltonian $H_{\mathcal{M}}$, particularly, a measurement of the dichotomous observable M as specified by Eq. (28). In general, however, wave- and particle-like statistics are basis dependent. It is easy to show that there exists another basis in which the wave- and the particle-like behavior are interchanged, i.e., the eigenbasis of the observable $R(\frac{\pi}{4})^\dagger M R(\frac{\pi}{4})$. Notwithstanding, in the setting of coherent control, the material eigenbasis is the preferred basis.

4 Quantum Erasure Coherent Control

Our goal is to create scenarios in which genuine, nontrivial features of quantum interference are the origin of coherent phase control. As a first scenario of this kind we propose a generalized coherent phase control scenario based on quantum erasure, in which quantum entanglement and nonclassical correlations play a role. This provides a measurement scheme by which an open configuration can be transformed into a closed configuration in a nontrivial way in order to probe and verify the nonclassicality of the scenario. We follow up on this aspect in Sec. 4.4.

4.1 Welcher-Weg Marking And Nontrivial CCI Configurations

The duality relation $\mathfrak{W}^2 + \mathfrak{P}^2 \leq 1$ provides a quantitative measure of the fact that any *a priori* WWI (as specified by the asymmetry \mathfrak{P} of the CCI) must cause a loss of interference contrast \mathfrak{W} in the measurement statistics of the output ports. A second source of WWI may be found in other degrees of freedom that are part of the material system or of the radiation field. We will now deal with them in greater detail—with a special focus on the role of the radiation.

The process by which degrees of freedom acquire WWI is called “welcher-weg marking” (WWM). The degrees of freedom involved in WWM, commonly referred to as the welcher-weg marker, can be understood in terms of observation and measurement, and is linked to an outward flow of information

from the path degree of freedom to the marker. In general, this flow is mediated by an entangling interaction, that is, the monitoring of the path degree of freedom by the marker creates an entangled state, in which the path degree of freedom and marker are in a quantum superposition. This being the case, one cannot ascribe realistic properties to *either* of the two parties; the properties of the first system depend on the choice of measurement performed on the second inasmuch as the state of the second system is determined by the observable being measured on the first. In the context of two-path interference, these quantum correlations can result in the distinguishability of path alternatives, if they correspond to a recording of WWI. According to the complementarity principle, this would lead to a reduction of interference contrast.

Consider then the role of entanglement and WWM in our agenda. A coherent control scenario in which both entanglement and WWM participate could be properly classified as quantum coherent control. Below we utilize the CCI to develop such a model scenario, starting with a CCI with unbiased transition amplitudes [with respect to the output ports, cf. Eq. (37)] and populating just one of the two input ports. That is, we set $p_\sigma = 1$ for $\sigma = +1$ or $\sigma = -1$. The final state of the total system is then

$$\tilde{\rho}(\infty) = \frac{1}{\sum_{\nu \in \mathcal{D}_-} (\langle \tilde{\psi}_{+1,\sigma\nu}^1 | \tilde{\psi}_{+1,\sigma\nu}^1 \rangle \langle \tilde{\chi}^1 | \tilde{\chi}^1 \rangle + \langle \tilde{\psi}_{-1,\sigma\nu}^N | \tilde{\psi}_{-1,\sigma\nu}^N \rangle \langle \tilde{\chi}^N | \tilde{\chi}^N \rangle)} \times \sum_{\nu \in \mathcal{D}_-} \left[R\left(\frac{\pi}{4}\right)^\dagger (|\tilde{\psi}_{+1,\sigma\nu}^1\rangle |\tilde{\chi}^1\rangle + |\tilde{\psi}_{-1,\sigma\nu}^N\rangle |\tilde{\chi}^N\rangle) \times (\langle \tilde{\psi}_{+1,\sigma\nu}^1 | \langle \tilde{\chi}^1 | + \langle \tilde{\psi}_{-1,\sigma\nu}^N | \langle \tilde{\chi}^N |) R\left(\frac{\pi}{4}\right) \right], \quad (55)$$

where the sums over the quantum number ν are over the input domain \mathcal{D}_- . In this expression, the path and radiation states are such that $|\tilde{\chi}^1\rangle$ correlates with the path labeled +1, and $|\tilde{\chi}^N\rangle$ with the path -1. This situation introduces a complication: the radiation field is not only driving the dynamics, but it can additionally act as a welcher-weg marker. In the setting of coherent control, however, these two roles conflict. Phase-sensitive control relies on the indistinguishability of the pathways, but WWM can inhibit the control by making the pathways distinguishable.

In conventional coherent control, we would simply measure M and determine the output port populations $\langle \frac{1}{2}(\mathbb{1} + \eta M) \rangle$ with $\eta = \pm 1$. Such an experiment would not provide any insight into the correlated nature of the paths ± 1 and the radiation, and hence into this quantum feature. In what can be called an extended control experiment, we join the measurement of M with a measurement of a radiation field observable $O_{\mathcal{R}}$. In this case, correlations can have an impact, and they may be exploited to gain such insight. In fact, given sufficient control over the field,¹ two antithetic measurement strategies are conceivable [94]: the ‘‘optimum welcher-weg

¹We will not concern ourselves with the very details and practical experimental

measurement” and quantum erasure. Both are useful for the agenda of developing a fully quantum control scenario, and both are explained in detail below. In the first, one tries to make the interferometer as open as possible and to extract as much WWI as possible. Although this minimizes the phase control—the strategy is in fact contrary to the general principle of coherent control as quoted on page 23—, the procedure may still be beneficial since the goal is to introduce quantum correlations. The second strategy is quantum erasure, where one attempts to close the interferometer as much as possible, which also gives as much phase control as possible. The logic behind the choice between the two antithetic strategies is provided by the nonclassical principle of complementarity. The existence of that choice is a distinctive feature of the extended coherent control scheme.

We discuss these strategies below, emphasizing once again that our goal is not to enhance the extent of control. Indeed, the closed configuration is known to provide maximum control in this scenario, i.e., maximum sensitivity to the value of the phase.

4.1.1 Welcher-Weg Measurements

In accord with Eq. (55), WWI may be acquired via a measurement $O_{\mathcal{R}}$ on the radiation field \mathcal{R} that can distinguish $|\tilde{\chi}^1\rangle$ and $|\tilde{\chi}^N\rangle$ —provided that they are distinguishable to some degree. A measure of the acquired amount of WWI is the welcher-weg *knowledge* $\mathfrak{K}(O_{\mathcal{R}})$ which is always greater than or equal to the predictability [Eq. (45)] $\mathfrak{P} = \mathfrak{K}(\mathbb{1}_{\mathcal{R}})$. Significantly, Ref. 94 proves that the duality relation $\mathfrak{V}^2 + \mathfrak{P}^2 \leq 1$ can be generalized to the duality relation

$$\mathfrak{V}(O_{\mathcal{R}})^2 + \mathfrak{K}(O_{\mathcal{R}})^2 \leq 1, \quad (56)$$

where $\mathfrak{V}(O_{\mathcal{R}})$ denotes the fringe visibility in the CCI’s output ports under joint measurement of $O_{\mathcal{R}}$.² For projective measurements, $O_{\mathcal{R}}^2 = O_{\mathcal{R}}$, \mathfrak{K} is computable from

$$\mathfrak{K}(O_{\mathcal{R}}) = \left| \left\langle R\left(\frac{\pi}{4}\right)^\dagger M R\left(\frac{\pi}{4}\right) O_{\mathcal{R}} \right\rangle \right| + \left| \left\langle R\left(\frac{\pi}{4}\right)^\dagger M R\left(\frac{\pi}{4}\right) (\mathbb{1}_{\mathcal{R}} - O_{\mathcal{R}}) \right\rangle \right|. \quad (57)$$

The first term quantifies the knowledge $\mathfrak{K}_{\text{click}}$ obtained from measurement events with the outcome 1 (i.e., detector clicks), whereas the second term specifies the knowledge $\mathfrak{K}_{\text{no-click}}$ gained from events with outcome 0 (no

requirements of such control, which are well enough discussed elsewhere [88, 100, 101]. However, we will discuss a realistic case of control in Sec. 4.3.

²Note that, since there cannot be any measurement $O_{\mathcal{R}}$ that reduces the interference contrast, we have $\mathfrak{V}(O_{\mathcal{R}}) \geq \mathfrak{V}(\mathbb{1}_{\mathcal{R}}) = \mathfrak{V}$ and, further, an additional duality relation, $\mathfrak{V}^2 + \mathfrak{K}(O_{\mathcal{R}})^2 \leq 1$, which is less strong than Eq. (56), but stronger than $\mathfrak{V}^2 + \mathfrak{P}^2 \leq 1$.

click). For the state (55), the knowledge amounts to

$$\begin{aligned} \mathfrak{R}(O_{\mathcal{R}}) = & \left| w_{+1} \frac{\langle \tilde{\chi}^1 | O_{\mathcal{R}} | \tilde{\chi}^1 \rangle}{\langle \tilde{\chi}^1 | \tilde{\chi}^1 \rangle} - w_{-1} \frac{\langle \tilde{\chi}^N | O_{\mathcal{R}} | \tilde{\chi}^N \rangle}{\langle \tilde{\chi}^N | \tilde{\chi}^N \rangle} \right| \\ & + \left| w_{+1} \left(1 - \frac{\langle \tilde{\chi}^1 | O_{\mathcal{R}} | \tilde{\chi}^1 \rangle}{\langle \tilde{\chi}^1 | \tilde{\chi}^1 \rangle} \right) - w_{-1} \left(1 - \frac{\langle \tilde{\chi}^N | O_{\mathcal{R}} | \tilde{\chi}^N \rangle}{\langle \tilde{\chi}^N | \tilde{\chi}^N \rangle} \right) \right|. \end{aligned} \quad (58)$$

If we want to acquire a maximum of WWI (in order to realize a maximally open CCI), we should not, however, restrict ourselves to projective measurements, which are, in general, not optimal. However, even without explicitly finding the optimal measurement, we can still calculate the welcher-weg knowledge it would provide. Specifically, the highest amount of WWI acquirable in any measurement of the field is determined by the radiative *distinguishability* $\mathfrak{D}_{\mathcal{R}} = \sup_{O_{\mathcal{R}}} \mathfrak{R}(O_{\mathcal{R}})$ [94], given by [92]

$$\begin{aligned} \mathfrak{D}_{\mathcal{R}} = \text{Tr} \left| \int \! \! \int d\mu \left(\langle +1\mu | R(\frac{\pi}{4}) \tilde{\rho}(\infty) R(\frac{\pi}{4})^\dagger | +1\mu \rangle \right. \right. \\ \left. \left. - \langle -1\mu | R(\frac{\pi}{4}) \tilde{\rho}(\infty) R(\frac{\pi}{4})^\dagger | -1\mu \rangle \right) \right|. \end{aligned} \quad (59)$$

where the trace of the norm is defined as $\text{Tr}|X| = \text{Tr}\sqrt{X^\dagger X}$.

For the state (55), we find from Eq. (59) that the radiative distinguishability is

$$\mathfrak{D}_{\mathcal{R}} = \sqrt{1 - 4w_{+1}w_{-1} \frac{|\langle \tilde{\chi}^1 | \tilde{\chi}^N \rangle|^2}{\langle \tilde{\chi}^1 | \tilde{\chi}^1 \rangle \langle \tilde{\chi}^N | \tilde{\chi}^N \rangle}}, \quad (60)$$

which becomes equal to \mathfrak{P} for indistinguishable, and unity for orthogonal, radiative out-states, i.e., $\mathfrak{R}(O_{\mathcal{R}}) = \mathfrak{D}_{\mathcal{R}} = 1$. With the latter, the paths are fully distinguished,³ the duality relation Eq. (56) indicates the absence of interference, $\mathfrak{V}(O_{\mathcal{R}}) = 0$, giving the fully particle-like statistics of the open CCI configuration o (Sec. 3.1). The optimum welcher-weg measurement thus demonstrates the significance of correlations between the path and the radiation field. The extent to which they are nonclassical is addressed below.

4.1.2 Quantum Erasure

With the quantum erasure measurement scheme, we select a statistical subensembles for which the path alternatives are indistinguishable. In doing so, we can recover maximum fringe contrast [92, 102–105] and thus a maximum of phase control. What is remarkable about this is that the

³If we failed to optimize the measurement, then, due to $\mathfrak{R}(O_{\mathcal{R}}) \geq \mathfrak{P}$, we would be at most as ignorant about the paths as without any welcher-weg measurement.

phase control can originate entirely from a nontrivial quantum interference effect. For quantum erasure to work, we again have to join the result of a measurement of M with that of an optimally chosen $O_{\mathcal{R}}$. The largest attainable fringe contrast—and thus phase controllability—in such a procedure is quantified by the radiative *coherence* $\mathfrak{C}_{\mathcal{R}} = \sup_{O_{\mathcal{R}}} \mathfrak{V}(O_{\mathcal{R}})$ [94], which is the counterpart of the radiative distinguishability, $\mathfrak{D}_{\mathcal{R}}$, introduced above.

For an unbiased CCI, the radiative coherence is given by

$$\mathfrak{C}_{\mathcal{R}} = 2 \operatorname{Tr} \left| \int d\mu \langle +1\mu | R(\frac{\pi}{4}) \tilde{\rho}(\infty) R(\frac{\pi}{4})^\dagger | -1\mu \rangle \right| \quad (61a)$$

which, for the final state (55), reduces to

$$\mathfrak{C}_{\mathcal{R}} = 2 \frac{|\sum_{\nu} \langle \tilde{\psi}_{+1,\sigma\nu}^1 | \tilde{\psi}_{+1,\sigma\nu}^N \rangle| \operatorname{Tr} |\tilde{\chi}^1\rangle \langle \tilde{\chi}^N|}{\sum_{\nu} (\langle \tilde{\psi}_{+1,\sigma\nu}^1 | \tilde{\psi}_{+1,\sigma\nu}^1 \rangle \langle \tilde{\chi}^1 | \tilde{\chi}^1 \rangle + \langle \tilde{\psi}_{-1,\sigma\nu}^N | \tilde{\psi}_{-1,\sigma\nu}^N \rangle \langle \tilde{\chi}^N | \tilde{\chi}^N \rangle)} \quad (61b)$$

and, in the case of (at least slightly) distinguishable final radiative states, $|\langle \tilde{\chi}^1 | \tilde{\chi}^N \rangle| > 0$, to

$$\mathfrak{C}_{\mathcal{R}} = \mathfrak{V} \frac{\sqrt{\langle \tilde{\chi}^1 | \tilde{\chi}^1 \rangle \langle \tilde{\chi}^N | \tilde{\chi}^N \rangle}}{|\langle \tilde{\chi}^1 | \tilde{\chi}^N \rangle|}. \quad (61c)$$

If the final radiative states, $|\tilde{\chi}^1\rangle$ and $|\tilde{\chi}^N\rangle$, are indistinguishable (i.e., proportional to one another), then $\mathfrak{C}_{\mathcal{R}} = \mathfrak{V}$, and we cannot improve the control; otherwise, we have $\mathfrak{C}_{\mathcal{R}} > \mathfrak{V}$. According to wave-particle complementarity as quantified by the duality relation (56), succeeding to completely restore the fringe contrast, $\mathfrak{V}(O_{\mathcal{R}}) = \mathfrak{C}_{\mathcal{R}} = 1$, means to fully reverse the WWM, $\mathfrak{K}(O_{\mathcal{R}}) = 0$. This situation realizes the closed CCI configuration and thus full phase control in an *entirely nontrivial* way.

The measurement strategies discussed here—optimum welcher-weg measurement, quantum erasure, and nonoptimum mixes thereof—will in general deliver a blend of particle- and wavelike statistics, which goes beyond Bohr’s original version of complementarity. Interestingly, it turns out that the experimenter has a choice between measurement strategies even after detecting the output port event (i.e. after the “click”). In fact, *when* the choice is made has no impact on the measurement statistics. This is the essence of the delayed choice gedanken experiment [76, 106], whose relevance for the demonstration of quantum coherent control is discussed in Sec. 5.

4.2 The Special Case of Symmetric CCIs

Below we derive optimum welcher-weg and quantum erasure measurements for the case of a symmetric CCI. In this example, WWM involves only the radiative degrees of freedom. For simplicity, we populate only one input

port (i.e., $p_\sigma = 1$ for either $\sigma = -1$ or 1), and assume unbiased transition amplitudes, as defined in Eq. (37). Additionally, we stipulate that

$$\sqrt{\langle \tilde{\chi}^1 | \tilde{\chi}^1 \rangle} T_1[\hat{f}_2](+1\mu, \sigma\nu) = \exp\{-i\gamma[\hat{f}_1, \hat{f}_2](+1, \sigma)\} \\ \times \sqrt{\langle \tilde{\chi}^N | \tilde{\chi}^N \rangle} T_N[\hat{f}_1](+1\mu, \sigma\nu) \quad (62)$$

for all $\mu \in \mathcal{D}_+$ and $\nu \in \mathcal{D}_-$, the same symmetry condition as in Eq. (47a). Note that, once again, the phase $\gamma = \gamma[\hat{f}_1, \hat{f}_2](+1, \sigma)$ is independent of both μ and ν . The CCI's output port labels and the remaining material degrees of freedom are therefore not correlated, excluding the latter from WWM.

With the above restrictions, the final state of the system becomes

$$\tilde{\rho}(\infty) = \prod_{\mathcal{D}_+} d\mu \prod_{\mathcal{D}_+} d\mu' \frac{\sum_\nu T_1[\hat{f}_2](+1\mu, \sigma\nu) T_1^*[\hat{f}_2](+1\mu', \sigma\nu)}{\sum_\nu \langle \tilde{\psi}_{+1, \sigma\nu}^1 | \tilde{\psi}_{+1, \sigma\nu}^1 \rangle} \\ \times R\left(\frac{\pi}{4}\right)^\dagger \frac{1}{\sqrt{2}} \left(| +1\mu \rangle \frac{|\tilde{\chi}^1\rangle}{\sqrt{\langle \tilde{\chi}^1 | \tilde{\chi}^1 \rangle}} - e^{i\gamma} | -1\mu \rangle \frac{|\tilde{\chi}^N\rangle}{\sqrt{\langle \tilde{\chi}^N | \tilde{\chi}^N \rangle}} \right) \\ \times \frac{1}{\sqrt{2}} \left(\langle +1\mu' | \frac{\langle \tilde{\chi}^1 |}{\sqrt{\langle \tilde{\chi}^1 | \tilde{\chi}^1 \rangle}} - e^{-i\gamma} \langle -1\mu' | \frac{\langle \tilde{\chi}^N |}{\sqrt{\langle \tilde{\chi}^N | \tilde{\chi}^N \rangle}} \right) R\left(\frac{\pi}{4}\right). \quad (63)$$

From this we find

$$\mathfrak{P} = 0, \quad \mathfrak{D}_{\mathcal{R}} = \sqrt{1 - \frac{|\langle \tilde{\chi}^1 | \tilde{\chi}^N \rangle|^2}{\langle \tilde{\chi}^1 | \tilde{\chi}^1 \rangle \langle \tilde{\chi}^N | \tilde{\chi}^N \rangle}}, \quad (64a)$$

$$\mathfrak{V} = \frac{|\langle \tilde{\chi}^1 | \tilde{\chi}^N \rangle|}{\sqrt{\langle \tilde{\chi}^1 | \tilde{\chi}^1 \rangle \langle \tilde{\chi}^N | \tilde{\chi}^N \rangle}}, \quad \mathfrak{C}_{\mathcal{R}} = 1. \quad (64b)$$

Hence, these quantities “saturate” the duality relations with $\mathfrak{V}^2 + \mathfrak{D}_{\mathcal{R}}^2 = 1$ and $\mathfrak{C}_{\mathcal{R}}^2 + \mathfrak{P}^2 = 1$. That is, the duality relations now provide a direct relationship, as opposed to an inequality, between the quantities in Eq. (64b). Note that since the duality relation (56) holds for all measurements $O_{\mathcal{R}}$, it specifically holds for the measurements that maximize the acquired WWI, $\mathfrak{K}(O_{\mathcal{R}}) = \mathfrak{D}_{\mathcal{R}}$, and restore the most fringe contrast, $\mathfrak{V}(O_{\mathcal{R}}) = \mathfrak{C}_{\mathcal{R}}$, respectively [94, 99].

In order to find optimal measurements $O_{\mathcal{R}}$ (for which either a maximum of WWI is obtained, or full interference contrast is restored, respectively), consider the ket in the second line of Eq. (63). This state *almost* looks like a standard example of an entangled state [107], but the radiation states $|\tilde{\chi}^1\rangle$ and $|\tilde{\chi}^N\rangle$ are in general nonorthogonal. However, there is an alternative form of the ket that involves only orthogonal states [108], and is of great value below. It reads

$$\sum_{\pm} \sqrt{\lambda_{\pm}} |\pm_{\mathcal{M}}\rangle |\pm_{\mathcal{R}}\rangle, \quad (65)$$

where

$$\lambda_{\pm} = \frac{1 \pm \mathfrak{A}}{2}, \quad (66a)$$

$$\begin{aligned} |\pm_{\mathcal{M}}\rangle &= R\left(\frac{\pi}{4}\right)^{\dagger} \frac{1}{\sqrt{2}} (\pm e^{-i\phi} | +1\mu\rangle - e^{i\gamma} | -1\mu\rangle) \\ &= \pm e^{-i(\phi-\gamma)/2} \left(\cos \frac{\phi+\gamma}{2} |\pm 1\mu\rangle - i \sin \frac{\phi+\gamma}{2} |\mp 1\mu\rangle \right), \end{aligned} \quad (66b)$$

and

$$|\pm_{\mathcal{R}}\rangle = \frac{1}{2\sqrt{\lambda_{\pm}}} \left(\pm e^{i\phi} \frac{|\tilde{\chi}^1\rangle}{\sqrt{\langle \tilde{\chi}^1 | \tilde{\chi}^1 \rangle}} + \frac{|\tilde{\chi}^N\rangle}{\sqrt{\langle \tilde{\chi}^N | \tilde{\chi}^N \rangle}} \right) \quad (66c)$$

with phase $\phi = \text{Arg}\langle \tilde{\chi}^1 | \tilde{\chi}^N \rangle$ as in Eq. (51). Here $\langle \pm_{\mathcal{R}} | \pm_{\mathcal{R}} \rangle = 1$ and $\langle \pm_{\mathcal{R}} | \mp_{\mathcal{R}} \rangle = 0$, whereas the states $| +_{\mathcal{M}} \rangle$ and $| -_{\mathcal{M}} \rangle$ are orthogonal, but in general (e.g., continuum states) not normalized. Their dependence on μ and σ is understood, though not explicitly stated.

Equation (65) is similar to a *Schmidt decomposition* [57, 109], in which the factors $\sqrt{\lambda_{\pm}}$ would be referred to as the *Schmidt coefficients*. The difference to a standard Schmidt decomposition is that the $|\pm_{\mathcal{R}}\rangle$ are improper (unnormalizable) states. Despite this difference, we will refer to Eq. (65) as a Schmidt decomposition and to $\sqrt{\lambda_{\pm}}$ as the Schmidt coefficients.

If $|\tilde{\chi}^1\rangle$ and $|\tilde{\chi}^N\rangle$ are linearly independent, then both Schmidt coefficients are finite and the state (65) is entangled. In general, however, that does not imply that $\tilde{\varrho}(\infty)$ in Eq. (63) is entangled. That is, since it is a mixed state, correlations may be classical. Here, however, $\tilde{\varrho}(\infty)$ contains the same entanglement as the state (65), if the remaining degrees of freedom of the material system (everything except the labels ± 1) are ignored.⁴ A quantitative measure of the entanglement strength is provided by the *concurrence* \mathfrak{c} [57, 110]. For the case described here, it is given by

$$\mathfrak{c} = \sqrt{2(1 - \sum_{\pm} \lambda_{\pm}^2)} \quad (67a)$$

$$= \sqrt{1 - \mathfrak{A}^2}, \quad (67b)$$

which varies smoothly from 0 for a product state, to 1, for a maximally entangled state for which the Schmidt coefficients are equal. This can only happen for fully distinguishable radiative out-states and hence vanishing interference.

Here, in accord with Eqs. (64b) and (67), the distinguishability and the concurrence seem to be equal, $\mathfrak{D}_{\mathcal{R}} = \mathfrak{c}$, which is an explicit statement that,

⁴This is easily justifiable in the case in which the material Hilbert space has the structure of a tensor product between a two-dimensional Hilbert space, \mathcal{H}_2 , for the CCI port labels ± 1 and another Hilbert space, $\mathcal{H}_{\perp 2}$, for the remaining degrees of freedom, such that $\mathcal{H}_{\mathcal{M}} \otimes \mathcal{H}_{\mathcal{R}} = \mathcal{H}_{\perp 2} \otimes \mathcal{H}_2 \otimes \mathcal{H}_{\mathcal{R}}$. Then the state (63) admits a similar decomposition into $\tilde{\varrho}_{\perp 2}(\infty) \otimes \tilde{\varrho}_{2 \otimes \mathcal{R}}(\infty)$, where the mixed state $\tilde{\varrho}_{\perp 2}(\infty)$ is not correlated with anything and $\tilde{\varrho}_{2 \otimes \mathcal{R}}(\infty)$ is pure and entangled.

in this example, the distinguishability is quantum and not the result of classical correlations [111]. Below we discuss whether this provides sufficient leverage for probing the nonclassicality of the scenario. To do so, we begin by designing an optimum welcher-weg measurement.

4.2.1 An Optimum Welcher-Weg Measurement

It is only possible to obtain additional WWI through a measurement of the radiation field if $\mathfrak{D}_{\mathcal{R}} > 0$. The acquired welcher-weg knowledge, $\mathfrak{K}(O_{\mathcal{R}})$, depends on the observable $O_{\mathcal{R}}$, and we can derive an optimum welcher-weg observable for which $\mathfrak{K}(O_{\mathcal{R}}) = \mathfrak{D}_{\mathcal{R}}$. For the symmetric CCI with $w_{+1} = w_{-1} = \frac{1}{2}$ examined here, it is

$$O_{\mathcal{R}} = \frac{1}{\sqrt{1 - \mathfrak{V}^2}} \left(\frac{|\tilde{\chi}^N\rangle\langle\tilde{\chi}^N|}{\langle\tilde{\chi}^N|\tilde{\chi}^N\rangle} - \frac{|\tilde{\chi}^1\rangle\langle\tilde{\chi}^1|}{\langle\tilde{\chi}^1|\tilde{\chi}^1\rangle} \right) \quad (68)$$

which has an eigendecomposition $O_{\mathcal{R}} = \Pi_{\mathcal{R}}^{\pm} - \Pi_{\bar{\mathcal{R}}}^{\pm}$, where $\Pi_{\mathcal{R}}^{\pm} = (|+\mathcal{R}\rangle \pm |-\mathcal{R}\rangle)(\langle+\mathcal{R}| \pm \langle-\mathcal{R}|)/2$. Consequentially, the measurement of the ± 1 eigenvalue reduces the state $\tilde{\rho}(\infty)$ to

$$\tilde{\rho}_{\mathcal{M}}^{\pm}(\infty) = \sum_{\nu} R\left(\frac{\pi}{4}\right)^{\dagger} \left| \tilde{\psi}_{\sigma\nu}^{\pm} \right\rangle \left\langle \tilde{\psi}_{\sigma\nu}^{\pm} \right| R\left(\frac{\pi}{4}\right) \quad (69a)$$

with

$$\begin{aligned} \left| \tilde{\psi}_{\sigma\nu}^{\pm} \right\rangle = & \sqrt{\frac{1 \mp \sqrt{1 - \mathfrak{V}^2}}{2 \sum_{\nu'} \langle \tilde{\psi}_{+1,\sigma\nu'}^1 | \tilde{\psi}_{+1,\sigma\nu'}^1 \rangle}} e^{-i\phi} \left| \tilde{\psi}_{+1,\sigma\nu}^1 \right\rangle \\ & + \sqrt{\frac{1 \pm \sqrt{1 - \mathfrak{V}^2}}{2 \sum_{\nu'} \langle \tilde{\psi}_{-1,\sigma\nu'}^N | \tilde{\psi}_{-1,\sigma\nu'}^N \rangle}} \left| \tilde{\psi}_{-1,\sigma\nu}^N \right\rangle. \end{aligned} \quad (69b)$$

For $\mathfrak{V} \rightarrow 0$, these states becomes fully particle-like: $\tilde{\rho}_{\mathcal{M}}^{-}(\infty)$ describes the state after excitation in a one-photon process, whereas $\tilde{\rho}_{\mathcal{M}}^{+}(\infty)$ describes the result of N -photon excitation. According to Eq. (67b), $\mathfrak{V} = 0$ also means $\mathfrak{c} = 1$, i.e. the quantum correlations described by the state $\tilde{\rho}(\infty)$ are maximal. Successful extraction of full WWI therefore suggests a strong nonclassicality to the scenario. However, as we shall see, that is not sufficient to prove it.

4.2.2 An Optimum What-Phase Measurement

Consider the intricacies of the complementary quantum erasure scheme, where phase control can emerge as a nontrivial quantum interference effect. In Eq. (63), the final state $\tilde{\rho}(\infty)$ is written in a way that puts emphasis on the particle-like property of the CCI labels. However, as shown above, an equally valid description (or “as-if reality” [92, 112]) is in terms of the Schmidt

decomposition (65), in which the material system is in a superposition of the two wavelike states $|\pm_{\mathcal{M}}\rangle$, one corresponding to fringes $|\!|_{+\mathcal{M}}\rangle$, in conjunction with the fringe marker state $|+\mathcal{R}\rangle$ and the other to antifringes $|\!|_{-\mathcal{M}}\rangle$, with the orthogonal antifringe marker state $|-\mathcal{R}\rangle$. The goal of quantum erasure is to realize one of these wavelike alternatives.

As an illustration, consider the joint measurement statistics of $\frac{1}{2}(\mathbb{1} + \eta M)$ and some radiative projector $O_{\mathcal{R}}$ with $O_{\mathcal{R}}^2 = O_{\mathcal{R}}$. Using the Schmidt decomposition (65), the statistics can be immediately obtained. On the one hand, within the subensemble for which we measure the $O_{\mathcal{R}}$ eigenvalue $+1$, i.e., the subensemble of click events, we observe the output port statistics

$$\begin{aligned} \frac{\langle \frac{1}{2}(\mathbb{1}_{\mathcal{M}} + \eta M)O_{\mathcal{R}} \rangle}{\langle O_{\mathcal{R}} \rangle} &= \frac{1}{\langle O_{\mathcal{R}} \rangle} \left\{ \frac{\lambda_+}{2} [1 + \eta \cos(\phi + \gamma)] \langle +_{\mathcal{R}} | O_{\mathcal{R}} | +_{\mathcal{R}} \rangle \right. \\ &\quad - \sqrt{\lambda_+ \lambda_-} \eta \sin(\phi + \gamma) \text{Im} \langle +_{\mathcal{R}} | O_{\mathcal{R}} | -_{\mathcal{R}} \rangle \\ &\quad \left. + \frac{\lambda_-}{2} [1 - \eta \cos(\phi + \gamma)] \langle -_{\mathcal{R}} | O_{\mathcal{R}} | -_{\mathcal{R}} \rangle \right\}, \end{aligned} \quad (70a)$$

where $\langle O_{\mathcal{R}} \rangle = \sum_{\pm} \lambda_{\pm} \langle \pm_{\mathcal{R}} | O_{\mathcal{R}} | \pm_{\mathcal{R}} \rangle$ is the weight of the subensemble. On the other hand, for the subensemble to the eigenvalue 0—the no-click subensemble—with

$$\begin{aligned} \frac{\langle \frac{1}{2}(\mathbb{1}_{\mathcal{M}} + \eta M)(\mathbb{1}_{\mathcal{R}} - O_{\mathcal{R}}) \rangle}{1 - \langle O_{\mathcal{R}} \rangle} &= \frac{1}{1 - \langle O_{\mathcal{R}} \rangle} \left\{ \frac{1}{2} [1 + \eta \mathfrak{V} \cos(\phi + \gamma)] \right. \\ &\quad \left. - \langle \frac{1}{2}(\mathbb{1}_{\mathcal{M}} + \eta M)O_{\mathcal{R}} \rangle \right\}. \end{aligned} \quad (70b)$$

Using Eq. (70a), it is easy to construct a projector $O_{\mathcal{R}}$ that restores full fringe visibility, $\mathfrak{V}(O_{\mathcal{R}}) = 1$. Formally, a perfect choice is

$$O_{\mathcal{R}} = |+\mathcal{R}\rangle\langle +_{\mathcal{R}}|. \quad (71)$$

With this, the statistics of the click subensemble becomes

$$\frac{\langle \frac{1}{2}(\mathbb{1}_{\mathcal{M}} + \eta M)O_{\mathcal{R}} \rangle}{\langle O_{\mathcal{R}} \rangle} = \frac{1}{2} [1 + \eta \cos(\phi + \gamma)] \quad (72)$$

with weight $\langle O_{\mathcal{R}} \rangle = \lambda_+$. Indeed, this expression describes a fringe pattern with maximal contrast. The choice (71) works, because the projection onto $|+\mathcal{R}\rangle$ reduces the decomposition (65) to a product state. Since WWM relies here fully on the entanglement between the final state of the marker and the path alternatives, the interference can be fully recovered. A less abstract explanation is that the field is detected in a state for which a distinction between the two excitation processes is not possible. The WWI has been *erased*.

With $O_{\mathcal{R}}$ as in Eq. (71), a fully saturated interference pattern also shows in the subensemble for which the detector does not click,

$$\frac{\langle \frac{1}{2}(\mathbb{1}_{\mathcal{M}} + \eta M)(\mathbb{1}_{\mathcal{R}} - O_{\mathcal{R}}) \rangle}{1 - \langle O_{\mathcal{R}} \rangle} = \frac{1}{2}[1 - \eta \cos(\phi + \gamma)], \quad (73)$$

where $1 - \langle O_{\mathcal{R}} \rangle = \lambda_-$. At first glance, this result seems at odds with the limited visibility \mathfrak{V} when no measurement on the field is carried out. However, there is no contradiction, since the weighted average

$$\langle O_{\mathcal{R}} \rangle \frac{\langle \frac{1}{2}(\mathbb{1}_{\mathcal{M}} + \eta M)O_{\mathcal{R}} \rangle}{\langle O_{\mathcal{R}} \rangle} + (1 - \langle O_{\mathcal{R}} \rangle) \frac{\langle \frac{1}{2}(\mathbb{1}_{\mathcal{M}} + \eta M)(\mathbb{1}_{\mathcal{R}} - O_{\mathcal{R}}) \rangle}{1 - \langle O_{\mathcal{R}} \rangle} \quad (74)$$

of both interference patterns is a sum of fringes and antifringes, which, in general, has less contrast than either pattern (\mathfrak{V} in this case).

In contrast to the optimum welcher-weg measurement scheme, a successful demonstration of quantum erasure would not only suggest nonclassicality, but also imply a genuinely quantum interference origin for phase control in the experiment. Sec. 4.4 discusses whether or not this would also be a valid rigorous proof. Before that, however, we address in Sec. 4.3 how “quantum erasure coherent control” could be done under more realistic conditions, i.e., conditions under which a measurement of $O_{\mathcal{R}} = |+\mathcal{R}\rangle\langle +\mathcal{R}|$ [Eq. (71)] is not available.

4.3 Quantum Erasure with Displaced Photon Threshold Measurements

The observable $O_{\mathcal{R}}$ in Eq. (71) is formally the best choice for quantum erasure, but it may not be the most practical. For an arbitrary radiative in-state $|\chi\rangle$, it may not be possible to realize a projection onto the state $|+\mathcal{R}\rangle$. We can illustrate and resolve this issue via an example of perfect WWM. Consider the case where the radiation field is initialized in the nonclassical $(n_1 + n_2)$ -photon wavepacket state

$$|\chi\rangle = \frac{1}{\sqrt{n_1!}} (a^\dagger[\hat{f}_1])^{n_1} \frac{1}{\sqrt{n_2!}} (a^\dagger[\hat{f}_2])^{n_2} |\text{vac}\rangle, \quad (75)$$

where $n_1 \geq N$, $n_2 \geq 1$, and where the amplitude functions f_1, f_2 have disjoint support and meet the requirements of the 1 vs. N coherent phase control as stated in Sec. 2.1. Then, according to Eqs. (24), the final (path conditioned) radiation states are

$$|\tilde{\chi}^1\rangle = \frac{1}{\sqrt{n_1!}} (a^\dagger[\hat{f}_1])^{n_1} \frac{\sqrt{n_2}}{\sqrt{(n_2 - 1)!}} (a^\dagger[\hat{f}_2])^{n_2 - 1} |\text{vac}\rangle \quad (76a)$$

and

$$|\tilde{\chi}^N\rangle = \frac{\sqrt{n_1(n_1 - 1) \cdots (n_1 - N + 1)}}{\sqrt{(n_1 - N)!}} (a^\dagger[\hat{f}_1])^{n_1 - N} \frac{1}{\sqrt{n_2!}} (a^\dagger[\hat{f}_2])^{n_2} |\text{vac}\rangle. \quad (76b)$$

These states are orthogonal, $\langle \tilde{\chi}^1 | \tilde{\chi}^N \rangle = 0$, and therefore $\phi = 0$, $\mathfrak{V} = 0$, and $\mathfrak{D} = 1$. Full WWI is thus available.

Complete WWI can be acquired by measuring the total light intensity $I \sim \text{Tr}[H_{\mathcal{R}} \tilde{\rho}(\infty)]$ [113], which can be understood as counting the final numbers of photons in the modes [114]. In principle, as described in the previous section, this WWI can be removed by a projection of the field into $|+\mathcal{R}\rangle$ or $|-\mathcal{R}\rangle$. Yet, by definition [cf. Eq. (66c)], these states are coherent superpositions of $|\tilde{\chi}^1\rangle$ and $|\tilde{\chi}^N\rangle$ and thus are *entangled* multimode Fock states. Hence, it is very difficult to implement a projection into one of them. However, there is an experimentally feasible alternative, a so-called “displaced photon threshold measurement” which can be defined as

$$O_{\mathcal{R}} = D^\dagger[-f](2|\text{vac}\rangle\langle\text{vac}| - \mathbf{1}_{\mathcal{R}})D[-f], \quad (77)$$

where

$$D[-f] = \exp(a[f] - a^\dagger[f]) = D^\dagger[f] \quad (78)$$

is a displacement operator in continuous Fock space. Such a displaced photon threshold measurement can be realized in a homodyne detection scheme that employs a click/no-click detector,⁵ an auxiliary coherent light source, and a beam splitter with an almost ideal transmission. In the beam splitter, prior to feeding it into the detector, the light is superposed with a coherent state

$$|-f\rangle = D[-f]|\text{vac}\rangle = e^{-\|f\|^2/2} \sum_{n=0}^{\infty} \frac{1}{n!} (a^\dagger[-f])^n |\text{vac}\rangle \quad (79)$$

from the auxiliary source whose radiation is characterized by the amplitude function $-f$. In those cases where the eigenvalue 1 is found (i.e., the absence of a click in the detector), the radiation field is projected into the coherent state $|f\rangle = D[f]|\text{vac}\rangle$. The visibility of the fringes observed in this subensemble is then:

$$\mathfrak{V}_{\text{no-click}} = \frac{1}{2\langle f|f\rangle\langle f|f\rangle} \left| \langle +\mathcal{R}|f\rangle|^2 - \langle +\mathcal{R}|f\rangle\langle f|-\mathcal{R}\rangle + \langle -\mathcal{R}|f\rangle\langle f|+\mathcal{R}\rangle - \langle -\mathcal{R}|f\rangle|^2 \right|, \quad (80)$$

⁵A click/no-click detector, also referred to as a threshold detector, is a photodetector that does not resolve the number of photons. It responds if it detects one or more photons, but its signal will not differentiate between one photon and two or more photons. A threshold detector with unit efficiency for all frequencies and polarizations is described by the dichotomous observable $[|\text{vac}\rangle\langle\text{vac}| - (\mathbf{1}_{\mathcal{R}} - |\text{vac}\rangle\langle\text{vac}|)]$. A click corresponds to an event with one or more photons and the eigenvalue -1 . The eigenvalue 1 is assigned to the photon-less no-click event.

where $\langle |f\rangle\langle f| \rangle = (|\langle +_{\mathcal{R}}|f\rangle|^2 + |\langle -_{\mathcal{R}}|f\rangle|^2)/2$ is the probability to not detect a click. For the radiation states (76), these expressions become

$$\mathfrak{V}_{\text{no-click}} = \frac{2\sqrt{n_1!(n_1-N)!n_2} |(\hat{f}_1, f)|^N |(\hat{f}_2, f)|}{(n_1-N)!n_2 |(\hat{f}_1, f)|^{2N} + n_1! |(\hat{f}_2, f)|^2} \quad (81)$$

and

$$\begin{aligned} \langle |f\rangle\langle f| \rangle &= \frac{|(\hat{f}_1, f)|^{2(n_1-N)} |(\hat{f}_2, f)|^{2(n_2-1)}}{4e^{\|f\|^2} n_1! (n_1-N)! n_2!} \\ &\quad \times \left[(n_1-N)! n_2 |(\hat{f}_1, f)|^{2N} + n_1! |(\hat{f}_2, f)|^2 \right]. \end{aligned} \quad (82)$$

The visibility $\mathfrak{V}_{\text{no-click}}$ can then be optimized by tuning the intensity, proportional to the norm $\|f\|$ of the amplitude function f , of the auxiliary coherent light field described by the state $|f\rangle$. The visibility becomes maximal, $\mathfrak{V}_{\text{no-click}} = 1$, for

$$\|f\| = \left(\frac{|(\hat{f}_1, \hat{f})|^N}{|(\hat{f}_2, \hat{f})|} \sqrt{n_2 \frac{(n_1-N)!}{n_1!}} \right)^{\frac{1}{1-N}} \quad (83)$$

with $\hat{f} = f/\|f\|$.⁶ That means, given the right intensity of the auxiliary field (which, according to the above equation, only depends on the number of photons in the incident radiation and the absolute overlaps $|(\hat{f}_1, \hat{f})|$, $|(\hat{f}_2, \hat{f})|$ of the amplitude functions), one achieves full coherent control over the label η of the material system,

$$\frac{\langle \frac{1}{2}(\mathbb{1}_{\mathcal{M}} + \eta M)|f\rangle\langle f| \rangle}{\langle |f\rangle\langle f| \rangle} = \frac{1}{2} \{ 1 + \eta \cos[\gamma + N \text{Arg}(\hat{f}_1, \hat{f}) - \text{Arg}(\hat{f}_2, \hat{f})] \}, \quad (84)$$

in the event that the detector does not fire.⁷ Subject to the constraint (83), one now optimizes this probability, by finding $\max_{\hat{f}} \langle |f\rangle\langle f| \rangle$. For convenience, we restrict our attention to $N = 2$. In this case, the expectation value $\langle |f\rangle\langle f| \rangle$ is maximized by

$$\hat{f} = \alpha \hat{f}_1 + \beta \hat{f}_2, \quad (85a)$$

where

$$|\alpha| = |(\hat{f}_1, \hat{f})| = \frac{1}{\sqrt{u}}, \quad |\beta| = |(\hat{f}_2, \hat{f})| = \sqrt{1 - \frac{1}{u}}, \quad (85b)$$

⁶With $\|f\|$ as in Eq. (83), $\mathfrak{R}(O_{\mathcal{R}}) = \mathfrak{R}_{\text{no-click}} = \mathfrak{R}_{\text{click}} = 0$. It is thus impossible to identify the excitation process by which the output port is reached.

⁷Note that the phase relationship between the incoming radiation and auxiliary field, $\text{Arg}(\hat{f}_i, \hat{f})$, offers an additional control opportunity.

and

$$u = \frac{1}{4} \left(3 + \sqrt{1 + \frac{8n_2(n_1+2n_2-2)}{n_1(n_1-1)}} \right). \quad (85c)$$

The maximum is given by

$$\langle |f\rangle \langle f| \rangle = \frac{(u-1)^{n_1+2n_2-2}}{n_1!(n_2-1)!} \left[\frac{n_1(n_1-1)}{n_2} \right]^{n_1+n_2-1} e^{-\frac{n_1(n_1-1)}{n_2}u(u-1)}. \quad (86)$$

For two photons in the first and one photon in the second incident wavepacket, $n_1 = 2$, $n_2 = 1$, and $\langle |f\rangle \langle f| \rangle = e^{-3/2}/2 \simeq 0.11$, which is also the largest possible value for any valid choice of n_1 and n_2 . That means that the statistical weight of the no-click subensemble is 11% at best. The remaining 89% contribute to the click subensemble where one observes interference fringes with contrast

$$\mathfrak{V}_{\text{click}} = \frac{\langle |f\rangle \langle f| \rangle}{1 - \langle |f\rangle \langle f| \rangle} \mathfrak{V}_{\text{no-click}} = \frac{1}{2e^{3/2} - 1} \simeq 0.13, \quad (87)$$

much less than for the no click subensemble, but still better than without quantum erasure. Note that we were unable to improve over these numbers, with or without condition (83).

4.4 Can Welcher-Weg Or What-Phase Measurements Rigorously Probe Nonclassicality?

The question addressed in this section is whether or not the measurement strategies discussed above can serve as rigorous verifications of the nonclassical principle of complementarity, of true quantum coherent control, and, in the case of quantum erasure, of genuinely quantum interference. For the example of quantum erasure, let us reiterate why this might be the case. In the above examples, the WWI is accompanied by quantum entanglement between the material system and the radiation field: measuring the former in one of the states $R(\frac{\pi}{4})^\dagger |\tilde{\psi}_{+1,\sigma\nu}^1\rangle$ or $R(\frac{\pi}{4})^\dagger |\tilde{\psi}_{-1,\sigma\nu}^1\rangle$ is equivalent to detecting the latter in either $|\tilde{\chi}^1\rangle$ or $|\tilde{\chi}^N\rangle$, respectively. The projection on a path ignorant marker state ($|+\mathcal{R}\rangle$ or $|-\mathcal{R}\rangle$) results in the interference reappearing; quantum erasure is complete. Based on this finding, one can speculate that an erasure of WWI generally involves the dissolution of quantum entanglement. If that were indeed true, then successful quantum erasure, as indicated by the recovery of interference, would be able to certify the presence of entanglement. Thus, we may ask whether or not quantum erasure necessarily implies quantum entanglement

The answer is, in general, unfortunately, no. The example studied in Sec. 4.2 is an exceptional, *pure-state case* where quantum entanglement is prerequisite to WWI, and WWI is prerequisite to the recovery of interference. However, as we discuss in the following, that causal chain breaks when mixed

states are considered. However, if we can guarantee that the system is in a pure state, then quantum erasure ensures quantum entanglement and rigorously verifies quantumness in the control scenario.

Considering, however, the difficulty of preparing the pure state case, we examine the general case, below. In that case:

Interference recovery does not require the presence of WWI. In fact, the term “quantum erasure” is a misnomer. Sometimes, interference can be restored in cases for which there is no WWI (and no quantum entanglement) to begin with. This is known as “nonerasing quantum erasure” [94]. The function of quantum erasure is solely to prepare subensembles within which the interference contrast is maximal [92, 115]. This can include the removal of WWI, but it also may not.

WWI does not rely on quantum entanglement. For example, if the state $\tilde{\varrho}(\infty)$ of Eq. (63) were to decohere into a mixture with respect to the path labels ± 1 , then the WWI would remain intact, but would exist as classical, rather than quantum, correlations. These correlations could still be removed by postselection, yet the recovery of an interference pattern would not be possible (i.e., WWI can be erased without regaining any interference contrast). That is, the procedure would not be able to bring back the cross-term contributions that are necessary for interference, but that were lost due to decoherence.

Interference recovery does not certify quantum entanglement. In some cases and contrary to the situation just described, interference contrast can be restored from a fully classical, mixed state. Below we give such an example (adapted from Ref. 94). It counters the proposition that quantum erasure is a reliable test for nonclassical correlations (or any correlations for that matter) unless the state is pure. To see this, consider the case in which condition (37) is replaced by

$$T_1[\hat{f}_2](+1\mu, \sigma\nu) = \sigma T_1[\hat{f}_2](-1\mu, \sigma\nu), \quad (88a)$$

$$T_N[\hat{f}_1](+1\mu, \sigma\nu) = -\sigma T_N[\hat{f}_1](-1\mu, \sigma\nu). \quad (88b)$$

We further require the validity of Eq. (62) and demand that

$$T_1[\hat{f}_2](+1\mu, \sigma\nu) = \exp\{-i\gamma[\hat{f}_1, \hat{f}_2](+1, \sigma)\} T_1[\hat{f}_2](+1\mu, -\sigma\nu), \quad (89a)$$

$$T_N[\hat{f}_2](+1\mu, \sigma\nu) = \exp\{i\gamma[\hat{f}_1, \hat{f}_2](+1, \sigma)\} T_N[\hat{f}_2](+1\mu, -\sigma\nu), \quad (89b)$$

as well as

$$\gamma[\hat{f}_1, \hat{f}_2](+1, +1) = -\gamma[\hat{f}_1, \hat{f}_2](+1, -1). \quad (89c)$$

Finally, let us assume that the material system starts in the state (30) with

$$\frac{p_{+1}}{\sum_{\nu \in \mathcal{D}_-} \delta_{M_{\nu,+1}}} = \frac{p_{-1}}{\sum_{\nu \in \mathcal{D}_-} \delta_{M_{\nu,-1}}}, \quad (90)$$

i.e., in an incoherent (classical) mixture with equal population of the CCI input ports ± 1 . In this situation, the final state will be

$$\begin{aligned} \tilde{\rho}(\infty) = & \sum_{\mathcal{D}_+}^f d\mu \sum_{\mathcal{D}_+}^f d\mu' \frac{\sum_{\nu} T_1[\hat{f}_2](+1\mu, +1\nu) T_1^*[\hat{f}_2](+1\mu', +1\nu)}{\sum_{\nu} \langle \tilde{\psi}_{+1,+1\nu}^1 | \tilde{\psi}_{+1,+1\nu}^1 \rangle} \\ & \times R(\frac{\pi}{4})^\dagger \frac{1}{2} \left[\left(\frac{|+1\mu\rangle |\tilde{\chi}^1\rangle}{\sqrt{2\langle \tilde{\chi}^1 | \tilde{\chi}^1 \rangle}} - e^{i\gamma} \frac{|-1\mu\rangle |\tilde{\chi}^N\rangle}{\sqrt{2\langle \tilde{\chi}^N | \tilde{\chi}^N \rangle}} \right) \right. \\ & \times \left(\frac{\langle +1\mu' | \langle \tilde{\chi}^1 |}{\sqrt{2\langle \tilde{\chi}^1 | \tilde{\chi}^1 \rangle}} - e^{-i\gamma} \frac{\langle -1\mu' | \langle \tilde{\chi}^N |}{\sqrt{2\langle \tilde{\chi}^N | \tilde{\chi}^N \rangle}} \right) \\ & + \left(\frac{|+1\mu\rangle |\tilde{\chi}^N\rangle}{\sqrt{2\langle \tilde{\chi}^N | \tilde{\chi}^N \rangle}} - e^{i\gamma} \frac{|-1\mu\rangle |\tilde{\chi}^1\rangle}{\sqrt{2\langle \tilde{\chi}^1 | \tilde{\chi}^1 \rangle}} \right) \\ & \left. \times \left(\frac{\langle +1\mu' | \langle \tilde{\chi}^N |}{\sqrt{2\langle \tilde{\chi}^N | \tilde{\chi}^N \rangle}} - e^{-i\gamma} \frac{\langle -1\mu' | \langle \tilde{\chi}^1 |}{\sqrt{2\langle \tilde{\chi}^1 | \tilde{\chi}^1 \rangle}} \right) \right] R(\frac{\pi}{4}). \quad (91) \end{aligned}$$

where $\gamma = \gamma[\hat{f}_1, \hat{f}_2](+1, +1)$. That is an average of Eq. (63) and Eq. (63) with the path labels $+1$ and -1 interchanged. Therefore, the state (91) does not represent any correlations—neither classical nor quantum—between the path labels and the radiation field. One calculates

$$\mathfrak{P} = 0, \quad \mathfrak{D}_{\mathcal{R}} = 0, \quad (92a)$$

$$\mathfrak{V} = \frac{|\langle \tilde{\chi}^1 | \tilde{\chi}^N \rangle|}{\sqrt{\langle \tilde{\chi}^1 | \tilde{\chi}^1 \rangle \langle \tilde{\chi}^N | \tilde{\chi}^N \rangle}} |\cos \phi|, \quad \mathfrak{C}_{\mathcal{R}} = |\cos \phi| \quad (92b)$$

with $\phi = \text{Arg}\langle \tilde{\chi}^1 | \tilde{\chi}^N \rangle$. Thus, if $\langle \tilde{\chi}^1 | \tilde{\chi}^N \rangle = 0$, then the fringe visibility can be fully restored because the state (91) contains cross terms

$$\frac{\langle \frac{1}{2}(\mathbf{1}_{\mathcal{M}} + \eta M) | +\mathcal{R} \rangle \langle +\mathcal{R} |}{\langle |+\mathcal{R}\rangle \langle +\mathcal{R} |} = \frac{1}{2}(1 + \eta \cos \gamma), \quad (93)$$

although $\mathfrak{D}_{\mathcal{R}} = 0$. We thus have a case of nonerasing quantum erasure.

To conclude, welcher-weg and quantum erasure measurement schemes can, in general, neither demonstrate the recording of WWI, nor can they unambiguously certify the presence of quantum entanglement [92]. Although, in our description of the scenario of Sec. 4.2, it is quantum entanglement that

mediates path knowledge and quantum interference that establishes control, the question about the nonclassicality of an actual coherent phase control experiment cannot be answered on the grounds of those measurement schemes alone. The presence of quantum entanglement, nonclassical correlations, and true quantum coherent control has to be certified by additional, more stringent means (as discussed in Sec. 6 below). However, this is not to say that the proposed quantum erasure coherent phase control experiment is useless. First, it is of practical utility to restore a maximum amount of phase controllability. Second, in combination with an optimum welcherweg measurement, quantum erasure allows for demonstrating wave-particle complementarity. And third, if an experiment managed to demonstrably produce the state (63) and if quantum erasure succeeded, then the scenario would be indeed be quantum (even nonclassical), and phase control would originate from genuinely quantum interference. The problem is that the state (63) may not be the only possible description. From a foundational perspective, one must show that there is no other, classical explanation for the measurement results.

5 Delayed Choice Coherent Control

Below we continue the search for unconventional, demonstrably quantum phase control scenarios. The first scenario, the quantum erasure control scheme discussed above (Sec. 4), was based on the principle of complementarity. The second scenario below will be based on another hallmark of quantum mechanics: delayed choice. As explained below, the alternative scenario solves a conceptual issue of quantum erasure phase control.

Complementarity in quantum mechanics implies that the experimenter can select from a set of measurement strategies in order to observe particle-like, wavelike, or any arbitrary intermediate statistics [92, 116]. This is in stark contrast to classical physics, which invariably classifies every object as either particle or wave; never can an entity subscribe to either property *ad libitum*. Complementarity also applies in the setting of quantum erasure, where a subensemble with wavelike statistics is chosen and where the timing of that choice is irrelevant for the outcome of the experiment [76, 102]. Quantum erasure can therefore be a particular realization of the so-called delayed-choice gedanken experiment [106, 115].

Delayed-choice experiments were proposed by Wheeler to display the fundamental difference that the principle of complementarity places between classical and quantum physics. In order to render it impossible for an object to “know” *a priori* whether or not to display the wave or the particle property, delayed-choice experiments aim to sever any causal link between the object and the interferometer until it has entered it.

Quantum erasure adheres to the aims of delayed choice by conditioning the interference property on the outcome of a measurement performed on

an auxiliary system, the welcher-weg marker. This allows for choosing *a posteriori* between the open interferometer configuration *o* with associated particle-like statistics—in which case the tracing of paths may be possible—to the closed configuration *c* and associated wavelike statistics—for which the path alternatives are at least partially indistinguishable. This also applies to the examples studied in Sec. 4.2, where the choice of, say, the wave property, could be postponed to a time after the measurement of the output port label. According to quantum theory, this can occur in direct violation of classical realism and thus suggests the nonclassicality of coherent control. That is a significant step towards the goal to create a demonstrably quantum control scenario.

Yet, one might deem that particular demonstration as unsatisfactory, since the preparation of the wave property—and thus phase control—is *detached* from the light-matter scattering processes of coherent control. Rather, an additional process, quantum erasure, has to be performed on top of the original coherent control experiment. For the scope of this article, we would prefer a situation in which the wave property emerges more directly from the scattering processes.

As a solution we propose another generalized coherent control experiment in which the CCI delivers the wave and the particle property directly and in superposition [77]. This experiment will allow one to select either the open or the closed CCI configuration on demand (and at any time) by flipping a “quantum switch”. Prior to turning that switch, it will be unknowable whether the CCI output port statistics are that of a wave or a particle, i.e., whether phase control is possible or not, a violation of classical realism. In this regard, this proposed scenario is entitled to be called quantum coherent control.

As we shall see, the positions of the quantum switch are represented by two (nearly) orthogonal states of the radiation field. That means that, in contrast to the quantum eraser, the choice between wave and particle is not a choice between two complementary, noncommuting field observables, but rather between two orthogonal projections.

5.1 The Simultaneously Both Open And Closed Configuration

In the following, we consider two field configurations,

$$|\chi_o\rangle = g_{1o}(a^\dagger[\hat{f}_{1o}])g_{2o}(a^\dagger[\hat{f}_{2o}])|\text{vac}\rangle \quad (94a)$$

and

$$|\chi_c\rangle = g_{1c}(a^\dagger[\hat{f}_{1c}])g_{2c}(a^\dagger[\hat{f}_{2c}])|\text{vac}\rangle. \quad (94b)$$

The former, $|\chi_o\rangle$, is assumed to implement an open CCI o ,

$$T_1[\hat{f}_{2o}](\eta\mu, \sigma\nu) \propto \delta_{\eta, -\sigma}, \quad (95a)$$

$$T_N[\hat{f}_{1o}](\eta\mu, \sigma\nu) \propto \delta_{\eta, \sigma} \quad (95b)$$

whereas the latter, $|\chi_c\rangle$, implements a closed CCI c ,

$$T_1[\hat{f}_{2c}](+1\mu, \sigma\nu) = T_1[\hat{f}_{2c}](-1\mu, \sigma\nu), \quad (95c)$$

$$T_N[\hat{f}_{1c}](+1\mu, \sigma\nu) = -T_N[\hat{f}_{1c}](-1\mu, \sigma\nu). \quad (95d)$$

These relations are adopted from Eqs. (36) and (37), respectively. In both cases, the incoming light is prepared in a semi-classical coherent state:

$$g_{io}(x) = \exp(\|f_{io}\|x - \|f_{io}\|^2/2), \quad (96a)$$

$$g_{ic}(x) = \exp(\|f_{ic}\|x - \|f_{ic}\|^2/2), \quad (96b)$$

$i = 1, 2$. These states are eigenstates of the photon annihilation operator, and thus WWM does not occur [114]. We have

$$\|f_{2o}\|^{-1}|\tilde{\chi}_o^1\rangle = \|f_{1o}\|^{-N}|\tilde{\chi}_o^N\rangle = |\chi_o\rangle, \quad (97a)$$

$$\|f_{2c}\|^{-1}|\tilde{\chi}_c^1\rangle = \|f_{1c}\|^{-N}|\tilde{\chi}_c^N\rangle = |\chi_c\rangle, \quad (97b)$$

similar to Eq. (40). Coherent states are explicitly chosen with the intention of excluding postselection procedures like optimum welcher-weg measurements or quantum erasure from the experiment. That is, we have to realize delayed choice in a different way, for reasons explained below.

In order to carry out Wheeler's original delayed choice experiment in the setting of coherent phase control, we would have to both *randomize* and *postpone* the choice between an open and closed CCI. We could certainly do the former, i.e., randomize the configuration by deciding at random between either $|\chi_c\rangle$ or $|\chi_o\rangle$ as the initial state of the radiation field. However, since we decided to exclude WWM, the CCI does not allow us to postpone that decision. This is a major stumbling block, since randomization alone would not suffice if the alternatives "phase control" and "no control" were chosen in advance.⁸

The CCI is thus *not* compatible with Wheeler's delayed choice experiment. The only way of physically delaying the choice is to deviate both from the traditional coherent control schemes and from Wheeler's original idea. The goal is to guarantee the uncertainty and the unknowability of the CCI's interference property. One solution is to quantize the choice between open and closed [77] by preparing the field in a quantum-coherent superposition between the complementary configurations, i.e. in

$$|\chi\rangle = \frac{|\chi_o\rangle + |\chi_c\rangle}{\sqrt{2(1 + \langle\chi_o|\chi_c\rangle)}}, \quad (98)$$

⁸Mind that it is irrelevant whether or not the choice is known to us—it has to be unknowable *physically*.

where

$$\langle \chi_o | \chi_c \rangle = \exp \left[-\frac{1}{2} \left(\|f_{1o}\|^2 + \|f_{2o}\|^2 + \|f_{1c}\|^2 + \|f_{2c}\|^2 \right) \right]. \quad (99)$$

This state is quite unusual. It is composed out of two semi-classical, distinct states, each of which a direct product of two coherent states in, in total, four mutually orthogonal modes, i.e., $|\chi\rangle$ is a ‘‘cat state’’ [109]. It is an entangled coherent state with nonclassical correlations of the GHZ type [57, 117–119]. From an experimental point of view, handling $|\chi\rangle$ may prove difficult: the state will be very sensitive to decoherence, and its creation requires a special, highly nonlinear MZI that, at the time of this writing, is not readily available.⁹

5.2 Quantum Delayed Choice

However, assuming a system prepared in the state

$$\varrho(-\infty) = \frac{1}{\sum_{\nu \in \mathcal{D}_-} \delta_{M_\nu \sigma}} \sum_{\nu \in \mathcal{D}_-} |\sigma\nu\rangle \langle \sigma\nu| \otimes |\chi\rangle \langle \chi| \quad (100)$$

with σ either equal to $+1$ or to -1 , we can expect (following a similar calculation as in Appendix A) the final state to become approximately equal to

$$\begin{aligned} \tilde{\varrho}(\infty) = & \left[\sum_{\nu} \left(|\tilde{\psi}_{o,\sigma\nu}\rangle |\chi_o\rangle + |\tilde{\psi}_{c,\sigma\nu}\rangle |\chi_c\rangle \right) \left(\langle \tilde{\psi}_{o,\sigma\nu} | \langle \chi_o| + \langle \tilde{\psi}_{c,\sigma\nu} | \langle \chi_c| \right) \right] \\ & \times \left[\sum_{\nu} \left(\langle \tilde{\psi}_{o,\sigma\nu} | \tilde{\psi}_{o,\sigma\nu} \rangle + \langle \tilde{\psi}_{o,\sigma\nu} | \tilde{\psi}_{c,\sigma\nu} \rangle \langle \chi_o | \chi_c \rangle \right. \right. \\ & \left. \left. + \langle \tilde{\psi}_{c,\sigma\nu} | \tilde{\psi}_{o,\sigma\nu} \rangle \langle \chi_c | \chi_o \rangle + \langle \tilde{\psi}_{c,\sigma\nu} | \tilde{\psi}_{c,\sigma\nu} \rangle \right) \right]^{-1}, \quad (101) \end{aligned}$$

where the sums run over $\nu \in \mathcal{D}_-$. With the equivalent of Eq. (62),

$$\|f_{2c}\| T_1[\hat{f}_{2c}](+1\mu, \sigma\nu) = e^{-i\gamma_c} \|f_{1c}\|^N T_N[\hat{f}_{1c}](+1\mu, \sigma\nu) \quad (102)$$

and $\gamma_c = \gamma[\hat{f}_{1c}, \hat{f}_{2c}](+1, \sigma)$ for all $\mu \in \mathcal{D}_+$ and $\nu \in \mathcal{D}_-$, the wavelike state $|\tilde{\psi}_{c,\sigma\nu}\rangle$ becomes

$$\begin{aligned} |\tilde{\psi}_{c,\sigma\nu}\rangle = & 2\|f_{2c}\| \sum_{\mathcal{D}_+} d\mu T_1[\hat{f}_{2c}](+1\mu, \sigma\nu) \\ & \times e^{i\gamma_c/2} \left(\cos \frac{\gamma_c}{2} |+1\mu\rangle - i \sin \frac{\gamma_c}{2} |-1\mu\rangle \right). \quad (103a) \end{aligned}$$

⁹Specifically, an entangled coherent state with a single frequency, ω , is produced by letting laser light interfere with itself in a MZI in which one arm has been replaced with a strong Kerr nonlinearity [117]. Yet another nonlinear optical process is required to transform this state into an entangled coherent states with two frequencies, ω and $N\omega$, as required for $|\chi\rangle$.

For the particle-like state, on the other hand, we arrive at

$$\left| \tilde{\psi}_{o,\sigma\nu} \right\rangle = \|f_{2o}\| \sum_{\mathcal{D}_+} d\mu T_1[\hat{f}_{2o}](-\sigma\mu, \sigma\nu) \frac{1}{\sqrt{2}} (|-\sigma\mu\rangle - e^{i\gamma_o} |\sigma\mu\rangle), \quad (103b)$$

if we impose the requirement that

$$\|f_{2o}\| T_1[\hat{f}_{2o}](-\sigma\mu, \sigma\nu) = -e^{-i\gamma_o} \|f_{1o}\|^N T_N[\hat{f}_{1o}](\sigma\mu, \sigma\nu) \quad (104)$$

with $\gamma_o = \gamma[\hat{f}_{1o}, \hat{f}_{2o}](\sigma)$ for all $\mu \in \mathcal{D}_+$ and $\nu \in \mathcal{D}_-$.

If an experiment succeeded in creating the state $\tilde{\varrho}(\infty)$ of Eq. (101), then, according to quantum theory, the interference property would be physically guaranteed to be random: Eq. (101) describes a *coherent* “blend” [92] or “morphing” [77] between particle- and wavelike output port statistics that is conditioned on the state of the radiation field. Therefore, a measurement of the field allows for a delayed-choice determination of whether the system is in $|\tilde{\psi}_{c,\sigma\nu}\rangle$ or $|\tilde{\psi}_{o,\sigma\nu}\rangle$, thus whether the CCI displays phase control or no control.¹⁰ Such a coherent control experiment would be an example of “quantum delayed-choice” [51, 77–81, 120].

The effect of the coherent control process is reminiscent of “entanglement swapping” [121, 122]. Whereas, initially, the quantum correlations reside exclusively within the field (between coherent states in very different field modes), the CCI redistributes them such that, in the final state (101), quantum entanglement appears instead between the matter and the radiation. The similarity to the entangling swapping protocol means that the quantum delayed choice coherent control scenario relies on quantum entanglement as a resource.

5.3 A Comparison between Quantum Erasure And Quantum Delayed Choice

It is worthwhile to compare these proposed coherent control implementations of quantum erasure and quantum delayed choice. In the following, we list a number of differences and similarities:

- (i) In both cases, the interference property (i.e., phase control or no control) can be prepared after the output port of the CCI has been measured i.e., both approaches implement Wheeler’s delayed choice experiment.
- (ii) The quantum erasure coherent control scenario produces entanglement, whereas the quantum delayed choice coherent control scenario relies on quantum entanglement as a resource. However, this entanglement is not consumed, but is transformed and used to deliver the wave and

¹⁰Note that $|\chi_o\rangle$ and $|\chi_c\rangle$ are not orthogonal, cf. Eq. (99).

the particle property in superposition. In doing so, quantum delayed choice coherent control can demonstrate both complementarity and delayed choice in a fashion that is closer to the spirit of coherent control than it would be possible in a quantum eraser experiment.

- (iii) In the quantum erasure case, it is the choice between two complementary measurements on the light field that decides between phase control or no control. In quantum delayed choice, the choice between these alternative is *random* and dictated by the outcome of the measurement of a *single* observable.¹¹ This is due to the fact that the interference property is set by a quantum switch whose position is unknowable and nondeterministic, a consequence of the fundamental randomness of nature as manifest in quantum theory.
- (iv) Yet, how can a quantum delayed choice coherent control experiment demonstrate that its outcome is fundamentally random? It cannot, that is, not on its own. Like quantum erasure coherent control, quantum delayed choice coherent control alone is insufficient to rigorously certify nonclassicality. For illustration, consider the case in which the amplitudes $\|f_{1o}\|$, $\|f_{2o}\|$, $\|f_{1c}\|$, and $\|f_{2c}\|$ are macroscopic. Then $|\chi_o\rangle$ and $|\chi_c\rangle$ are readily distinguishable. Let us predict the outcome of a joint measurement of the CCI output ports and the population of a selection of modes of the radiation field. If these modes correspond to the closed configuration, i.e., if they are associated with the amplitude functions f_{1c} or f_{2c} , then the detection of one or more photons will be perfectly correlated with wavelike output port statistics and the absence of photons will be perfectly correlated with particle-like output port statistics. One will find that the case that applies is unpredictable. However, an experiment that establishes just that is not able to discriminate the observed statistics against those of the corresponding classical situation: a simple Bernoulli trial (i.e., essentially a coin flip) between the open and the closed CCI configuration. The experiment would not even demonstrate Wheeler's original version of delayed choice, because the statistics of the output port populations could as well have been fully determined from the moment of the field's creation, without any change to the results.

The last item on this list illustrates that, for a valid, credible, and meaningful demonstration of nonclassicality, and from a foundational perspective, *it is generally insufficient to acknowledge that observations are consistent with*

¹¹As originally discussed in Ref. 77, this result is at variance with Bohr's original view on complementarity, according to which the wave and the particle property manifest themselves only in complementary measurements corresponding to complementary experiments. In quantum delayed choice, however, both properties can be observed by measuring a single observable in a single experiment. The authors of Ref. 77 therefore propose to revise the phrasing of the principle and speak of complementarity of experimental data rather than complementary experiments.

quantum theory. Rather, it is necessary to show that they are inconsistent with all classical descriptions. The next section deals with this issue.

6 Towards Rigorous Experimental Certification of The Nonclassicality of Coherent Phase Control

The above discussion makes clear that neither the quantum erasure nor the quantum delayed choice scenario (Secs. 4 and 5, respectively) are stringent enough to ensure truly nonclassical control scenarios. In this section, we show how the nonclassicality of these scenarios can be certified, i.e., we clarify to what extent classical explanations of the experimental observations can be excluded. This is the final step in demonstrating quantum coherent control.

Such a certification of nonclassicality and related problems are of course not new. Rather, these issues have led to major advances in understanding the foundations and basic principles of quantum mechanics. Specifically, Bell test experiments have been devised and executed in order to show the untenability of local realism [57, 123–125], and Leggett-Garg test experiments have been performed to refute classical theories combining macrorealism and noninvasive measurability [44, 126–128]. These (and most other) tests assume the existence of classical probability distributions for the measurement statistics, in particular, joint distributions that account for all inquired marginal probabilities, independent of the measurement. From this assumption, constraints on the statistics of certain measurement outcomes can be derived that are usually expressed in terms of an inequality (cf. Bell-CHSH inequalities and Leggett-Garg inequalities), violations of which are then rigorous indicators of nonclassicality (barring loopholes). In these derivations, the formalism of quantum mechanics (or any other nonclassical theory) is nowhere used. This is crucial, because bounds on classical behavior can only be acquired from within classical physics. Moreover, in a discussion about the necessity of nonclassical theories to describe certain aspects of nature, arguments originating from within quantum mechanics (or other nonclassical theories) are not allowed. Nobody who refutes nonclassicality would accept them.

6.1 A Bell Inequality Test for Coherent Control

The ultimate purpose of Bell inequality experiments has been to settle the question of whether nature obeys *local realism*. *Realism* is mentioned at the beginning of Sec. 2; it is the idea that all properties and values of a system exist prior to, and independent of, their measurement. Quantum theory refutes realism, classical physics does not. *Locality*, on the other hand,

refers to the assumption that interaction between spatially distant physical systems is not possible. Although classical and quantum mechanics are local theories, both of them can predict nonlocal correlations that stem from local processes like coupling, interaction, and scattering. If nature satisfied local realism, then two space-like separated measurement events would never be able to influence one another, since a signal heralding the measurement outcome from one event to the other would have to travel faster than the speed of light. Such influence is excluded by special relativity.

Numerous Bell test experiments have been conducted [49, 62–64, 129–132], some with considerable violations of the inequality. Experiments usually implement tests based on the Clauser-Horne-Shimony-Holt (CHSH) inequality [57, 125] that is an extension of Bell’s original inequality. Both inequalities provide bounds for the correlations between measurement outcomes obtained from a bipartite system. The CHSH inequality, in particular, is derived for the case where two observables, each with two possible outcomes, are measured on both subsystems. Here we use this inequality where the first subsystem is the pair of output ports of the CCI and the second subsystem is a collection of relevant modes of the radiation field.

6.2 The Case of Quantum Erasure Coherent Control

For the certification of nonclassicality in the quantum erasure coherent control scenario of Sec. 4.2, we propose the following CHSH inequality:

$$|\langle B \rangle| = |\langle O_{\mathcal{M}} \otimes O_{\mathcal{R}} \rangle + \langle O'_{\mathcal{M}} \otimes O_{\mathcal{R}} \rangle + \langle O_{\mathcal{M}} \otimes O'_{\mathcal{R}} \rangle - \langle O'_{\mathcal{M}} \otimes O'_{\mathcal{R}} \rangle| \leq 2, \quad (105)$$

where we introduced the Bell operator B and the four dichotomous observables $O_{\mathcal{M}}$, $O'_{\mathcal{M}}$, $O_{\mathcal{R}}$, and $O'_{\mathcal{R}}$, defined below. One can then easily verify that the inequality (105) holds for classical physics. If we denote $o_{\mathcal{M}}$, $o'_{\mathcal{M}}$, $o_{\mathcal{R}}$, and $o'_{\mathcal{R}}$ the possible outcomes (± 1) of the observables of the Bell operator, then clearly $-2 \leq o_{\mathcal{M}}o_{\mathcal{R}} + o'_{\mathcal{M}}o_{\mathcal{R}} + o_{\mathcal{M}}o'_{\mathcal{R}} - o'_{\mathcal{M}}o'_{\mathcal{R}} \leq 2$. However, in quantum mechanics, the largest possible expectation value of a Bell-CHSH operator is the Tsirelson bound, $2\sqrt{2}$ [133, 134]. We shall see that, in quantum erasure coherent control, the inequality (105) can be violated and even equality, $|\langle B \rangle| = 2\sqrt{2}$, be achieved. In accord with Bell’s theorem, this implies that the physics does not abide by local realism.

Consider now the four observables $O_{\mathcal{M}}$, $O'_{\mathcal{M}}$, $O_{\mathcal{R}}$, and $O'_{\mathcal{R}}$. The first two are sensitive only to the CCI output labels:

$$O_{\mathcal{M}} = \frac{1}{\sqrt{2 - \mathfrak{V}^2}} \left[-\sqrt{1 - \mathfrak{V}^2} \sigma_{\mathcal{M}}^1 - \sin(\phi + \gamma) \sigma_{\mathcal{M}}^2 + \cos(\phi + \gamma) \sigma_{\mathcal{M}}^3 \right], \quad (106a)$$

$$O'_{\mathcal{M}} = \frac{1}{\sqrt{2 - \mathfrak{V}^2}} \left[\sqrt{1 - \mathfrak{V}^2} \sigma_{\mathcal{M}}^1 - \sin(\phi + \gamma) \sigma_{\mathcal{M}}^2 + \cos(\phi + \gamma) \sigma_{\mathcal{M}}^3 \right], \quad (106b)$$

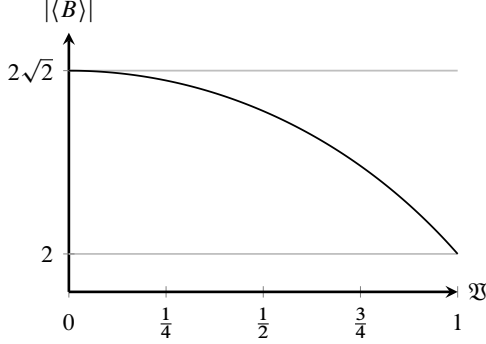


Figure 8: Absolute Bell expectation value $|\langle B \rangle|$ with respect to the state (63) as a function of the visibility \mathfrak{V} . Maximum violation, $|\langle B \rangle| = 2\sqrt{2}$, occurs for $\mathfrak{V} = 0$.

where

$$\sigma_{\mathcal{M}}^1 = \int d\mu (|+1\mu\rangle\langle-1\mu| + |-1\mu\rangle\langle+1\mu|), \quad (107a)$$

$$\sigma_{\mathcal{M}}^2 = \int d\mu (-i|+1\mu\rangle\langle-1\mu| + i|-1\mu\rangle\langle+1\mu|), \quad (107b)$$

$$\sigma_{\mathcal{M}}^3 = M = \int d\mu (|+1\mu\rangle\langle+1\mu| - |-1\mu\rangle\langle-1\mu|) \quad (107c)$$

are Hermitian, unitary pseudospin operators (the equivalents of the Pauli spin matrices). The visibility \mathfrak{V} is the same as in Eq. (64b) (page 35), and the phases ϕ and γ are defined in Eqs. (51) and (62) (pages 29 and 35, respectively). The second two observables are sensitive only to the radiation:

$$O_{\mathcal{R}} = \frac{1}{\sqrt{1-\mathfrak{V}^2}} \left(\frac{|\tilde{\chi}^N\rangle\langle\tilde{\chi}^N|}{\langle\tilde{\chi}^N|\tilde{\chi}^N\rangle} - \frac{|\tilde{\chi}^1\rangle\langle\tilde{\chi}^1|}{\langle\tilde{\chi}^1|\tilde{\chi}^1\rangle} \right) \quad (108a)$$

and

$$O'_{\mathcal{R}} = |+\mathcal{R}\rangle\langle+\mathcal{R}| - |-\mathcal{R}\rangle\langle-\mathcal{R}|, \quad (108b)$$

where $|\pm\mathcal{R}\rangle$ are the orthonormal radiative states derived in Sec. 4.2 [cf. Eq. (66c)]. With these operators and the final state $\bar{\rho}(\infty)$ of the quantum erasure coherent control scenario given in Eq. (63), we have

$$|\langle B \rangle| = |\text{Tr}[B\bar{\rho}(\infty)]| = 2\sqrt{2-\mathfrak{V}^2}, \quad (109)$$

see Fig. 8. Clearly $|\langle B \rangle|$ reaches the Tsirelson bound $2\sqrt{2}$ for vanishing visibility, i.e., $\mathfrak{V} = 0$, a result that is impossible classically.

Several points are worth noting. First, the field observables Eq. (108) are known from Sec. 4.2. In particular, $O_{\mathcal{R}}$ is an optimal observable for a welcher-weg measurement [cp. Eq. (68)], whereas $O'_{\mathcal{R}}$ is optimal for

quantum erasure [cp. Eq. (71)]. In this sense, $O_{\mathcal{R}}$ and $O'_{\mathcal{R}}$ are maximally complementary. Second, although there is an intimate relation, testing the Bell inequality (105) is *not* the same as combining the results from an optimum welcher-weg measurement and from quantum erasure. For a proper Bell test, the field observables have to be joint in a particular way with material observables, e.g. $O_{\mathcal{M}}$ and $O'_{\mathcal{M}}$ from above, that are different from M and also probe coherences between the CCI output ports. Third, the maximum Bell violation is achieved for vanishing visibility, $\mathfrak{V} = 0$, which, according to the discussion in Sec. 4.2, is equivalent to a maximum of radiative distinguishability $\mathfrak{D}_{\mathcal{R}}$ and a maximum of quantum entanglement \mathfrak{c} .¹² This is in agreement with the fact that all states with maximum Bell violation are the equivalent of a direct sum of maximally quantum entangled singlet states [135]. Finally, due to the presence of coherences between $|\tilde{\chi}^1\rangle$ and $|\tilde{\chi}^N\rangle$, a measurement of the field observable $O'_{\mathcal{R}}$ may not be possible. Therefore, in a manner similar to what is done in Sec. 4.3, one could instead consider another set of operators that substitute $O_{\mathcal{R}}$ and $O'_{\mathcal{R}}$ and that are given in terms of displaced photon threshold measurement observables. We leave this as an exercise to the interested reader.

6.3 The Case of Quantum Delayed Choice Coherent Control

Consider now the quantum delayed choice coherent control scenario introduced in Sec. 5.2. As in the case of quantum erasure coherent control above, we propose a Bell-CHSH inequality test for certifying nonclassicality. The Bell operator B is, however, different from that used in the previous section; it needs to be adapted to the physical situation described by the state (101). We restrict attention, as an example, to a special case where particle-like and wavelike statistics occur with equal probabilities, i.e. we add the requirement that

$$2\|f_{2c}\| T_1[\hat{f}_{2c}](+1\mu, \sigma\nu) = e^{i\kappa} \|f_{2o}\| T_1[\hat{f}_{2o}](-\sigma\mu, \sigma\nu) \quad (110)$$

with $\kappa = \kappa[\hat{f}_{2o}, \hat{f}_{2c}](\sigma)$ for all $\mu \in \mathcal{D}_+$ and $\nu \in \mathcal{D}_-$. Further, we fix the relationship between the relative phases of the transition amplitudes by setting

$$\gamma_o = -\phi - \frac{\pi}{2}, \quad \sigma = -1, \quad (111)$$

$$\gamma_c = \phi, \quad \kappa = -2\phi - \pi, \quad (112)$$

independently of $\nu \in \mathcal{D}_-$. Here, the new free phase parameter ϕ replaces all other phase parameters, and the input port has been set to -1 . With

¹²Recall that, for $\mathfrak{V} = 0$, the final states of the radiation field, $|\tilde{\chi}^1\rangle$ and $|\tilde{\chi}^N\rangle$, are orthogonal and thus fully distinguishable.

these assumptions, the state (101) becomes

$$\begin{aligned} \tilde{\rho}(\infty) &= \left(\|f_{2o}\|^2 \int_{\mathcal{D}_+} d\mu \sum_{\nu \in \mathcal{D}_-} |T_1[\hat{f}_{2o}](+1\mu, -1\nu)|^2 \right)^{-1} \\ &\times \sum_{\nu \in \mathcal{D}_-} \frac{\left(|\tilde{\psi}_{o,-1\nu}\rangle|\chi_o\rangle + |\tilde{\psi}_{c,-1\nu}\rangle|\chi_c\rangle \right) \left(\langle\tilde{\psi}_{o,-1\nu}| \langle\chi_o| + \langle\tilde{\psi}_{c,-1\nu}| \langle\chi_c| \right)}{2 - \frac{1}{\sqrt{2}} \langle\chi_o|\chi_c\rangle [\cos\phi + \cos(2\phi) - \sin\phi]}, \end{aligned} \quad (113)$$

where

$$|\tilde{\psi}_{o,-1\nu}\rangle = \|f_{2o}\| \int_{\mathcal{D}_+} d\mu T_1[\hat{f}_{2o}](+1\mu, -1\nu) \frac{1}{\sqrt{2}} \left(|+1\mu\rangle + ie^{-i\phi}|-1\mu\rangle \right) \quad (114a)$$

and

$$\begin{aligned} |\tilde{\psi}_{c,-1\nu}\rangle &= \|f_{2o}\| \int_{\mathcal{D}_+} d\mu T_1[\hat{f}_{2o}](+1\mu, -1\nu) \\ &\times e^{-3i\phi/2} \left(-\cos\frac{\phi}{2} |+1\mu\rangle + i\sin\frac{\phi}{2} |-1\mu\rangle \right) \end{aligned} \quad (114b)$$

are the particle-like and the wavelike CCI state, respectively. The overlap $\langle\chi_o|\chi_c\rangle$ is real and the same as in Eq. (99).

Since most phases and interferometer imbalances have been eliminated, the only remaining variables are the overlap $\langle\chi_o|\chi_c\rangle$ and the phase ϕ that, unless stated otherwise, are treated below as arbitrary and controllable.¹³ Since there is no single Bell test that would be applicable to all settings of these two variables. One has to construct a family of Bell tests that take these settings into account. This can be done using a method similar to that outlined in Ref. 108. Due to the complexity of the expressions, we only give the result for $\langle B \rangle$ with respect to the state (113):

$$\langle B \rangle = 2 \sqrt{1 + \frac{(1 - \langle\chi_o|\chi_c\rangle^2)[2 + \sin(2\phi)]}{\left\{ 2 - \frac{1}{\sqrt{2}} \langle\chi_o|\chi_c\rangle [\cos\phi + \cos(2\phi) - \sin\phi] \right\}^2}}. \quad (115)$$

This expression is plotted in Fig. 9(a). The expectation value is seen to be larger than 2 for all $\langle\chi_o|\chi_c\rangle < 1$. In other words, Bell tests can be found and violated for practically all relevant values of ϕ and $\langle\chi_o|\chi_c\rangle$. Moreover, $\langle B \rangle$

¹³The overlap $\langle\chi_o|\chi_c\rangle$ is always between 0 and 1, since, as we explain in what follows, the bounds of that interval are not achievable practically. On the one hand, the value 0 is not physical. Since it would imply an infinite population of the field. For macroscopic populations, $\langle\chi_o|\chi_c\rangle$ can, however, come indistinguishably close to 0. The value 1, on the other hand, is equivalent to the absence of all incoming light, where there would be no dynamics, no coherent control, and nothing to measure.

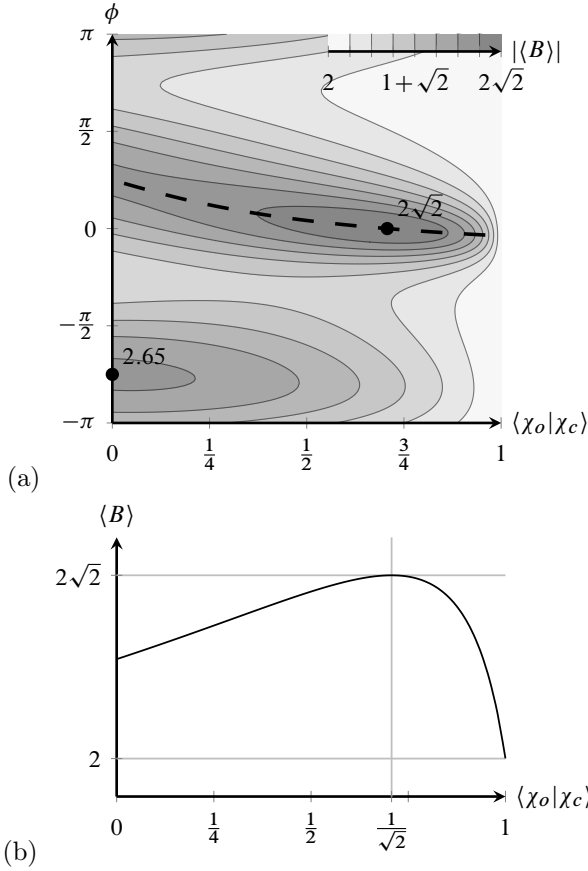


Figure 9: (a) Contour plot of the absolute Bell expectation value $|\langle B \rangle|$ with respect to the state (113) [from Eq. (115)] as a function of the phase ϕ and the overlap $\langle \chi_o | \chi_c \rangle$. Higher values have a darker shade (see scale in upper right corner). The dashed black line is the position of the global maximum of $|\langle B \rangle|$ with respect to ϕ , but for fixed $\langle \chi_o | \chi_c \rangle$. This shows how, for given $\langle \chi_o | \chi_c \rangle$, one would have to choose ϕ to achieve the highest possible Bell violation. Local maxima are labeled and indicated with a dot. Especially noteworthy is the saturation of the Bell violation at the Tsirelson bound $2\sqrt{2}$ for $\phi = 0$ and $\langle \chi_o | \chi_c \rangle = 1/\sqrt{2}$. (b) Plot of Eq. (118), which is a cut through panel (a) at $\phi = 0$.

can reach the global maximum Tsirelson bound of $2\sqrt{2}$, for the particular pair of values: $\phi = 0$ and $\langle \chi_o | \chi_c \rangle = 1/\sqrt{2}$. The latter value corresponds to a minuscule field amplitude with a significant population of the vacuum mode.

In the following, we explore the neighborhood of the global maximum of $\langle B \rangle$ and identify the specific Bell test that gives rise to it. We expect that, in an experiment, ϕ can be controlled better than $\langle \chi_o | \chi_c \rangle$. Therefore, we fix ϕ at 0 below and derive a Bell operator family that adapts to any given value of $\langle \chi_o | \chi_c \rangle$. As in Sec. 6.2, each Bell operator B is comprised of four dichotomous observables, two of which are sensitive to the matter \mathcal{M} and two to the radiation \mathcal{R} . They are:

$$O_{\mathcal{M}} = \frac{1}{\sqrt{6 - 4\sqrt{2}\langle \chi_o | \chi_c \rangle}} \left[\left(-\sqrt{2} + \langle \chi_o | \chi_c \rangle - \sqrt{1 - \langle \chi_o | \chi_c \rangle^2} \right) \sigma_{\mathcal{M}}^2 + \left(-\sqrt{2} + \langle \chi_o | \chi_c \rangle + \sqrt{1 - \langle \chi_o | \chi_c \rangle^2} \right) \sigma_{\mathcal{M}}^3 \right], \quad (116a)$$

$$O'_{\mathcal{M}} = \frac{1}{\sqrt{6 - 4\sqrt{2}\langle \chi_o | \chi_c \rangle}} \left[\left(-\sqrt{2} + \langle \chi_o | \chi_c \rangle + \sqrt{1 - \langle \chi_o | \chi_c \rangle^2} \right) \sigma_{\mathcal{M}}^2 + \left(-\sqrt{2} + \langle \chi_o | \chi_c \rangle - \sqrt{1 - \langle \chi_o | \chi_c \rangle^2} \right) \sigma_{\mathcal{M}}^3 \right], \quad (116b)$$

with $\sigma_{\mathcal{M}}^2, \sigma_{\mathcal{M}}^3$ from Eqs. (107), and

$$O_{\mathcal{R}} = \frac{1}{1 - \langle \chi_o | \chi_c \rangle^2} [-\langle \chi_o | \chi_c \rangle (|\chi_c\rangle\langle \chi_c| + |\chi_o\rangle\langle \chi_o|) + |\chi_c\rangle\langle \chi_o| + |\chi_o\rangle\langle \chi_c|], \quad (117a)$$

$$O'_{\mathcal{R}} = \frac{1}{\sqrt{1 - \langle \chi_o | \chi_c \rangle^2}} (|\chi_c\rangle\langle \chi_c| - |\chi_o\rangle\langle \chi_o|). \quad (117b)$$

The expectation value of the Bell operator $B = O_{\mathcal{M}} \otimes O_{\mathcal{R}} + O'_{\mathcal{M}} \otimes O_{\mathcal{R}} + O_{\mathcal{M}} \otimes O'_{\mathcal{R}} - O'_{\mathcal{M}} \otimes O'_{\mathcal{R}}$ with respect to the state (113) with $\phi = 0$ is

$$\langle B \rangle = \frac{2\sqrt{6 - 4\sqrt{2}\langle \chi_o | \chi_c \rangle}}{2 - \sqrt{2}\langle \chi_o | \chi_c \rangle}. \quad (118)$$

A plot of that is shown in Fig. 9(b). At the maximum, where $\langle B \rangle = 2\sqrt{2}$, i.e., at $\langle \chi_o | \chi_c \rangle = 1/\sqrt{2}$, the material observables become particularly simple. They are $O_{\mathcal{M}} = -\sigma_{\mathcal{M}}^2$ and $O'_{\mathcal{M}} = -\sigma_{\mathcal{M}}^3 = -M$.

As before, measuring the observables $O_{\mathcal{R}}$ and $O'_{\mathcal{R}}$ pose a serious experimental challenge. Therefore, a switch to displaced photon measurements of a kind similar to what was discussed in Sec. 4.3 may be necessary. See Ref. 136 for further information.

7 Application To Photoelectron Spin Polarization Control in Alkali Photoionization

Here, we apply this formalism to a specific example used throughout the remainder of the article, phase-coherent control of the spin polarization of an electron emitted in an 1 vs. 2 photoionization process from a heavy alkali atom [136]. This control scenario is an extension of Elliott's two-color photoionization experiments on alkali atoms [14, 15, 32, 33], which demonstrated that the angular distribution of an emitted photoelectron can be controlled by the relative phase between two ionizing laser beams. The sensitivity to phase was attributed to quantum interference between competing ionization processes. However, as discussed in Sec. 1, phase sensitivity by itself does not suffice to guarantee quantum interference.

The control scenario below deviates from the original experiment in two ways: (i) the control target is the polarization of the spin of the emitted photoelectron, rather than its angular distribution. Hence, the binary alternatives of the electron's spin- $\frac{1}{2}$ allow for a straightforward definition of the dichotomous observable M , and (ii) the framework of the controlherent control interferometer (CCI) allows us to demonstrate true quantum features. For this section, the goal is to show that the spin polarization control example can implement a CCI as defined in Sec. 2. Hence, although some of the details of this example are well known, casting the problem as a CCI immediately allows us to apply all the results in Sec. 2 to this scenario.

7.1 A Model for The Material Degrees of Freedom

Below we introduce a simple photoionization model for the alkali atom. Note first, that in the weak-field limit, the scattering recoil of the atom will be small, so if the atom is tightly confined [137, 138], then we can neglect its motional degrees of freedom which would otherwise result in distinguishable pathways. Further we can neglect all but the outermost electron of the atom. The atomic Hamiltonian, hence, reduces to an effective single-electron Hamiltonian with bound and continuum contributions:

$$H_{\mathcal{M}} = \sum_{nljm_j} E_{nlj} |nljm_j\rangle\langle nljm_j| + \int_0^{\infty} dE E \sum_{ljm_j} |Eljm_j^+\rangle\langle Eljm_j^+|, \quad (119)$$

where the states are described by the principle quantum number (n), the orbital (l) and the total angular momenta (j), and the projection (m_j) of the total angular momentum onto the quantization axis, chosen as the laboratory's \hat{z} -axis below. The bound eigenstates $|nljm_j\rangle$ are hydrogen-like, with energies E_{nlj} that depend on l and j due to spin-orbit coupling. The bound state sum in Eq. (119), begins at the electron's ground state which, for alkali metals, is spin- $\frac{1}{2}$ and is denoted $|n0\frac{1}{2}m_j\rangle$, where n equals the

metal's atomic number. Using Clebsch-Gordan coefficients, we can expand the bound eigenstates in the position basis:

$$\langle \mathbf{X} | n l j m_j \rangle = \sum_{m_l m_s} \langle l m_l \frac{1}{2} m_s | j m_j \rangle R_{nlj}(X) Y_{l m_l}(\hat{\mathbf{X}}) | m_s \rangle. \quad (120)$$

Here, R_{nlj} denotes a solution of the radial Schrödinger equation, $Y_{l m_l}$ is a spherical harmonic, m_l is the \hat{z} -axis projection of the orbital angular momentum, and $| m_s \rangle$ describes the electron spin, also in \hat{z} direction. The continuum states are, to good approximation, the asymptotic scattering out-states of energy E in the partial wave expansion for a screened Coulomb potential [89, 139]. In this article, we use two different, but equivalent sets of continuum states, $| E l j m_j^+ \rangle$ and

$$| \mathbf{K} m_s^+ \rangle = \frac{\hbar}{\sqrt{m_e K}} \sum_{l m_l} Y_{l m_l}(\hat{\mathbf{K}}) \sum_{j m_j} \langle l m_l \frac{1}{2} m_s | j m_j \rangle | E(K) l j m_j^+ \rangle. \quad (121)$$

The latter states are eigenstates of $H_{\mathcal{M}}$ with energy $E(K) = \hbar^2 K^2 / 2m_e$. Here \mathbf{K} is the electron's asymptotic outgoing wavevector, $\hat{\mathbf{K}}$ its direction and K its length. An expansion analogous to Eq. (120) also exists for the continuum wave functions $\langle \mathbf{X} | E l j m_j^+ \rangle$. For an alkali atom, the radial part in that expansion can be taken as a Coulomb function that obeys

$$R_{Elj}(X) \underset{X \rightarrow \infty}{\sim} i^l e^{i\varpi_{Klj}} \sqrt{\frac{2m}{\pi \hbar^2 K}} \times \frac{1}{X} \sin \left[KX + \frac{1}{K} \ln(2KX) - \frac{1}{2} l \pi + \varpi_{Klj} + \delta_K \right], \quad (122)$$

where ϖ_{Klj} is the partial wave Coulomb phase shift and δ_K is the quantum defect.

7.2 The Proposed Experiment

Consider then the setup for the experiment, and the associated implementation of the CCI. We assume an ideal, spherically shaped electron detector centered around the atom, all in the vacuum. The detector is large and can measure both the electron position on the surface, and its spin polarization with respect to a constant global axis. The atom is initially in its ground state, in an incoherent mixture of spin up and down,

$$\varrho_{\mathcal{M}}(-\infty) = \sum_{m_j} p_{m_j} | n 0 \frac{1}{2} m_j \rangle \langle n 0 \frac{1}{2} m_j |. \quad (123)$$

It is ionized with a pair of weak light pulses with $\varrho_{\mathcal{R}}(-\infty) = |\chi\rangle \langle \chi|$, whereupon a photoelectron is emitted. The outgoing matter and light waves are described by the final state $\varrho(\infty)$.

The control target defines the input and output ports of the CCI as the electron's spin polarization. The input ports are thus associated with the spin polarization m_j of the electronic ground state $|n0\frac{1}{2}m_j\rangle$, and the output ports are identified with the spin projection m_s of the outgoing matter wave $|\mathbf{K}m_s^+\rangle$. Hence, the material observable M is defined as

$$M = \sum_{nlm_l m_s} 2m_s |nlm_l m_s\rangle \langle nlm_l m_s| + \int d\mathbf{K} \sum_{m_s} 2m_s |\mathbf{K}m_s^+\rangle \langle \mathbf{K}m_s^+|, \quad (124)$$

where the factor of 2 ensures that M has the eigenvalues $+1$ and -1 .¹⁴

The incoming light is quasi-monochromatic around frequencies 2ω and ω , and the detection is limited to photoelectrons with kinetic energy $E(K) \approx E_- + 2\hbar\omega$, where $E_- = E_{n0\frac{1}{2}}$, hence \mathcal{D}_- is a region in \mathbf{K} -space clustered around $E(K)$. We make further adjustments to \mathcal{D}_+ below.

Using the approach in Sec. 2.1, we project the total density operator of electron and radiation onto \mathcal{D}_+ to obtain:

$$\begin{aligned} \tilde{\rho}(\infty) = \tilde{p}^{-1} \sum_{m_s, m'_s = \pm\frac{1}{2}} \sum_{m_j = \pm\frac{1}{2}} p_{m_j} & \left(|\tilde{\psi}_{m_s, m_j}^1\rangle |\tilde{\chi}^1\rangle + |\tilde{\psi}_{m_s, m_j}^2\rangle |\tilde{\chi}^2\rangle \right) \\ & \times \left(\langle \tilde{\psi}_{m'_s, m_j}^1 | \langle \tilde{\chi}^1 | + \langle \tilde{\psi}_{m'_s, m_j}^2 | \langle \tilde{\chi}^2 | \right) \end{aligned} \quad (125)$$

with \tilde{p} the normalization. The ket

$$|\tilde{\psi}_{m_s, m_j}^1\rangle = \int_{\mathcal{D}_+} d\mathbf{K} T_1 [f_2](\mathbf{K}m_s, m_j) |\mathbf{K}m_s^+\rangle, \quad (126)$$

is the final scattering state of a single ionization event, and $|\tilde{\psi}_{m_s, m_j}^2\rangle$ is an analogous expression for the final state of a two-photon photon ionization event. Note that these states are defined in terms of the one- and two-photon scattering probability amplitudes, T_1 and T_2 . For monochromatic cw light, these amplitudes are well known [32, 33]. However, here we deal with quasi-monochromatic light pulses. The approach in Sec. 2.1, specifically

¹⁴Since M need not be sensitive to anything but the electron's spin, we assemble M 's point spectrum [the first term in Eq. (124)] from the spin-orbit product states $|nlm_l m_s\rangle$. In alkali metals, the electron's spin and orbit are strongly coupled, and these states are in general not eigenstates of the Hamiltonian $H_{\mathcal{M}}$. This is in violation of the provisions of Sec. 2.2, according to which M and $H_{\mathcal{M}}$ are required to commute. However, this will not be an issue below, since the properties of M matter only with respect to the initial and the final states in the scattering problem. There is no issue with respect to \mathcal{D}_+ , since M is diagonal in all continuum states of $H_{\mathcal{M}}$, including those in \mathcal{D}_+ . We only have to concern ourselves with \mathcal{D}_- . The set \mathcal{D}_- represents the ground state for which spin-orbit coupling is absent. Therefore, the state $|n0\frac{1}{2}m_j\rangle$ is identical to the spin-orbit product state $|n00m_s\rangle$ with $m_s = m_j$. Hence, M is also diagonal with respect to all states in \mathcal{D}_- .

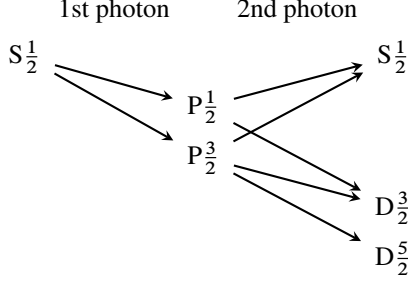


Figure 10: Electric dipole selection rules between lj -states in one- and two-photon absorption. These two processes are distinguishable by the final orbital angular momenta, in particular, the separation into states with even (S, D) and those with odd parity (P).

Eq. (27a), gives

$$\begin{aligned}
 T_1[\hat{f}_2](\mathbf{K}m_s, m_j) &= 2\pi i \int d\mathbf{k} \sum_{\lambda} \delta[E_- - E(K) + \hbar\omega(k)] \hat{f}_2(\mathbf{k}, \lambda) \\
 &\times (-i)\hbar\mathcal{E}(k) \frac{\hbar}{\sqrt{m_e K}} \sum_{m'_l} Y_{1m'_l}(\hat{\mathbf{K}}) \sum_{j'm'_j} \langle 1m'_l \frac{1}{2}m_s | j'm'_j \rangle \\
 &\times A_1[1j'm'_j, 0\frac{1}{2}m_j; \hat{\mathbf{e}}(\mathbf{k}, \lambda)] D_1[E(K)1j', n0\frac{1}{2}], \quad (127)
 \end{aligned}$$

where

$$\begin{aligned}
 A_1(l'j'm'_j, lj m_j; \hat{\mathbf{e}}) &= \sqrt{\frac{2l+1}{2l'+1}} \langle l0 10 | l'0 \rangle \sum_{m_l m'_l} \sum_{q=-1}^1 \varepsilon_q \langle lm_l 1q | l'm'_l \rangle \\
 &\times \sum_{m_s} \langle l'm'_l \frac{1}{2}m_s | j'm'_j \rangle \langle lm_l \frac{1}{2}m_s | j m_j \rangle, \quad (128a)
 \end{aligned}$$

is the first-order angular dipole matrix element and

$$D_1(E'l'j', nlj) = e \int_0^{\infty} dx x^3 R_{E'l'j'}^*(x) R_{nlj}(x) \quad (128b)$$

is the first-order radial integral [140, 141]. The D_1 integrals, not explicitly calculated here, serve as empirical parameters below.

Figure 10 illustrates the selection rules for the single-photon transition, which are enforced by A_1 , i.e., T_1 only connects the ground state to P continuum states with $l' = 1$. Moreover, A_1 determines the contributions of σ ($\Delta m_j = \pm 1$) and π transitions ($\Delta m_j = 0$) to the transition amplitude.

These primarily depend on the projections $\varepsilon_q = \hat{\varepsilon} \cdot \hat{e}_q^*$ of the field polarization $\hat{\varepsilon}$ onto the spherical basis vectors $\hat{e}_{\pm 1} = \mp(\hat{x} \pm i\hat{y})/\sqrt{2}$, $\hat{e}_0 = \hat{z}$. Figure 10 also shows the selection rules for the two-photon process (only partial waves with $l' = 0$ or 2 contribute) arising from the second-order angular dipole matrix element

$$A_2(l'j'm'_j, l''j'', ljm_j; \hat{\varepsilon}, \hat{\varepsilon}') = \sum_{m''_j} A_1(l'j'm'_j, l''j''m''_j; \hat{\varepsilon}) \times A_1(l''j''m''_j, ljm_j; \hat{\varepsilon}'), \quad (129a)$$

that, together with the second-order radial integral

$$D_2(E'l'j', l''j'', nlj; k) = \sum_{n''} \frac{D_1(E'l'j', n''l''j'')D_1(n''l''j'', nlj)}{E_{nlj} - E_{n''l''j''} + \hbar ck + i0} + \int_0^\infty dE'' \frac{D_1(E'l'j', E''l''j'')D_1(E''l''j'', nlj)}{E_{nlj} - E'' + \hbar ck + i0}, \quad (129b)$$

enters the two-photon transition amplitude

$$\begin{aligned} T_2[\hat{f}_1](\mathbf{K}m_s, m_j) &= -2\pi i \\ &\times \int d\mathbf{k}_1 \sum_{\lambda_1} \int d\mathbf{k}_2 \sum_{\lambda_2} \delta[E_- - E(K) + \sum_{i=1}^2 \hbar\omega(k_i)] \\ &\times \hat{f}_1(\mathbf{k}_1, \lambda_1) (-i)\hbar\mathcal{E}(k_1) \hat{f}_1(\mathbf{k}_2, \lambda_2) (-i)\hbar\mathcal{E}(k_2) \frac{\hbar}{\sqrt{m_e K}} \sum_{l'm'_l} Y_{l'm'_l}(\hat{\mathbf{K}}) \\ &\times \sum_{j'm'_j} \langle l'm'_l \frac{1}{2}m_s | j'm'_j \rangle \sum_{j''} A_2[l'j'm'_j, 1j'', 0\frac{1}{2}m_j; \hat{\varepsilon}(\mathbf{k}_1, \lambda_1), \hat{\varepsilon}(\mathbf{k}_2, \lambda_2)] \\ &\times D_2[E(K)l'j', 1j'', n0\frac{1}{2}; k_2]. \quad (130) \end{aligned}$$

These expressions were derived from Eq. (27b), and the arguments of A_2 and D_2 refer to the particular photoionization channels. For example, $D_2[E(K)2\frac{5}{2}, 1\frac{3}{2}, n0\frac{1}{2}]$ is the radial matrix element leading from the $S\frac{1}{2}$ ground state $|n0\frac{1}{2}m_j\rangle$ via intermediate $P\frac{3}{2}$ orbitals to the $D\frac{5}{2}$ continuum state $|E(K)D\frac{5}{2}m'_j\rangle$.

Since the states accessed by the two ionization pathways are of different parity and angular momentum, the outgoing matter wave is a welcher-weg marker that, in principle, allows one to acquire absolute path knowledge. As discussed in Sec. 4.1, this situation excludes phase control completely. This can be rectified by rendering the path knowledge physically inaccessible, i.e., by quantum erasure. This procedure is applied below to obtain phase control.

The welcher-weg information is encoded in the matter angular distribution. Hence, the measurement of M has to be combined with a measurement

of an observable that is sensitive to the electron's angular spread. However, the observable has to be such that the ionization pathways are indistinguishable in at least one of its eigenspaces. The simplest (though not optimal) observable fulfilling this requirement corresponds to a single segment of the spherically shaped detector, chosen so that, if it detects an electron, there is no way of telling whether its matter wave had even or odd parity (i.e., whether the electron was emitted in a single- or a two-photon process).

Effectively, with this prescription, the measurement is restricted to a narrow solid angle around a single direction, denoted $\hat{\mathbf{K}}_+$. Consequently, \mathcal{D}_+ is confined in both energy and direction $\hat{\mathbf{K}}$. We define $\hat{\mathbf{K}}_+ = \mathbf{K}_+/K_+$ with $\mathbf{K}_+ = |\mathcal{D}_+|^{-1} \int_{\mathcal{D}_+} d\mathbf{K} \mathbf{K}$, the average of \mathbf{K} over \mathcal{D}_+ , $K_+ = \|\mathbf{K}_+\|$ its length, and $|\mathcal{D}_+| = \int_{\mathcal{D}_+} d\mathbf{K}$, the volume of \mathcal{D}_+ . That is, we achieve quantum erasure by measuring the differential cross section.

The states $|\tilde{\psi}_{m_s, m_j}^1\rangle$ and $|\tilde{\psi}_{m_s, m_j}^2\rangle$ depend on the size and shape of \mathcal{D}_+ , but given the narrow confinement of \mathcal{D}_+ , it is justified to assume that T_1 and T_2 vary weakly over \mathcal{D}_+ . Hence, T_1 and T_2 are evaluated at \mathbf{K}_+ instead of \mathbf{K} , i.e., we approximate

$$|\tilde{\psi}_{m_s, m_j}^1\rangle \simeq T_1[\hat{f}_2](\mathbf{K}_+ m_s, m_j) \int_{\mathcal{D}_+} d\mathbf{K} |\mathbf{K} m_s^+\rangle \quad (131a)$$

and

$$|\tilde{\psi}_{m_s, m_j}^2\rangle \simeq T_2[\hat{f}_1](\mathbf{K}_+ m_s, m_j) \int_{\mathcal{D}_+} d\mathbf{K} |\mathbf{K} m_s^+\rangle. \quad (131b)$$

7.3 Implementation of The Open And The Closed CCI Configurations

Below we show how to implement the open and the closed configuration with the photoelectron spin CCI. These configurations are needed for the quantum erasure and the quantum delayed choice coherent control experiments described above.

Consider first the open CCI. As explained in Sec. 3.1, the open configuration is maximally biased. This is reflected in the following prescription: if the atom's initial state is spin up (or down), then a photoelectron emitted in single-photon ionization has to arrive at the detector with spin down (up), and a photoelectron emitted in double-photon ionization must arrive with spin up (down). That is:

$$T_1[\hat{f}_{2o}](\mathbf{K}_+ m_s, m_j) \propto \delta_{m_s, -m_j}, \quad (132a)$$

$$T_2[\hat{f}_{1o}](\mathbf{K}_+ m_s, m_j) \propto \delta_{m_s, m_j}, \quad (132b)$$

i.e., Eqs. (36) applied to the photoelectron spin control scenario. In addition,

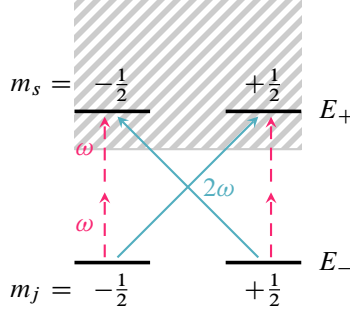


Figure 11: (color online) In the open configuration o , single-photon ionization (solid blue) only undergoes a σ -transition with $|m_j - m'_s| = 1$, whereas two-photon ionization (dashed red) leaves the electronic spin unchanged. The processes are distinguishable from one another due to their different outcomes.

we stipulate the symmetry condition

$$\sqrt{\langle \tilde{\chi}_o^1 | \tilde{\chi}_o^1 \rangle} |T_1[\hat{f}_{2o}](\mathbf{K}_+ - m_j, m_j)| = \sqrt{\langle \tilde{\chi}_o^2 | \tilde{\chi}_o^2 \rangle} |T_2[\hat{f}_{1o}](\mathbf{K}_+ m_j, m_j)| \quad (133)$$

adapted from Eq. (47). With Eq. (133), the single- and the double-photon process have equal *a priori* probabilities.

In the following, we specify suitable parameters that allow T_1 and T_2 to fulfill the conditions (132) and (133), the direction $\hat{\mathbf{K}}_+$ pointing to the detector, the wavepackets' directions of incidence, and the wavepackets' polarizations. Wavepacket properties are described by the amplitude functions f_{1o}, f_{2o} .

For the direction of detection, we choose

$$\hat{\mathbf{K}}_+ = \frac{1}{\sqrt{3}}(\sqrt{2}\hat{\mathbf{x}} - \hat{\mathbf{z}}), \quad (134)$$

a choice that will work for both open and closed configurations.

With regard to the wavepackets, we concentrate on the simplifying case where the amplitude functions cluster around a single direction of incidence ($\hat{\mathbf{k}}_{1o}$ and $\hat{\mathbf{k}}_{2o}$, respectively) and a single polarization ($\hat{\mathbf{e}}_{1o}, \hat{\mathbf{e}}_{2o}$). In such a case, we can approximate

$$f_{2o}(\mathbf{k}, \lambda) \simeq \alpha_{2o} \sqrt{\ell_{2o}^{-3} u_{2o}[\ell_{2o}^{-1}(\mathbf{k} - \mathbf{k}_{2o})]} \hat{\mathbf{e}}_{2o} \cdot \hat{\mathbf{e}}(\mathbf{k}_{2o}, \lambda) \quad (135)$$

(and equivalently f_{1o}), where α_{2o} is an average amplitude with phase φ_{2o} and absolute value $|\alpha_{2o}| = \|f_{2o}\|$. Here, u_{2o} is a positive bump function that minimizes the error of the approximation. Such a function has compact support around the origin, a unit volume integral, and a unit average extent

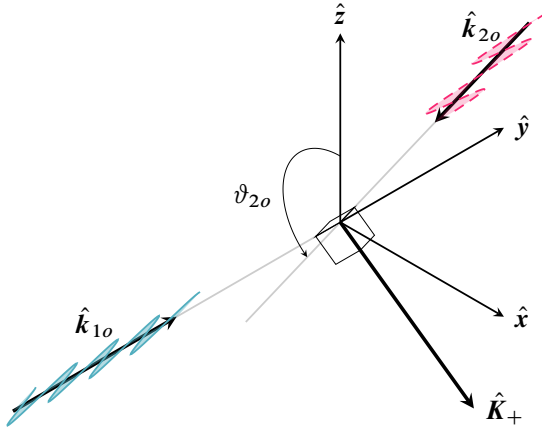


Figure 12: (color online) Scattering geometry of the open configuration o with incident light wavevectors $\hat{\mathbf{k}}_{1o} = \hat{\mathbf{y}}$ and $\hat{\mathbf{k}}_{2o}$ with projection $\hat{\mathbf{k}}_{2o} \cdot \hat{\mathbf{z}} = \cos \vartheta_{2o} = -\sqrt{2/3}$. The emitted photoelectron is detected in the direction $\hat{\mathbf{K}}_+$, which, together with $\hat{\mathbf{k}}_{2o}$ and $\hat{\mathbf{k}}_{1o}$, forms a right-handed orthogonal triad that is rotated from the laboratory's reference frame by $3\pi/2 - \vartheta_{2o} = \pi - \arctan \sqrt{2}$ around the $\hat{\mathbf{y}}$ -axis. The alkali atom is located at the origin. The polarization of the incoming radiation is indicated in color (shades of gray). The open configuration employs linearly polarized light.

that is scaled to ℓ_{2o} . In essence, ℓ_{2o} quantifies the average extent of f_{2o} in \mathbf{k} -space. Since f_{2o} is concentrated around $\hat{\mathbf{k}}_{2o}$, ℓ_{2o} is small.

The open configuration is then engineered by setting

$$\hat{\mathbf{k}}_{2o} = \hat{\mathbf{y}}, \quad \hat{\boldsymbol{\varepsilon}}_{2o} = \frac{1}{\sqrt{3}}(\hat{\mathbf{x}} + \sqrt{2}\hat{\mathbf{z}}), \quad (136a)$$

$$\hat{\mathbf{k}}_{1o} = -\frac{1}{\sqrt{3}}(\hat{\mathbf{x}} + \sqrt{2}\hat{\mathbf{z}}), \quad \hat{\boldsymbol{\varepsilon}}_{1o} = \hat{\mathbf{y}}, \quad (136b)$$

where the incoming light is chosen as linearly polarized. The geometry of the experiment is visualized in Fig. 12. With the above parameter choices, the transition amplitudes become

$$T_1[\hat{f}_{2o}](\mathbf{K}_+ + \frac{1}{2}, +\frac{1}{2}) = T_1[\hat{f}_{2o}](\mathbf{K}_+ - \frac{1}{2}, -\frac{1}{2}) = 0, \quad (137a)$$

$$\begin{aligned} T_1[\hat{f}_{2o}](\mathbf{K}_+ + \frac{1}{2}, -\frac{1}{2}) &= -T_1[\hat{f}_{2o}](\mathbf{K}_+ - \frac{1}{2}, +\frac{1}{2}) = e^{i\varphi_{2o}} \\ &\times \int d\mathbf{k} \delta[E_- - E_+ + \hbar\omega(k)] \sqrt{u_{2o}[\ell_{2o}^{-1}(\mathbf{k} - \mathbf{k}_{2o})]} \\ &\times \frac{\sqrt{\pi}\hbar^2 \mathcal{E}(k)}{3\sqrt{\ell_{2o}^3 m_e K_+}} [-D_1(E_+ 1\frac{1}{2}, n0\frac{1}{2}) + D_1(E_+ 1\frac{3}{2}, n0\frac{1}{2})], \end{aligned} \quad (137b)$$

$$\begin{aligned} T_2[\hat{f}_{1o}](\mathbf{K}_+ + \frac{1}{2}, +\frac{1}{2}) &= T_2[\hat{f}_{1o}](\mathbf{K}_+ - \frac{1}{2}, -\frac{1}{2}) = e^{2i\varphi_{1o}} \\ &\times \int d\mathbf{k}_1 \int d\mathbf{k}_2 \delta[E_- - E_+ + \sum_{i=1}^2 \hbar\omega(k_i)] \\ &\times \sqrt{u_{1o}[\ell_{1o}^{-1}(\mathbf{k}_1 - \mathbf{k}_{1o})]} \sqrt{u_{1o}[\ell_{1o}^{-1}(\mathbf{k}_2 - \mathbf{k}_{1o})]} \frac{\sqrt{\pi}\hbar^3 \mathcal{E}(k_1)\mathcal{E}(k_2)}{\sqrt{45}\ell_{1o}^3 \sqrt{m_e K_+}} \\ &\times [5D_2(E_+ 0\frac{1}{2}, 1\frac{1}{2}, n0\frac{1}{2}; k_2) + 10D_2(E_+ 0\frac{1}{2}, 1\frac{3}{2}, n0\frac{1}{2}; k_2) \\ &\quad - 5D_2(E_+ 2\frac{3}{2}, 1\frac{1}{2}, n0\frac{1}{2}; k_2) - D_2(E_+ 2\frac{3}{2}, 1\frac{3}{2}, n0\frac{1}{2}; k_2) \\ &\quad - 9D_2(E_+ 2\frac{5}{2}, 1\frac{3}{2}, n0\frac{1}{2}; k_2)], \end{aligned} \quad (137c)$$

and

$$T_2[\hat{f}_{1o}](\mathbf{K}_+ + \frac{1}{2}, -\frac{1}{2}) = T_2[\hat{f}_{1o}](\mathbf{K}_+ - \frac{1}{2}, +\frac{1}{2}) = 0, \quad (137d)$$

where $E_+ = E(K_+)$. Note that, if the spin-orbit coupling were absent, then the radial integrals D_1 and D_2 would add to zero and T_1 and T_2 would vanish. However, spin-orbit coupling is typically present, and T_1 and T_2 are finite with, in general, the second-order amplitude T_2 much smaller than its counterpart T_1 .

In Eqs. (137), the integrals over the bump functions u_{2o} and u_{1o} ensure the agreement between the photon energy $2\hbar\omega$ and the ionization energy $E_+ - E_-$ in relation to the energy spreading, $\hbar\ell_{2o}$ and $\hbar\ell_{1o}$, respectively.

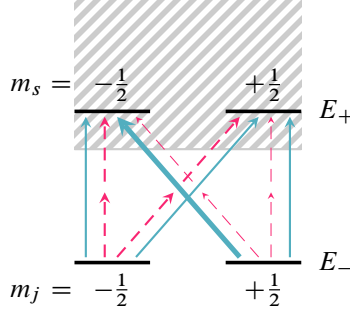


Figure 13: In the closed configuration c , the processes are not distinguishable by their outcomes, since the transition amplitudes between all spin combinations are finite and unbiased. Our proposed implementation deviates from the demanded behavior. Only for $m_j = -\frac{1}{2}$ [and $D_2(E_+ 2\frac{5}{2}, 1\frac{3}{2}, n0\frac{1}{2}; k_2) = 0$], the amplitudes are unbiased. However, for $m_j = +\frac{1}{2}$, they are biased, illustrated here by the width of the arrows.

If ℓ_{2o} (or ℓ_{1o}) is small enough, all functions under the integral, except the δ -term and u_{2o} (u_{1o}), can be approximated by their value at k_{2o} (k_{1o}). The integral then reduces to a numerical factor $\eta_{2o}^2 I_{2o} / \hbar c$ ($\eta_{1o}^5 I_{1o} / \hbar c$), where I_{2o} (I_{1o}) is dimensionless.

To conclude the open configuration discussion, note, from Eqs. (137), that T_1 and T_2 fulfill conditions (132). Condition (133) can be implemented by adjusting $\sqrt{\langle \tilde{\chi}_o^1 | \tilde{\chi}_o^1 \rangle}$ and $\sqrt{\langle \tilde{\chi}_o^2 | \tilde{\chi}_o^2 \rangle}$ that, for coherent states [as in Eqs. (96b)], become equal to $|\alpha_{1o}|^2$ and $|\alpha_{2o}|$, respectively.

Consider now the closed configuration which, according to Sec. 3.2, is characterized by completely unbiased, symmetric transition amplitudes [Eqs. (37) and (47)]. In the photoelectron spin control scenario, these conditions are

$$T_1[\hat{f}_{2c}](\mathbf{K}_+ + \frac{1}{2}, m_j) = T_1[\hat{f}_{2c}](\mathbf{K}_+ - \frac{1}{2}, m_j), \quad (138a)$$

$$T_2[\hat{f}_{1c}](\mathbf{K}_+ + \frac{1}{2}, m_j) = -T_2[\hat{f}_{1c}](\mathbf{K}_+ - \frac{1}{2}, m_j) \quad (138b)$$

and

$$\sqrt{\langle \tilde{\chi}_c^1 | \tilde{\chi}_c^1 \rangle} |T_1[\hat{f}_{2c}](\mathbf{K}_+ + \frac{1}{2}, m_j)| = \sqrt{\langle \tilde{\chi}_c^2 | \tilde{\chi}_c^2 \rangle} |T_2[\hat{f}_{1c}](\mathbf{K}_+ + \frac{1}{2}, m_j)|. \quad (139)$$

Fig. 13 provides a graphical representation of Eqs. (138). The challenge is to find settings $\hat{\mathbf{K}}_+$, \hat{f}_{1c} , and \hat{f}_{2c} so that T_1 and T_2 satisfy Eqs. (138) and (139), independent of the values of the radial integrals D_1 and D_2 that depend on the energy $E(K)$ and on the particular alkali atom used.

We adopt a similar approximation as above for the open configuration.

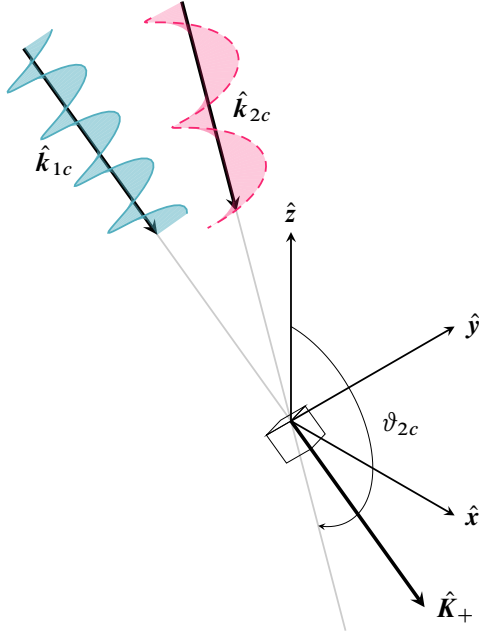


Figure 14: (color online) Scattering geometry of the closed configuration c with the alkali atom at the center, Wavepacket polarizations are indicated in color (shades of gray). The amplitude function f_{1c} of the first wavepacket is concentrated around the incident direction $\hat{\mathbf{k}}_{1c} = \hat{\mathbf{K}}_+$, and the circular polarization $\hat{\mathbf{e}}_{1c}$. $\hat{\mathbf{k}}_{1c}$ makes an angle of $\pi - \text{arccsc}(3) \simeq 2.80\text{rad}$ with the $\hat{\mathbf{z}}$ -axis. The second wavepacket (described by f_{2c}) is incident from the direction $\hat{\mathbf{k}}_{2c}$, for which $\hat{\mathbf{k}}_{2c} \cdot \hat{\mathbf{z}} = \cos \vartheta_{2c} = -2\sqrt{2}/3$. Its polarization $\hat{\mathbf{e}}_{2c}$ is elliptical.

That is, we approximate

$$f_{2c}(\mathbf{k}, \lambda) \simeq \alpha_{2c} \sqrt{\ell_{2c}^{-3} u_{2c} [\ell_{2c}^{-1}(\mathbf{k} - \mathbf{k}_{2c})]} \hat{\boldsymbol{\varepsilon}}_{2c} \cdot \hat{\boldsymbol{\varepsilon}}(\mathbf{k}_{2c}, \lambda) \quad (140)$$

and equivalently f_{1c} . We then set

$$\hat{\mathbf{k}}_{2c} = \frac{1}{\sqrt{3}}(\sqrt{2}\hat{\mathbf{x}} - \hat{\mathbf{z}}), \quad (141a)$$

$$\hat{\boldsymbol{\varepsilon}}_{2c} = \frac{1}{\sqrt{14}} \left[\sqrt{5+3\sqrt{2}} \frac{1}{\sqrt{3}}(-\hat{\mathbf{x}} - \sqrt{2}\hat{\mathbf{z}}) - i\sqrt{9-3\sqrt{2}}\hat{\mathbf{y}} \right], \quad (141b)$$

$$\hat{\mathbf{k}}_{1c} = \frac{1}{3}(\hat{\mathbf{x}} - 2\sqrt{2}\hat{\mathbf{z}}), \quad (141c)$$

$$\hat{\boldsymbol{\varepsilon}}_{1c} = \frac{1}{\sqrt{2}} \left[\frac{1}{3}(2\sqrt{2}\hat{\mathbf{x}} + \hat{\mathbf{z}}) + i\hat{\mathbf{y}} \right]. \quad (141d)$$

$\hat{\mathbf{K}}_+$ stays as it is [cf. Eq. (134)] as shown in Fig. 14. The transition amplitudes then become

$$\begin{aligned} T_1[\hat{f}_{2c}](\mathbf{K}_+ + \tfrac{1}{2}, +\tfrac{1}{2}) &= \frac{1}{1 + \sqrt{2}} T_1[\hat{f}_{2c}](\mathbf{K}_+ - \tfrac{1}{2}, +\tfrac{1}{2}) = \\ &- T_1[\hat{f}_{2c}](\mathbf{K}_+ + \tfrac{1}{2}, -\tfrac{1}{2}) = -T_1[\hat{f}_{2c}](\mathbf{K}_+ - \tfrac{1}{2}, -\tfrac{1}{2}) = e^{i\varphi_{2c}} \\ &\quad \times \int d\mathbf{k} \delta[E_- - E_+ + \hbar\omega(k)] \sqrt{u_{2c}[\ell_{2c}^{-1}(\mathbf{k} - \mathbf{k}_{2c})]} \\ &\times \frac{\sqrt{\pi\hbar^2\mathcal{E}(k)}}{3\sqrt{7}\ell_{2c}^3 m_e K} \sqrt{3 - \sqrt{2}} [D_1(E_+ 1\frac{1}{2}, n0\frac{1}{2}) - D_1(E_+ 1\frac{3}{2}, n0\frac{1}{2})] \end{aligned} \quad (142a)$$

and

$$\begin{aligned}
T_2[\hat{f}_{1c}](\mathbf{K}_+, m_s, m_j) &= e^{2i\varphi_{1c}} \int d\mathbf{k}_1 \int d\mathbf{k}_2 \delta[E_- - E_+ + \sum_{i=1}^2 \hbar\omega(k_i)] \\
&\times \sqrt{u_{1c}[\ell_{1c}^{-1}(\mathbf{k}_1 - \mathbf{k}_{1c})]} \sqrt{u_{1c}[\ell_{1c}^{-1}(\mathbf{k}_2 - \mathbf{k}_{1c})]} \frac{\sqrt{\pi} i \hbar^3 \mathcal{E}(k_1) \mathcal{E}(k_2)}{90 \sqrt{m_e K_+}} \\
&\times \left\{ \begin{array}{l}
(-1 + \sqrt{2}) [5D_2(E_+ 2\frac{3}{2}, 1\frac{1}{2}, n0\frac{1}{2}; k_2) \\
+ D_2(E_+ 2\frac{3}{2}, 1\frac{3}{2}, n0\frac{1}{2}; k_2) \\
- 3(7 + 5\sqrt{2}) D_2(E_+ 2\frac{5}{2}, 1\frac{3}{2}, n0\frac{1}{2}; k_2)] \quad \text{if } m_s = \frac{1}{2} \text{ and } m_j = \frac{1}{2}, \\
(-1 + \sqrt{2}) [-5D_2(E_+ 2\frac{3}{2}, 1\frac{1}{2}, n0\frac{1}{2}; k_2) \\
- D_2(E_+ 2\frac{3}{2}, 1\frac{3}{2}, n0\frac{1}{2}; k_2) \\
+ 6D_2(E_+ 2\frac{5}{2}, 1\frac{3}{2}, n0\frac{1}{2}; k_2)] \quad \text{if } m_s = -\frac{1}{2} \text{ and } m_j = \frac{1}{2}, \\
(1 + \sqrt{2}) [5D_2(E_+ 2\frac{3}{2}, 1\frac{1}{2}, n0\frac{1}{2}; k_2) \\
+ D_2(E_+ 2\frac{3}{2}, 1\frac{3}{2}, n0\frac{1}{2}; k_2) \\
- 6D_2(E_+ 2\frac{5}{2}, 1\frac{3}{2}, n0\frac{1}{2}; k_2)] \quad \text{if } m_s = \frac{1}{2} \text{ and } m_j = -\frac{1}{2}, \\
(1 + \sqrt{2}) [-5D_2(E_+ 2\frac{3}{2}, 1\frac{1}{2}, n0\frac{1}{2}; k_2) \\
- D_2(E_+ 2\frac{3}{2}, 1\frac{3}{2}, n0\frac{1}{2}; k_2) \\
+ 3(7 - 5\sqrt{2}) D_2(E_+ 2\frac{5}{2}, 1\frac{3}{2}, n0\frac{1}{2}; k_2)] \quad \text{if } m_s = -\frac{1}{2} \text{ and } m_j = -\frac{1}{2}.
\end{array} \right. \tag{142b}
\end{aligned}$$

Evidently, T_1 and T_2 do not yet fulfil the conditions (138). First, in Eq. (142a), $T_1[\hat{f}_{2c}](\mathbf{K}_+ - \frac{1}{2}, +\frac{1}{2})$ deviates from the required behavior, being too large by a factor of $(1 + \sqrt{2})$. By contrast, the T_1 for the other values of m_s and m_j are as unbiased as required, and they have the correct signs. Therefore, the issue can be avoided by using the input port $m_j = -\frac{1}{2}$, i.e., by setting $p_{\frac{1}{2}} = 0$ and $p_{-\frac{1}{2}} = 1$ in $\varrho_{\mathcal{M}}(-\infty)$ [Eq. (123) on page 59].

Second, as can be seen from Eq. (142b), T_2 is different for all four possible combinations of $m_s = \pm\frac{1}{2}$ and $m_j = \pm\frac{1}{2}$, because the second-order radial integral $D_2(E_+ 2\frac{5}{2}, 1\frac{3}{2}, n0\frac{1}{2}; k_2)$ enters in all four cases with a different prefactor. This problem cannot be solved by altering $\hat{\mathbf{K}}_+$, $\hat{\mathbf{k}}_{2c}$, $\hat{\mathbf{e}}_{2c}$, $\hat{\mathbf{k}}_{1c}$, or $\hat{\mathbf{e}}_{1c}$. In order to fulfill the conditions (138), we have to impose a requirement on $D_2(E_+ 2\frac{5}{2}, 1\frac{3}{2}, n0\frac{1}{2}; k_2)$, e.g.,

$$D_2(E_+ 2\frac{5}{2}, 1\frac{3}{2}, n0\frac{1}{2}; k_2) = 0. \tag{143}$$

That is, one has to find an energy E_+ or system, where the transition to

$D_{\frac{5}{2}}$ is negligible compared to the transition to $D_{\frac{3}{2}}$.¹⁵

The final task is to balance the magnitudes of $T_1[\hat{f}_{2c}](\mathbf{K}_+ + \frac{1}{2}, m_j)$ and $T_2[\hat{f}_{1c}](\mathbf{K}_+ + \frac{1}{2}, m_j)$ in accordance with Eq. (139). This can be achieved by adjusting $\sqrt{\langle \tilde{\chi}_c^1 | \tilde{\chi}_c^1 \rangle}$ and $\sqrt{\langle \tilde{\chi}_c^2 | \tilde{\chi}_c^2 \rangle}$ (or $|\alpha_{1c}|^2$ and $|\alpha_{2c}|$, respectively, in the case of coherent states of incoming light).

In summary, this section shows how to build an open and a closed CCI for the specific example of photoelectron spin control. With the settings as in Eqs. (134) and (141), it is possible to do the quantum erasure coherent control experiment of Sec. 4. The quantum delayed choice coherent control scenario of Sec. 5 can be implemented with a combination of Eqs. (134), (136) and (141). The existence of a single direction of detection $\hat{\mathbf{K}}_+$ [Eq. (134)] that works for both the open and the closed configuration makes this possible. See Ref. 136 for further details.

8 Facing the Loopholes

In any test of a Bell inequality, one has to deal with three loopholes: locality, fair-sampling, and freedom-of-choice. Only if the Bell violation occurs under simultaneous closing of these loopholes, does a Bell inequality provide a stringent test for local realism. As discussed below, this presents a significant challenge in the case of photoelectron spin control. Indeed, closing these loopholes had been one of the major problems in fundamental physics for a long time [142].

Locality loophole. In both the quantum erasure and the quantum delayed choice coherent control scenario, the locality loophole arises from the possibility that the measurement outcome of the spin polarization is influenced by the measurement of the light, or vice versa. The skeptic's suspicion is that the choice of the measurement observable, or of its measurement outcome, could have been heralded with subluminal or luminal speed from the location of the photodetection to the location of the spin detection.

This locality loophole can be closed by separating both the choice of observable and the measurement events of either subsystem by space-like distances, excluding any causal influence. Additional confidence could be built by deliberately randomizing the observable choices using random numbers generated by quantum random number generators.

¹⁵If only the input port $m_j = -\frac{1}{2}$ is used, then the stipulation that

$$D_2(E_+ 2\frac{5}{2}, 1\frac{3}{2}, n0\frac{1}{2}; k_2) = \frac{2}{93} (9 + 5\sqrt{2}) \\ \times [5D_2(E_+ 2\frac{3}{2}, 1\frac{1}{2}, n0\frac{1}{2}; k_2) + D_2(E_+ 2\frac{3}{2}, 1\frac{3}{2}, n0\frac{1}{2}; k_2)]$$

is a possible solution to the bias issue as well.

In the case of photoelectron spin control, closing the locality loophole seems like an almost insurmountable challenge.

Fair-sampling or detection loophole. This loophole recognizes that every detection is imperfect, and electron spin detectors are particularly flawed: only a small fraction of the photoelectrons can be collected, and an even smaller fraction has a discernible spin. With such a small detection efficiency, the detected electron spins may not be representative of the entire statistical ensemble, and they may suggest a violation of local realism despite the fact that the entirety of spins still obeys it. Equivalent issues, albeit less severe, exist for the detection of the light.

The detection loophole can be dealt with in two ways. Either one relies on “fair sampling” (i.e., the supplementary hypothesis that the sample of detected spins is representative of the whole sample), or one closes the loophole by increasing the efficiency above a certain threshold ($2\sqrt{2} - 2 \simeq 83\%$ [143]). However, with present technology, this threshold is unattainable for electron spin detection. Thus, in the photoelectron spin experiment, the assumption of fair sampling would have to be adopted to close this loophole.

Freedom-of-choice loophole. This loophole arises from the assumption that the choice of the observables on the electron spin and the light is independent and free of properties of the physical system being measured, or of some local hidden variable. If this freedom were denied, and if all choices were completely deterministic, then the outcome of the Bell measurements would have been determined in advance.

This is a loophole for local realism and, in a completely deterministic world, it cannot be closed [144]. If nature is nondeterministic, however, then the problem of freedom-of-choice can be solved by having a space-like separation between the control event and the choice of the measurement observables [62]. But again, for photoelectron spin control, this is a rather difficult undertaking.

Closing all these loopholes simultaneously (for any physical process) had been one of the most significant and difficult problems in foundational physics. It has only been overcome recently for entangled electron spins [62] and entangled photon pairs [63, 64]. With all the specific attributes of photoelectron spin control, however, repeating such a success would be extremely difficult. Furthermore, we could have discussed far simpler examples of quantum erasure [103, 105, 145], delayed choice [102, 146–148], and quantum delayed choice [51, 78, 79], based on established technology like linear quantum optics that is used routinely in applications of quantum information theory. Indeed, we do not propose photoelectron spin control to show that quantum erasure and quantum delayed choice are possible or to provide further evidence that nature violates local realism. Rather, we set

out to find the most quantum of the quantum phase control scenarios and the limits of their verification. It appears we have successfully examined these limits.

9 Conclusions

We began this article by noting that two-color weak-field phase control is analogous to a classical control phenomenon. Hence, it cannot be advertised as a true quantum interference effect. In a nutshell, there are several reasons why this is the case.

1. The control features of two-color weak-field phase control can be derived perturbatively from nonlinear response theory, an approach that applies to both classical and quantum matter. In both cases, nonlinear response theory predicts both the nonadditivity and the phase sensitivity of the response. (Nonadditivity implies that the collective response to the incident driving fields differs from the sum of the individual responses to each field component. Phase sensitivity refers to the dependence of the response on the phases of the field components. These are the features of two-color phase control.)
2. Perturbative nonlinear response theory separates the response into material and nonmaterial contributions. The phase sensitivity originates exclusively from the nonmaterial contributions. Since these contributions are classical, differences between a classical and quantum response can only result from quantitative differences in the material contribution. These differences are not related to either phase sensitivity or to quantum interference.
3. Formally, claiming that the observation of a phase-sensitive and non-additive response in experiments of coherent phase control is a demonstration of quantum interference is a logical fallacy known as the “affirmation of the consequent”. Agreement and consistency with a theory does not constitute a proof, even if no other explanation is known.

These points raised the question of how a conventional coherent control experiment in general, and a phase control experiment in particular, can be studied from a foundational perspective and developed into a genuinely and verifiably quantum interference phenomenon. This is the issue that was explored in the main part of this article. Specifically, we first introduced a general, unifying framework for studying all-optical control of matter using two-color light fields. The theory was derived under minimal assumptions. It is applicable to a wide variety of control targets including atoms, molecules, and bulk solids. The control field was treated in the continuous multimode formalism, a useful mathematical tool to account for realistic pulse profiles

that are compact both in space and in frequency. Furthermore, the approach allowed us to consider any choice of the light's photon statistics. We thus derived expressions that apply in equal measure to semiclassical and to quantum states of light, such as coherent state, Fock states, or squeezed states.

At the heart of this framework is a new kind of formal interferometer, the coherent control interferometer (CCI), which allowed us to reach a significant level of abstraction. It is defined in terms of its input and output ports as well as via a special set of scattering states that play the role of a binary path degree of freedom. By means of these prescriptions, knowing the path traversed in the CCI is equivalent to knowing the frequency of the light with which the matter has interacted.

Through the introduction of the CCI, the problem of phase control was translated into the language of common two-way interferometry, including interferometers such as the Young double-slit, the Mach-Zehnder interferometer, the Stern-Gerlach apparatus, and the Ramsey interferometer. This allowed detailed clarification of the concepts of waves, particles, and their complementarity in two-color phase control scenarios. These fundamental concepts are the keys to demonstrating quantum interference in coherent phase control. They are also of practical relevance, since, as we found, the success of phase control is always limited by the simultaneously acquirable amount of path knowledge. The development of the CCI allowed an approach to systematically exploring this relationship.

To this end, we proposed the quantum erasure coherent phase control scenario, in which the CCI is subject to which-path marking. Unlike conventional phase control scenarios, this one makes use of quantum light, which both controls the dynamics and becomes entangled with the matter in the process. As a consequence, the path taken through the CCI is marked, providing path knowledge that can be extracted, if not in practice then at least in principle. Phase control, therefore, has to be poor, unless the CCI is joint with a quantum erasure measurement of the outgoing quantum light. In this case, we found that control can be improved at the expense of the simultaneously acquired path knowledge, with limits set by quantitative wave-particle complementarity. We further found that, in the setting of the CCI, the Englert-Greenberger-Yasin duality relation $\mathcal{C}_{\mathcal{R}}^2 + \mathfrak{P}^2 \leq 1$ provides a quantitative relationship between the maximum controllability $\mathcal{C}_{\mathcal{R}}$ and the minimum path knowledge \mathfrak{P} acquirable in any measurement of the outgoing light. We derived the measurement observable that saturates the above duality relation, giving best possible phase control. We also showed how quantum erasure can be achieved in a homodyne measurement scheme with a so-called click/no-click photodetector that does not measure the number of photons. With quantitative wave-particle complementarity and quantum erasure, this proposed coherent control scenario can demonstrate two hallmark features of quantum mechanics.

As a second application of the CCI formalism we proposed the quantum delayed-choice coherent control scenario, designed to demonstrate Wheeler’s idea of delayed choice, another hallmark of quantum mechanics. This scenario, which employs quantum light as well, realizes two complementary situations simultaneously. In the first, phase control is absent, characterized by particle-like CCI output port statistics. In the second, phase control is present, and the CCI displays wave-like statistics. These two situations are coherently blended and conditioned on marker states of the outgoing light. We showed that this can be described in terms of entanglement between the radiation field and the control target. Our theory for quantum delayed-choice coherent control scenario predicts that, prior to measurement, it is impossible to know whether there will be phase control or not. Upon measurement, the case that applies will be random. This is the essence of quantum delayed-choice coherent phase control.

In the last section, we showed how these two scenarios, quantum erasure and the quantum delayed choice coherent control, are not only consistent with quantum theory, but are in fact inconsistent with every conceivable—or inconceivable—classical description. To this end, we constructed Bell inequality tests for each of the two proposed scenarios. For the quantum erasure scenario, we showed that a violation of the Bell inequality certifies that the erased path distinguishability has been of nonclassical origin. For the quantum delayed-choice scenario, on the other hand, we showed that a failed Bell test suggests that the outcome of the experiment has not only been unpredictable, but also nonclassically random. Thus, in both scenarios, a Bell inequality violation demonstrates that phase control originates from nontrivial and nonclassical interference effects. It is quantum coherent control.

To demonstrate the utility of this framework and the feasibility of the two proposed control scenarios, we examined the specific case of photoelectron spin control, where a heavy alkali atom is ionized by weak coherent ($\omega + 2\omega$) radiation. With this example, we expanded on the seminal two-color coherent phase control experiments of Elliott et al., in which, according to our discussion, control is analogous to a classical control phenomenon. In doing so, we showed how a well-known coherent phase control experiment can be modified to display quantum coherent control.

In conclusion, we proposed a general framework to examine various degrees of “quantumness” in phase control scenarios and paved the way for new coherent control experiments in which phase control will be a genuinely and verifiably quantum interference phenomenon. Applications of this approach to other molecular control scenarios is expected to be highly enlightening.

Acknowledgments

Financial support from the Natural Sciences and Engineering Research Council of Canada is gratefully acknowledged. T.S. thanks Christine Tewfik for her patience and support, and P.B. thanks Professor A. Steinberg for numerous discussions preliminary to this work.

Appendix A: The Longtime Limit of The Total Density Operator

Below, perturbation theory is used to solve the light-matter scattering problem for weak field unitary 1 vs. N coherent phase control dynamics, where $N = 2, 3, \dots$. Although standard quantum structures are simpler [3], we use the Liouville representation of quantum mechanics to allow a future extension to nonunitary dynamics. Here, Liouville space is a vector space of operators on the regular Hilbert space (such as Hamiltonians, observables, density operators, etc.), and superoperators are the operators acting on Liouville space. The time evolution superoperator $\mathcal{U}(t, t') = \exp[-i\mathcal{L}(t - t')/\hbar]$ solves the Liouville equation

$$i\hbar\partial_t\mathcal{U}(t, t') = \mathcal{L}\mathcal{U}(t, t'), \quad (144)$$

where $\mathcal{L} = \mathcal{L}_0 + \mathcal{V}$ the total Liouville superoperator of the system, corresponds to the commutator $[H, \cdot] = [H_0 + V, \cdot]$. Equation (144) is equivalent to the von Neumann equation for the density operator ϱ . For convenience, we define a free time evolution superoperator $\mathcal{U}_0(t, t')$ that solves the free Liouville equation $i\hbar\partial_t\mathcal{U}_0(t, t') = \mathcal{L}_0\mathcal{U}_0(t, t')$, with $\mathcal{L}_0 = \mathcal{L}_M + \mathcal{L}_R = [H_M + H_R, \cdot] = [H_0, \cdot]$ in which the material part of the system, \mathcal{M} , and the radiation field, \mathcal{R} , evolve independently of each other. The perturbation $\mathcal{V} = [V, \cdot]$ describes the light-matter interaction, treated within the electric dipole approximation. The initial state of the system is given by

$$|\varrho(-\infty)\rangle\rangle = |\varrho_M(-\infty)\rangle\rangle \otimes |\varrho_R(-\infty)\rangle\rangle, \quad (145a)$$

where

$$|\varrho_M(-\infty)\rangle\rangle = \sum_{\nu \in \mathcal{D}_-} p_\nu |\nu\nu\rangle\rangle \quad (145b)$$

and

$$|\varrho_R(-\infty)\rangle\rangle = |\chi\chi\rangle\rangle. \quad (145c)$$

These vectors are the Liouville representations of Eqs. (16), (8), and (18), respectively, i.e., $|\nu\nu\rangle\rangle$ corresponds to $|\nu\rangle\langle\nu|$, etc.

Consider then the scattering problem. Initially, as well as finally, the electromagnetic fields are far away from the material target and therefore

do not interact with it. Scattering theory provides a map, the scattering superoperator,

$$\mathcal{S} = \lim_{t \rightarrow \infty} \mathcal{U}_0(0, t/2) \mathcal{U}(t/2, -t/2) \mathcal{U}_0(-t/2, 0), \quad (146)$$

that relates a past asymptotic in-state $|\varrho(-\infty)\rangle\rangle$ to its future asymptotic out-state $|\varrho(\infty)\rangle\rangle$:

$$|\varrho(\infty)\rangle\rangle = \mathcal{S}|\varrho(-\infty)\rangle\rangle. \quad (147)$$

The superoperator \mathcal{S} has a perturbative expansion,

$$\mathcal{S} = 1 - 2\pi i \int dE \delta(E - \mathcal{L}_0) \mathcal{T}(E + i0) \delta(\mathcal{L}_0 - E), \quad (148)$$

with

$$\mathcal{T}(z) = \mathcal{V} + \mathcal{V} \mathcal{G}_0(z) \mathcal{T}(z) = \sum_{n=0}^{\infty} \mathcal{V} (\mathcal{G}_0(z) \mathcal{V})^n = \sum_{n=0}^{\infty} \mathcal{T}_n(z) \quad (149)$$

the transition superoperator, and with $\mathcal{G}_0(z) = (z - \mathcal{L}_0)^{-1}$, the unperturbed resolvent superoperator.

Restricting attention to only interesting asymptotic out-states (i.e., those characterized by the quantum number set \mathcal{D}_+), is equivalent to postselection, $|\varrho(\infty)\rangle\rangle \mapsto |\tilde{\varrho}(\infty)\rangle\rangle$, of the form

$$|\tilde{\varrho}(\infty)\rangle\rangle = \tilde{p}^{-1} \mathcal{P}_{\mathcal{D}_+} |\varrho(\infty)\rangle\rangle \quad (150a)$$

$$= \tilde{p}^{-1} \int_{\mathcal{D}_+} d\mu \int_{\mathcal{D}_+} d\mu' |\mu\mu'\rangle\rangle \langle\langle \mu\mu' | \varrho(\infty)\rangle\rangle, \quad (150b)$$

where

$$\tilde{p} = \int_{\mathcal{D}_+} d\mu \langle\langle \mu\mu, \mathbb{1}_{\mathcal{R}} | \varrho(\infty)\rangle\rangle. \quad (150c)$$

That is, the superoperator $\mathcal{P}_{\mathcal{D}_+}$ projects into the subspace spanned by $|\mu\mu'\rangle\rangle$, with μ, μ' in the domain \mathcal{D}_+ .

Below we calculate the leading terms in the perturbative expansion of $|\tilde{\varrho}(\infty)\rangle\rangle$. In coherent control, the material ground state $|\nu\nu\rangle\rangle$ and the relevant asymptotic out-states $|\mu\mu\rangle\rangle$ (and out-coherences $|\mu\mu'\rangle\rangle$) do not overlap. Hence $\mathcal{P}_{\mathcal{D}_+} |\varrho_{\mathcal{M}}(-\infty)\rangle\rangle = 0$, i.e., the zeroth-order term vanishes. The first-order term vanishes as well since it is proportional to matrix elements of the form $\langle\langle \mu\mu', \dots | \mathcal{V} | \nu\nu, \dots \rangle\rangle$ that evaluate to zero. The first nonzero term is, therefore, of at least second order. The first step in the calculation of that term is the evaluation of the second-order \mathcal{S} -matrix element

$$- 2\pi i \int dE \langle\langle \mu\mu', \{\mathbf{q}\kappa\} \{ \mathbf{q}'\kappa' \} | \times \delta(E - \mathcal{L}_0) \mathcal{T}_2(E + i0) \delta(\mathcal{L}_0 - E) | \nu\nu, \{\mathbf{k}\lambda\} \{ \mathbf{k}'\lambda' \} \rangle\rangle, \quad (151)$$

where the Liouville notations $|\nu\nu, \{\mathbf{k}\lambda\}\{\mathbf{k}'\lambda'\}\rangle\rangle$ and $|\mu\mu', \{\mathbf{q}\kappa\}\{\mathbf{q}'\kappa'\}\rangle\rangle$ correspond to

$$|\nu\rangle\langle\nu| \otimes |\mathbf{k}_1\lambda_1, \dots, \mathbf{k}_n\lambda_n\rangle\langle\mathbf{k}'_1\lambda'_1, \dots, \mathbf{k}'_{n'}\lambda'_{n'}| \quad (152a)$$

and

$$|\mu\rangle\langle\mu'| \otimes |\mathbf{q}_1\kappa_1, \dots, \mathbf{q}_m\kappa_m\rangle\langle\mathbf{q}'_1\kappa'_1, \dots, \mathbf{q}'_{m'}\kappa'_{m'}|, \quad (152b)$$

respectively. The numbers n and n' (m and m') are the initial (final) photon numbers in the field. The above vectors are eigenvectors of the free Liouville operator \mathcal{L}_0 . In particular,

$$\mathcal{L}_0|\nu\nu, \{\mathbf{k}\lambda\}\{\mathbf{k}'\lambda'\}\rangle\rangle = \hbar\omega(\{k\}, \{k'\}) = \sum_{i=1}^n \hbar\omega(k_i) - \sum_{i'=1}^{n'} \hbar\omega(k'_{i'}) \quad (153a)$$

and

$$\begin{aligned} \mathcal{L}_0|\mu\mu', \{\mathbf{q}\kappa\}\{\mathbf{q}'\kappa'\}\rangle\rangle &= \Delta_{\mu\mu'} + \hbar\omega(\{q\}, \{q'\}) = E_\mu - E_{\mu'} \\ &+ \sum_{j=1}^m \hbar\omega(q_j) - \sum_{j'=1}^{m'} \hbar\omega(q'_{j'}), \end{aligned} \quad (153b)$$

where E_μ denotes the eigenenergy of the eigenstate $|\mu\rangle$ of the material Hamiltonian $H_{\mathcal{M}}$ and $\hbar\omega(k) = \hbar ck$ is the energy of single-photon eigenstate $|\mathbf{k}\lambda\rangle$ of the field Hamiltonian $H_{\mathcal{R}}$.

With these, the second order \mathcal{S} -matrix element [Eq. (151)] becomes

$$\begin{aligned} &- 2\pi i \delta[\Delta_{\mu\mu'} + \hbar\omega(\{q\}, \{q'\}) - \hbar\omega(\{k\}, \{k'\})] \\ &\times \left\{ \langle\mu, \{\mathbf{q}\kappa\}|V|\nu, \{\mathbf{k}\lambda\}\rangle \frac{1}{\Delta_{\mu'\nu} + \hbar\omega(\{q'\}, \{k\}) + i0} \langle\nu, \{\mathbf{k}'\lambda'\}|V|\mu', \{\mathbf{q}'\kappa'\}\rangle \right. \\ &\left. + \langle\nu, \{\mathbf{k}'\lambda'\}|V|\mu', \{\mathbf{q}'\kappa'\}\rangle \frac{1}{-\Delta_{\mu'\nu} - \hbar\omega(\{q'\}, \{k\}) + i0} \langle\mu, \{\mathbf{q}\kappa\}|V|\nu, \{\mathbf{k}\lambda\}\rangle \right\}. \end{aligned} \quad (154)$$

The terms in the braces, $\{\dots + \dots\}$, can be illustrated graphically:

$$\begin{array}{ccc} \boxed{\nu\{\mathbf{k}\lambda\}|\nu\{\mathbf{k}'\lambda'\}} & \leftarrow & \boxed{\nu\{\mathbf{k}\lambda\}|\mu'\{\mathbf{q}'\kappa'\}} \\ & & \downarrow \\ \boxed{\mu\{\mathbf{q}\kappa\}|\mu'\{\mathbf{q}'\kappa'\}} & & \boxed{\mu\{\mathbf{q}\kappa\}|\nu\{\mathbf{k}'\lambda'\}} \\ & & \leftarrow & \boxed{\mu\{\mathbf{q}\kappa\}|\mu'\{\mathbf{q}'\kappa'\}} \end{array} + \begin{array}{ccc} \boxed{\nu\{\mathbf{k}\lambda\}|\nu\{\mathbf{k}'\lambda'\}} & & \boxed{\nu\{\mathbf{k}\lambda\}|\mu'\{\mathbf{q}'\kappa'\}} \\ & & \downarrow \\ \boxed{\mu\{\mathbf{q}\kappa\}|\mu'\{\mathbf{q}'\kappa'\}} & & \boxed{\mu\{\mathbf{q}\kappa\}|\nu\{\mathbf{k}'\lambda'\}} \\ & & \leftarrow & \boxed{\mu\{\mathbf{q}\kappa\}|\mu'\{\mathbf{q}'\kappa'\}} \end{array}. \quad (155)$$

The diagrams represent the two possible pathways through Liouville space that connect the in-vector $|\nu\nu, \{\mathbf{k}\lambda\}\{\mathbf{k}'\lambda'\}\rangle\rangle$ (shown in each case in the upper left corner) to the out-vector $|\mu\mu', \{\mathbf{q}\kappa\}\{\mathbf{q}'\kappa'\}\rangle\rangle$ (in the lower right corner). Liouville pathways describe the joint evolution of both bras and kets that comprise the system's density operator ρ [149]. The arrows correspond to transitions mediated by the light-matter coupling V . A horizontal arrow indicates action of V from the right, whereas a vertical arrow represents

action from the left. The above diagrams thus differ by the order these interactions take place.

Straightforward algebraic manipulation reduces Eq. (154) to

$$(-2\pi i) \delta[\Delta_{\nu\mu} + \hbar\omega(\{k\}, \{q\})] \langle \mu, \{\mathbf{q}\kappa\} | V | \nu, \{\mathbf{k}\lambda\} \rangle \\ \times 2\pi i \delta[\Delta_{\mu'\nu} + \hbar\omega(\{q'\}, \{k'\})] \langle \nu, \{\mathbf{k}'\lambda'\} | V | \mu', \{\mathbf{q}'\kappa'\} \rangle, \quad (156)$$

an expression which describes scattering events involving the emission or absorption of a photon. In the following, we concentrate on absorption only and set $m = n - 1$ and $m' = n' - 1$. Energy conservation is guaranteed by the δ -functions: Eq. (156) is nonzero only if the energy of the absorbed photon energy resonant with material states involved in the transition. Consequently, the second-order term can only appear in $|\tilde{\varrho}(\infty)\rangle\rangle$ if at least one incoming wavepacket carries photons with the required frequency. This is indeed the case in the 1 vs. N coherent phase control scenarios with $N = 2, 3, \dots$.

The second-order term

$$I_2 \equiv -2\pi i \int dE \mathcal{P}_{\mathcal{D}_+} \delta(E - \mathcal{L}_0) \mathcal{F}_2(E + i0) \delta(\mathcal{L}_0 - E) |\varrho(-\infty)\rangle\rangle \quad (157)$$

can be calculated from Eq. (156) by expanding the initial state $|\varrho(-\infty)\rangle\rangle$ in the Liouville basis $|\nu\nu', \{\mathbf{k}\lambda\}\{\mathbf{k}'\lambda'\}\rangle\rangle$, i.e. by using

$$|\varrho(-\infty)\rangle\rangle = \sum_{\nu \in \mathcal{D}_-} \int d\{\mathbf{k}\} \sum_{\{\lambda\}} \int d\{\mathbf{k}'\} \sum_{\{\lambda'\}} |\nu\nu, \{\mathbf{k}\lambda\}\{\mathbf{k}'\lambda'\}\rangle\rangle \\ \times \langle\langle \nu\nu, \{\mathbf{k}\lambda\}\{\mathbf{k}'\lambda'\} | \varrho(-\infty)\rangle\rangle. \quad (158)$$

Here we are interested in the result for the specific initial state (145) with the radiative part $|\varrho_{\mathcal{R}}(-\infty)\rangle\rangle$ corresponding to $|\chi\rangle\langle\chi|$, where

$$|\chi\rangle = g_1(a^\dagger[\hat{f}_1]) g_2(a^\dagger[\hat{f}_2]) |\text{vac}\rangle \quad (159)$$

[see Eq. (18) on page 14].

After a lengthy calculation, one obtains

$$I_2 = \sum_{\mathcal{D}_+} d\mu \sum_{\mathcal{D}_+} d\mu' |\mu\rangle\langle\mu'| \otimes \sum_{\nu \in \mathcal{D}_-} p_\nu T_1[\hat{f}_2](\mu, \nu) T_1^*[\hat{f}_2](\mu', \nu) \\ \times g_1(a^\dagger[\hat{f}_1]) g_2^{(1)}(a^\dagger[\hat{f}_2]) |\text{vac}\rangle \langle\text{vac}| g_1(a^\dagger[\hat{f}_1])^\dagger g_2^{(1)}(a^\dagger[\hat{f}_2])^\dagger, \quad (160)$$

where $T_1[\hat{f}_2](\mu, \nu)$ is as in Eq. (27a) on page 15. Eq. (160) illustrates that, to second order in \mathcal{V} , only the second wavepacket interacts with the material system, whereas the first wavepacket passes the matter unimpeded. Given that the quantum resonance condition is fulfilled, the second wavepacket undergoes change, from $g_2(a^\dagger[\hat{f}_2])|\text{vac}\rangle$ to $g_2^{(1)}(a^\dagger[\hat{f}_2])|\text{vac}\rangle$.

In 1 vs. N scenarios, there are only two other relevant orders in the perturbative expansion of $|\tilde{\varrho}(\infty)\rangle\rangle$: the $(N+1)^{\text{th}}$ and the $(2N)^{\text{th}}$ order. We focus first on the latter with $N=2$ for simplicity. Whereas the second-order term accounts for the absorption of a single photon from the second wavepacket only, the fourth-order term describes two-photon absorption exclusively from the first wavepacket. The fourth-order matrix element of \mathcal{S} with respect to $|\nu\nu, \{\mathbf{k}\lambda\}\{\mathbf{k}'\lambda'\}\rangle\rangle$ and $|\mu\mu', \{\mathbf{q}\kappa\}\{\mathbf{q}'\kappa'\}\rangle\rangle$ with initial photon numbers n and n' and final photon numbers $m = n - 2$ and $m' = n' - 2$, respectively, reads

$$\begin{aligned}
& 2\pi i \delta[\Delta_{\mu\mu'} + \hbar\omega(\{q\}, \{q'\}) - \hbar\omega(\{k\}, \{k'\})] \sum_{\xi, \xi'} \int d\{\mathbf{u}\} \sum_{\{\tau\}} \int d\{\mathbf{u}'\} \\
& \times \sum_{\{\tau'\}} \left[\begin{array}{c} \boxed{\nu\{\mathbf{k}\lambda\} | \nu\{\mathbf{k}'\lambda'\}} \leftarrow \boxed{\nu\{\mathbf{k}\lambda\} | \xi\{\mathbf{u}'\tau'\}} \leftarrow \boxed{\nu\{\mathbf{k}\lambda\} | \mu'\{\mathbf{q}'\kappa'\}} \\ \downarrow \xi\{\mathbf{u}\tau\} \mu'\{\mathbf{q}'\kappa'\} \\ \boxed{\xi\{\mathbf{u}\tau\} | \mu\{\mathbf{q}\kappa\}} \mu'\{\mathbf{q}'\kappa'\} \\ \\ \boxed{\nu\{\mathbf{k}\lambda\} | \nu\{\mathbf{k}'\lambda'\}} \leftarrow \boxed{\nu\{\mathbf{k}\lambda\} | \xi\{\mathbf{u}'\tau'\}} \\ \downarrow \xi\{\mathbf{u}\tau\} \mu'\{\mathbf{q}'\kappa'\} \\ \boxed{\xi\{\mathbf{u}\tau\} | \xi\{\mathbf{u}'\tau'\}} \leftarrow \boxed{\xi\{\mathbf{u}\tau\} | \mu'\{\mathbf{q}'\kappa'\}} \\ \downarrow \mu\{\mathbf{q}\kappa\} \mu'\{\mathbf{q}'\kappa'\} \\ \\ \boxed{\nu\{\mathbf{k}\lambda\} | \nu\{\mathbf{k}'\lambda'\}} \\ \downarrow \xi\{\mathbf{u}\tau\} \nu\{\mathbf{k}'\lambda'\} \leftarrow \boxed{\xi\{\mathbf{u}\tau\} | \xi\{\mathbf{u}'\tau'\}} \leftarrow \boxed{\xi\{\mathbf{u}\tau\} | \mu'\{\mathbf{q}'\kappa'\}} \\ \downarrow \mu\{\mathbf{q}\kappa\} \mu'\{\mathbf{q}'\kappa'\} \\ \\ \boxed{\nu\{\mathbf{k}\lambda\} | \nu\{\mathbf{k}'\lambda'\}} \leftarrow \boxed{\nu\{\mathbf{k}\lambda\} | \xi\{\mathbf{u}'\tau'\}} \\ \downarrow \xi\{\mathbf{u}\tau\} \mu'\{\mathbf{q}'\kappa'\} \\ \boxed{\xi\{\mathbf{u}\tau\} | \xi\{\mathbf{u}'\tau'\}} \\ \downarrow \mu\{\mathbf{q}\kappa\} \xi\{\mathbf{u}'\tau'\} \leftarrow \boxed{\mu\{\mathbf{q}\kappa\} | \mu'\{\mathbf{q}'\kappa'\}} \\ \\ \boxed{\nu\{\mathbf{k}\lambda\} | \nu\{\mathbf{k}'\lambda'\}} \\ \downarrow \xi\{\mathbf{u}\tau\} \nu\{\mathbf{k}'\lambda'\} \leftarrow \boxed{\xi\{\mathbf{u}\tau\} | \xi\{\mathbf{u}'\tau'\}} \\ \downarrow \mu\{\mathbf{q}\kappa\} \xi\{\mathbf{u}'\tau'\} \leftarrow \boxed{\mu\{\mathbf{q}\kappa\} | \mu'\{\mathbf{q}'\kappa'\}} \\ \\ \boxed{\nu\{\mathbf{k}\lambda\} | \nu\{\mathbf{k}'\lambda'\}} \\ \downarrow \xi\{\mathbf{u}\tau\} \nu\{\mathbf{k}'\lambda'\} \\ \downarrow \mu\{\mathbf{q}\kappa\} \nu\{\mathbf{k}'\lambda'\} \leftarrow \boxed{\mu\{\mathbf{q}\kappa\} | \xi\{\mathbf{u}'\tau'\}} \leftarrow \boxed{\mu\{\mathbf{q}\kappa\} | \mu'\{\mathbf{q}'\kappa'\}} \end{array} \right]. \quad (161)
\end{aligned}$$

The algebraic version of the first diagram in the brackets is

$$\begin{aligned}
& \langle \mu, \{\mathbf{q}\kappa\} | V | \xi, \{\mathbf{u}\tau\} \rangle \frac{1}{\Delta_{\mu'\xi} + \hbar\omega(\{q'\}, \{u\}) + i0} \langle \xi, \{\mathbf{u}\tau\} | V | \nu, \{\mathbf{k}\lambda\} \rangle \\
& \quad \times \frac{1}{\Delta_{\mu'\nu} + \hbar\omega(\{q'\}, \{k\}) + i0} \langle \xi', \{\mathbf{u}'\tau'\} | V | \mu', \{\mathbf{q}'\kappa'\} \rangle \\
& \quad \times \frac{1}{\Delta_{\xi'\nu} + \hbar\omega(\{u'\}, \{k\}) + i0} \langle \nu, \{\mathbf{k}'\lambda'\} | V | \xi', \{\mathbf{u}'\tau'\} \rangle. \quad (162)
\end{aligned}$$

According to Eq. (161), there are six different time-orderings in which the light-matter interaction V can act on the density matrix, each represented by a unique diagram. The Liouville pathways described by these diagrams can combine in various ways, and certain individual contributions can cancel when all paths are summed up.

The fourth-order term

$$I_4 \equiv -2\pi i \int dE \mathcal{P}_{\mathcal{D}_+} \delta(E - \mathcal{L}_0) \mathcal{T}_4(E + i0) \delta(\mathcal{L}_0 - E) |\varrho(-\infty)\rangle \quad (163)$$

can be obtained from Eq. (161) in a manner corresponding to the calculation of the second-order term (156), again using $|\varrho(-\infty)\rangle$ from Eq. (145). We arrive at

$$\begin{aligned}
I_4 = & \sum_{\mathcal{D}_+} d\mu \sum_{\mathcal{D}_+} d\mu' |\mu\rangle \langle \mu'| \otimes \sum_{\nu \in \mathcal{D}_-} p_\nu T_2[\hat{f}_1](\mu, \nu) T_2^*[\hat{f}_1](\mu', \nu) \\
& \times g_1^{(2)}(a^\dagger[\hat{f}_1]) g_2(a^\dagger[\hat{f}_2]) |\text{vac}\rangle \langle \text{vac}| g_1^{(2)}(a^\dagger[\hat{f}_1])^\dagger g_2(a^\dagger[\hat{f}_2])^\dagger. \quad (164)
\end{aligned}$$

It is instructive to compare Eq. (164) to the second-order result given in Eq. (160). Whereas, to second order in \mathcal{V} , only the second wavepacket scatters with the material, here, to fourth order, only the first wavepacket does so. Since two photons are absorbed, Eq. (164) features second-order (T_2) instead of first-order (T_1) transition amplitudes. Analogously, the function g_1 appears in the form of its second derivative. It is therefore a simple matter to correctly guess the $(2N)^{\text{th}}$ -order result. It reads as

$$\begin{aligned}
& \sum_{\mathcal{D}_+} d\mu \sum_{\mathcal{D}_+} d\mu' |\mu\rangle \langle \mu'| \otimes \sum_{\nu \in \mathcal{D}_-} p_\nu T_N[\hat{f}_1](\mu, \nu) T_N^*[\hat{f}_1](\mu', \nu) \\
& \quad \times g_1^{(N)}(a^\dagger[\hat{f}_1]) g_2(a^\dagger[\hat{f}_2]) |\text{vac}\rangle \langle \text{vac}| g_1^{(N)}(a^\dagger[\hat{f}_1])^\dagger g_2(a^\dagger[\hat{f}_2])^\dagger \quad (165)
\end{aligned}$$

with $T_N[\hat{f}_1](\mu, \nu)$ as in Eq. (27b) on page 16. This term is a leading contribution to 1 vs. N coherent phase control with $N > 1$.

The third and last contribution comes from the cross term that emerges in $(N + 1)^{\text{th}}$ order, e.g., order 3 for $N = 2$. In calculating the third-order \mathcal{S} -matrix elements, two cases must be distinguished. In the first, the ket

portion of the density matrix is subject to two-photon absorption, whereas the bra portion undergoes single-photon absorption, i.e., $m = n - 2$ and $m' = n' - 1$. The result is

$$\begin{aligned}
& -2\pi i \delta[\Delta_{\mu\mu'} + \hbar\omega(\{q\}, \{q'\}) - \hbar\omega(\{k\}, \{k'\})] \sum_{\xi} \int d\{\mathbf{u}\} \\
& \times \sum_{\{\tau\}} \left[\begin{array}{c} \boxed{\nu\{\mathbf{k}\lambda\}} \boxed{\nu\{\mathbf{k}'\lambda'\}} \leftarrow \boxed{\nu\{\mathbf{k}\lambda\}} \boxed{\mu'\{\mathbf{q}'\kappa'\}} \quad \boxed{\nu\{\mathbf{k}\lambda\}} \boxed{\nu\{\mathbf{k}'\lambda'\}} \\ \downarrow \quad \downarrow \quad \downarrow \quad \downarrow \quad \downarrow \quad \downarrow \\ \boxed{\xi\{\mathbf{u}\tau\}} \boxed{\mu'\{\mathbf{q}'\kappa'\}} + \boxed{\xi\{\mathbf{u}\tau\}} \boxed{\nu\{\mathbf{k}'\lambda'\}} \leftarrow \boxed{\xi\{\mathbf{u}\tau\}} \boxed{\mu'\{\mathbf{q}'\kappa'\}} \\ \downarrow \quad \downarrow \quad \downarrow \quad \downarrow \quad \downarrow \quad \downarrow \\ \boxed{\mu\{\mathbf{q}\kappa\}} \boxed{\mu'\{\mathbf{q}'\kappa'\}} \quad \boxed{\mu\{\mathbf{q}\kappa\}} \boxed{\mu'\{\mathbf{q}'\kappa'\}} \\ \\ \boxed{\nu\{\mathbf{k}\lambda\}} \boxed{\nu\{\mathbf{k}'\lambda'\}} \\ \downarrow \quad \downarrow \\ \boxed{\xi\{\mathbf{u}\tau\}} \boxed{\nu\{\mathbf{k}'\lambda'\}} \leftarrow \boxed{\xi\{\mathbf{u}\tau\}} \boxed{\mu'\{\mathbf{q}'\kappa'\}} \\ \downarrow \quad \downarrow \\ \boxed{\mu\{\mathbf{q}\kappa\}} \boxed{\mu'\{\mathbf{q}'\kappa'\}} \end{array} \right], \quad (166)
\end{aligned}$$

where the first diagram in the brackets can also be written as

$$\begin{aligned}
& \langle \mu, \{\mathbf{q}\kappa\} | V | \xi, \{\mathbf{u}\tau\} \rangle \frac{1}{\Delta_{\mu'\xi} + \hbar\omega(\{q'\}, \{u\}) + i0} \langle \xi, \{\mathbf{u}\tau\} | V | \nu, \{\mathbf{k}\lambda\} \rangle \\
& \times \frac{1}{\Delta_{\mu'\nu} + \hbar\omega(\{q'\}, \{k\}) + i0} \langle \nu, \{\mathbf{k}'\lambda'\} | V | \mu', \{\mathbf{q}'\kappa'\} \rangle. \quad (167)
\end{aligned}$$

The other case is the conjugate process, one might say, in which the ket loses a single photon and the bra loses two of them, i.e., $m = n - 1$, $m' = n' - 2$. As a result, the contribution is

$$\begin{aligned}
& 2\pi i \delta[\Delta_{\mu\mu'} + \hbar\omega(\{q\}, \{q'\}) - \hbar\omega(\{k\}, \{k'\})] \sum_{\xi'} \int d\{\mathbf{u}'\} \\
& \times \sum_{\{\tau'\}} \left[\begin{array}{c} \boxed{\nu\{\mathbf{k}\lambda\}} \boxed{\nu\{\mathbf{k}'\lambda'\}} \leftarrow \boxed{\nu\{\mathbf{k}\lambda\}} \boxed{\xi'\{\mathbf{u}'\tau'\}} \leftarrow \boxed{\nu\{\mathbf{k}\lambda\}} \boxed{\mu'\{\mathbf{q}'\kappa'\}} \\ \downarrow \quad \downarrow \quad \downarrow \quad \downarrow \quad \downarrow \quad \downarrow \\ \boxed{\mu\{\mathbf{q}\kappa\}} \boxed{\mu'\{\mathbf{q}'\kappa'\}} \\ \\ \boxed{\nu\{\mathbf{k}\lambda\}} \boxed{\nu\{\mathbf{k}'\lambda'\}} \leftarrow \boxed{\nu\{\mathbf{k}\lambda\}} \boxed{\xi'\{\mathbf{u}'\tau'\}} \\ \downarrow \quad \downarrow \quad \downarrow \quad \downarrow \\ \boxed{\mu\{\mathbf{q}\kappa\}} \boxed{\xi'\{\mathbf{u}'\tau'\}} \leftarrow \boxed{\mu\{\mathbf{q}\kappa\}} \boxed{\mu'\{\mathbf{q}'\kappa'\}} \\ \\ \boxed{\nu\{\mathbf{k}\lambda\}} \boxed{\nu\{\mathbf{k}'\lambda'\}} \\ \downarrow \quad \downarrow \\ \boxed{\mu\{\mathbf{q}\kappa\}} \boxed{\nu\{\mathbf{k}'\lambda'\}} \leftarrow \boxed{\mu\{\mathbf{q}\kappa\}} \boxed{\xi'\{\mathbf{u}'\tau'\}} \leftarrow \boxed{\mu\{\mathbf{q}\kappa\}} \boxed{\mu'\{\mathbf{q}'\kappa'\}} \end{array} \right], \quad (168)
\end{aligned}$$

where we can also write

$$\begin{aligned}
& \langle \mu, \{\mathbf{q}\kappa\} | V | \nu, \{\mathbf{k}\lambda\} \rangle \frac{1}{\Delta_{\mu'\nu} + \hbar\omega(\{q'\}, \{k\}) + i0} \langle \xi', \{\mathbf{u}'\tau'\} | V | \mu', \{\mathbf{q}'\kappa'\} \rangle \\
& \times \frac{1}{\Delta_{\xi'\nu} + \hbar\omega(\{u'\}, \{k\}) + i0} \langle \nu, \{\mathbf{k}'\lambda'\} | V | \xi', \{\mathbf{u}'\tau'\} \rangle \quad (169)
\end{aligned}$$

for the first term in the brackets. These expressions can be used to derive the third-order contribution to $\mathcal{P}_{\mathcal{D}_+}|\varrho(\infty)\rangle\rangle$ with $|\varrho(-\infty)\rangle\rangle$ as before. Afterwards, it is straightforward to obtain the terms that are relevant in the 1 vs. 2 control scenario. We skip these steps and directly generalize to the $(N+1)^{\text{th}}$ -order result for 1 vs. N coherent control. We find

$$\begin{aligned}
& -2\pi i \int dE \mathcal{P}_{\mathcal{D}_+} \delta(E - \mathcal{L}_0) \mathcal{T}_{N+1}(E + i0) \delta(\mathcal{L}_0 - E) |\varrho(-\infty)\rangle\rangle \\
& = \sum_{\mathcal{D}_+} d\mu \sum_{\mathcal{D}_+} d\mu' |\mu\rangle\langle\mu'| \otimes \sum_{\nu \in \mathcal{D}_-} p_\nu T_1[\hat{f}_2](\mu, \nu) T_N^*[\hat{f}_1](\mu', \nu) \\
& \times g_1(a^\dagger[\hat{f}_1]) g_2^{(1)}(a^\dagger[\hat{f}_2]) |\text{vac}\rangle\langle\text{vac}| g_1^{(N)}(a^\dagger[\hat{f}_1])^\dagger g_2(a^\dagger[\hat{f}_2])^\dagger \\
& + \text{h.c.}, \quad (170)
\end{aligned}$$

giving Eq. (23).

References

- [1] M. Shapiro and P. Brumer, *Quantum control of molecular processes*, 2nd ed. (Wiley-VCH, Weinheim, 2012).
- [2] S. Rice and M. Zhao, *Optical Control of Molecular Processes* (Academic Press, 2000).
- [3] M. Shapiro, J. W. Hepburn, and P. Brumer, *Chem. Phys. Lett.* **149**, 451 (1988).
- [4] G. Kurizki, M. Shapiro, and P. Brumer, *Phys. Rev. B* **39**, 3435 (1989).
- [5] E. Dupont, P. B. Corkum, H. C. Liu, M. Buchanan, and Z. R. Wasilewski, *Phys. Rev. Lett.* **74**, 3596 (1995).
- [6] I. Franco and P. Brumer, *Phys. Rev. Lett.* **97**, 040402 (2006).
- [7] I. Franco, M. Shapiro, and P. Brumer, *Phys. Rev. Lett.* **99**, 126802 (2007).
- [8] A. Apolonski, A. Poppe, G. Tempea, C. Spielmann, T. Udem, R. Holzwarth, T. W. Hädrsch, and F. Krausz, *Physical Review Letters* **85**, 740 (2000).
- [9] D. J. Jones, S. A. Diddams, J. K. Ranka, A. Stentz, R. S. Windeler, J. L. Hall, and S. T. Cundiff, *Science* **288**, 635 (2000).
- [10] D. J. Jackson and J. J. Wynne, *Phys. Rev. Lett.* **49**, 543 (1982).

- [11] P. Brumer and M. Shapiro, *Chem. Phys. Lett.* **126**, 541 (1986).
- [12] E. Baskin and M. Entin, *JETP Lett* **48** (1988).
- [13] N. Baranova, A. Chudinov, and B. Y. Zel'dovich, *Optics Communications* **79**, 116 (1990).
- [14] C. Chen and D. S. Elliott, *Phys. Rev. Lett.* **65**, 1737 (1990).
- [15] C. Chen, Y.-Y. Yin, and D. S. Elliott, *Phys. Rev. Lett.* **64**, 507 (1990).
- [16] C. Chan, P. Brumer, and M. Shapiro, *The Journal of chemical physics* **94**, 2688 (1991).
- [17] V. D. Kleiman, L. Zhu, X. Li, and R. J. Gordon, *The Journal of chemical physics* **102**, 5863 (1995).
- [18] L. Zhu, V. Kleiman, X. Li, S. P. Lu, K. Trentelman, and R. J. Gordon, *Science* **270**, 77 (1995).
- [19] M. Shapiro and P. Brumer, *J. Chem. Soc., Faraday Trans.* **93**, 1263 (1997).
- [20] A. Haché, Y. Kostoulas, R. Atanasov, J. L. P. Hughes, J. E. Sipe, and H. M. van Driel, *Phys. Rev. Lett.* **78**, 306 (1997).
- [21] Z.-M. Wang and D. S. Elliott, *Phys. Rev. Lett.* **87**, 173001 (2001).
- [22] F. Ehlötzky, *Physics Reports* **345**, 175 (2001).
- [23] R. D. R. Bhat and J. E. Sipe, *Phys. Rev. B* **72**, 075205 (2005).
- [24] J. Wahlstrand, J. Pipis, P. Roos, S. Cundiff, and R. Smith, *Applied physics letters* **89**, 241115 (2006).
- [25] A. Bolovinos, S. Cohen, and I. Lontos, *Phys. Rev. A* **77**, 023413 (2008).
- [26] B. Pasenow, H. Duc, T. Meier, and S. Koch, *Solid State Communications* **145**, 61 (2008).
- [27] D. G. Kuroda, C. P. Singh, Z. Peng, and V. D. Kleiman, *Science* **326**, 263 (2009).
- [28] K. M. Rao and J. E. Sipe, *Phys. Rev. B* **84**, 205313 (2011).
- [29] D. Antypas and D. Elliott, *Canadian Journal of Chemistry* **92**, 144 (2014).
- [30] R. A. Muniz and J. E. Sipe, *Phys. Rev. B* **91**, 085404 (2015).

- [31] R. Feynman, R. Leighton, and M. Sands, *The Feynman Lectures on Physics*, The Feynman Lectures on Physics No. v. 3 (Pearson/Addison-Wesley, 1963).
- [32] Y.-Y. Yin, C. Chen, D. S. Elliott, and A. V. Smith, *Phys. Rev. Lett.* **69**, 2353 (1992).
- [33] Y.-Y. Yin and D. S. Elliott, *Phys. Rev. A* **47**, 2881 (1993).
- [34] S. Flach, O. Yevtushenko, and Y. Zolotaryuk, *Phys. Rev. Lett.* **84**, 2358 (2000).
- [35] I. Franco, M. Spanner, and P. Brumer, *Chem. Phys.* **370**, 143 (2010).
- [36] M. Spanner, I. Franco, and P. W. Brumer, *Phys. Rev. A* **80**, 1 (2009).
- [37] H. Muller, P. Bucksbaum, D. Schumacher, and A. Zavriyev, *J. Phys. B* **23**, 2761 (1990).
- [38] H. Han and P. Brumer, *Chem. Phys. Lett.* **406**, 237 (2005).
- [39] V. Constantoudis and C. A. Nicolaides, *J. Chem. Phys.* **122**, 084118 (2005).
- [40] E. de Lima and M. de Aguiar, *Phys. Rev. A* **77**, 033406 (2008).
- [41] M. Ivanov, D. Bartram, and O. Smirnova, *Mol. Phys.* **110**, 1801 (2012).
- [42] G. Greenstein and A. Zajonc, *The Quantum Challenge: Modern Research on the Foundations of Quantum Mechanics, 2nd Edition* (Jones and Bennett, 2005).
- [43] A. J. Leggett, *Journal of Physics: Condensed Matter* **14**, R415 (2002).
- [44] A. J. Leggett, *Rep. Prog. Phys.* **71**, 022001 (2008).
- [45] B. Sheehy, B. Walker, and L. F. DiMauro, *Phys. Rev. Lett.* **74**, 4799 (1995).
- [46] W. Kauzmann, *Quantum Chemistry* (John Wiley, 2000).
- [47] R. Chance, A. Prock, and R. Silbey, *The Journal of Chemical Physics* **62**, 2245 (1975).
- [48] S. Duque, P. Brumer, and L. A. Pachón, *Phys. Rev. Lett.* **115**, 110402 (2015).
- [49] A. Aspect, J. Dalibard, and G. Roger, *Phys. Rev. Lett.* **49**, 1804 (1982).
- [50] Z. Y. Ou and L. Mandel, *Phys. Rev. Lett.* **61**, 50 (1988).

- [51] F. Kaiser, T. Coudreau, P. Milman, D. B. Ostrowsky, and S. Tanzilli, *Science* **338**, 637 (2012).
- [52] A. K. Ekert, *Phys. Rev. Lett.* **67**, 661 (1991).
- [53] C. H. Bennett, G. Brassard, C. Crépeau, R. Jozsa, A. Peres, and W. K. Wootters, *Phys. Rev. Lett.* **70**, 1895 (1993).
- [54] A. Steane, *Rep. Prog. Phys.* **61**, 117 (1998).
- [55] L. M. Duan, M. D. Lukin, J. I. Cirac, and P. Zoller, *Nature* **414**, 413 (2001).
- [56] N. Gisin, G. Ribordy, W. Tittel, and H. Zbinden, *Rev. Mod. Phys.* **74**, 145 (2002).
- [57] O. GÃijhne and G. TÃijsth, *Phys. Rep.* **474**, 1 (2009).
- [58] A. Ekert and R. Renner, *Nature* **507**, 443 (2014).
- [59] W. H. Zurek, *Physics Today* **44**, 36 (1991).
- [60] D. Salart, A. Baas, C. Branciard, N. Gisin, and H. Zbinden, *Nature* **454**, 861 (2008).
- [61] A. Winter, *Nature* **466**, 1053 (2010).
- [62] B. Hensen, H. Bernien, A. E. Dreau, A. Reiserer, N. Kalb, M. S. Blok, J. Ruitenber, R. F. L. Vermeulen, R. N. Schouten, C. Abellan, W. Amaya, V. Pruneri, M. W. Mitchell, M. Markham, D. J. Twitchen, D. Elkouss, S. Wehner, T. H. Taminiau, and R. Hanson, *Nature* **526**, 682 (2015).
- [63] M. Giustina, M. A. M. Versteegh, S. Wengerowsky, J. Handsteiner, A. Hochrainer, K. Phelan, F. Steinlechner, J. Kofler, J.-A. Larsson, C. Abellán, W. Amaya, V. Pruneri, M. W. Mitchell, J. Beyer, T. Gerrits, A. E. Lita, L. K. Shalm, S. W. Nam, T. Scheidl, R. Ursin, B. Wittmann, and A. Zeilinger, *Phys. Rev. Lett.* **115**, 250401 (2015).
- [64] L. K. Shalm, E. Meyer-Scott, B. G. Christensen, P. Bierhorst, M. A. Wayne, M. J. Stevens, T. Gerrits, S. Glancy, D. R. Hamel, M. S. Allman, K. J. Coakley, S. D. Dyer, C. Hodge, A. E. Lita, V. B. Verma, C. Lambrocco, E. Tortorici, A. L. Migdall, Y. Zhang, D. R. Kumor, W. H. Farr, F. Marsili, M. D. Shaw, J. A. Stern, C. Abellán, W. Amaya, V. Pruneri, T. Jennewein, M. W. Mitchell, P. G. Kwiat, J. C. Bienfang, R. P. Mirin, E. Knill, and S. W. Nam, *Phys. Rev. Lett.* **115**, 250402 (2015).
- [65] M. Schlosshauer, *Decoherence and the Quantum-to-Classical Transition* (Springer, 2007).

- [66] C. Zhuang, C. R. Paul, X. Liu, S. Maneshi, L. S. Cruz, and A. M. Steinberg, *Phys. Rev. Lett.* **111**, 233002 (2013).
- [67] H. Ohmura, T. Nakanaga, and M. Tachiya, *Phys. Rev. Lett.* **92**, 113002 (2004).
- [68] H. Ohmura and T. Nakanaga, *J. Chem. Phys.* **120**, 5176 (2004).
- [69] H. Ohmura, *Phys. Rev. A* **74**, 043410 (2006).
- [70] K. A. Pronin and A. D. Bandrauk, *Phys. Rev. B* **69**, 195308 (2004).
- [71] D. Sun, C. Divin, J. Rioux, J. E. Sipe, C. Berger, W. A. de Heer, P. N. First, and T. B. Norris, *Nano Letters* **10**, 1293 (2010).
- [72] E. J. Mele, P. Král, and D. Tománek, *Phys. Rev. B* **61**, 7669 (2000).
- [73] A. Najmaie, R. D. R. Bhat, and J. E. Sipe, *Phys. Rev. B* **68**, 165348 (2003).
- [74] J. Rioux, G. Burkard, and J. E. Sipe, *Phys. Rev. B* **83**, 195406 (2011).
- [75] R. A. Muniz and J. E. Sipe, *Phys. Rev. B* **89**, 205113 (2014).
- [76] X.-S. Ma, J. Koller, and A. Zeilinger, *Reviews of Modern Physics* **88**, 015005 (2016).
- [77] R. Ionicioiu and D. R. Terno, *Phys. Rev. Lett.* **107**, 230406 (2011).
- [78] J.-S. Tang, Y.-L. Li, X.-Y. Xu, G.-Y. Xiang, C.-F. Li, and G.-C. Guo, *Nat. Phot.* **6**, 602 (2012).
- [79] A. Peruzzo, P. Shadbolt, N. Brunner, S. Popescu, and J. L. O'Brien, *Science* **338**, 634 (2012).
- [80] S. S. Roy, A. Shukla, and T. S. Mahesh, *Phys. Rev. A* **85**, 022109 (2012).
- [81] R. Auccaise, R. M. Serra, J. G. Filgueiras, R. S. Sarthour, I. S. Oliveira, and L. C. Céleri, *Phys. Rev. A* **85**, 032121 (2012).
- [82] I. Franco and P. Brumer, *J. Phys. B* **41**, 074003 (2008).
- [83] L. Sirko and P. M. Koch, *Phys. Rev. Lett.* **89**, 274101 (2002).
- [84] M. Schetzen, *The Volterra and Wiener Theories of Nonlinear Systems* (Krieger Publishing Co., Inc., Melbourne, FL, USA, 2006).
- [85] M. Spanner, C. A. Arango, and P. Brumer, *J. Chem. Phys.* **133**, 059903 (2010).
- [86] M. O. Scully, B.-G. Englert, and H. Walther, *Nature* **351**, 111 (1991).

- [87] C. Cohen-Tannoudji, J. Dupont-Roc, and G. Grynberg, *Atom-Photon Interactions*, Wiley Science Paperback Series (Wiley, 1998).
- [88] L. Mandel and E. Wolf, *Optical Coherence and Quantum Optics* (Cambridge University Press, 1995).
- [89] J. R. Taylor, *Scattering theory* (Wiley, 1972).
- [90] J. A. Wheeler, in *Mathematical Foundations of Quantum Theory*, edited by A. R. Marlow (Academic Press, 1978).
- [91] R. P. Feynman, *The character of physical law*, Vol. 66 (MIT press, 1967).
- [92] B.-G. Englert, *Z. Naturforsch.* **54a**, 11 (1998).
- [93] B.-G. Englert, *Phys. Rev. Lett.* **77**, 2154 (1996).
- [94] B.-G. Englert and J. A. Bergou, *Opt. Commun.* **179**, 337 (2000).
- [95] W. K. Wootters and W. H. Zurek, *Phys. Rev. D* **19**, 473 (1979).
- [96] R. J. Glauber, *Ann. New York Acad. Sci.* **480**, 336 (1986).
- [97] D. M. Greenberger and A. Yasin, *Phys. Lett. A* **128**, 391 (1988).
- [98] L. Mandel, *Opt. Lett.* **16**, 1882 (1991).
- [99] G. Jaeger, A. Shimony, and L. Vaidman, *Phys. Rev. A* **51**, 54 (1995).
- [100] M. O. Scully and S. Zubairy, *Quantum Optics* (Cambridge University Press, 1997).
- [101] D. F. Walls and G. J. Milburn, *Quantum Optics* (Springer, 2008).
- [102] Y.-H. Kim, R. Yu, S. P. Kulik, Y. Shih, and M. O. Scully, *Phys. Rev. Lett.* **84**, 1 (2000).
- [103] S. P. Walborn, M. O. Terra Cunha, S. Pádua, and C. H. Monken, *Phys. Rev. A* **65**, 033818 (2002).
- [104] A. Bramon, G. Garbarino, and B. C. Hiesmayr, *Phys. Rev. Lett.* **92**, 020405 (2004).
- [105] Y. Aharonov and M. S. Zubairy, *Science* **307**, 875 (2005).
- [106] J. A. Wheeler, in *Quantum Theory and Measurement*, Princeton Series in Physics, edited by J. A. Wheeler and W. H. Zurek (Princeton Univ. Press, Princeton, NJ, 1984) Chap. I.13, pp. 182–213.
- [107] M. A. Horne, A. Shimony, and A. Zeilinger, *Phys. Rev. Lett.* **62**, 2209 (1989).

- [108] A. Mann, B. C. Sanders, and W. J. Munro, *Phys. Rev. A* **51**, 989 (1995).
- [109] M. Nielsen and I. Chuang, *Quantum Computation and Quantum Information* (Cambridge University Press, Cambridge, 2000).
- [110] R. Horodecki, P. Horodecki, M. Horodecki, and K. Horodecki, *Rev. Mod. Phys.* **81**, 865 (2009).
- [111] M. Jakob and J. A. Bergou, *Opt. Commun.* **283**, 827 (2010).
- [112] B.-G. Englert, *Eur. Phys. J.* **67**, 1 (2013).
- [113] R. Loudon, *The Quantum Theory of Light* (OUP Oxford, 2000).
- [114] J. Gong and P. Brumer, *J. Chem. Phys.* **132**, 054306 (2010).
- [115] P. G. Kwiat and B.-G. Englert, “Quantum erasing the nature of reality: or, perhaps, the reality of nature?” in *Science and Ultimate Reality: Quantum Theory, Cosmology, and Complexity*, edited by J. D. Barrow, P. C. W. Davies, and C. L. H. Jr. (Cambridge University Press, 2004) Chap. 15, p. 306.
- [116] N. Bohr, in *Quantum Theory and Measurement*, Princeton Series in Physics, edited by J. A. Wheeler and W. H. Zurek (Princeton Univ. Press, Princeton, NJ, 1984) Chap. I.1, p. 9.
- [117] B. Sanders, *Phys. Rev. A* **45**, 6811 (1992).
- [118] H. Jeong and N. B. An, *Phys. Rev. A* **74**, 022104 (2006).
- [119] D. M. Greenberger, M. A. Horne, A. Shimony, and A. Zeilinger, *Am. J. Phys.* **58**, 1131 (1990).
- [120] R. Stassi, A. Ridolfo, S. Savasta, R. Girlanda, and O. D. Stefano, *Europhys. Lett.* **99**, 24003 (2012).
- [121] M. Żukowski, A. Zeilinger, M. A. Horne, and A. K. Ekert, *Phys. Rev. Lett.* **71**, 4287 (1993).
- [122] S. Bose, V. Vedral, and P. L. Knight, *Phys. Rev. A* **57**, 822 (1998).
- [123] J. S. Bell, *Physics* **1**, 195 (1964).
- [124] J. Bell, *Rev. Mod. Phys.* **38**, 447 (1966).
- [125] J. F. Clauser, M. A. Horne, A. Shimony, and R. A. Holt, *Phys. Rev. Lett.* **23**, 880 (1969).
- [126] A. J. Leggett and A. Garg, *Phys. Rev. Lett.* **54**, 857 (1985).

- [127] C. Emary, N. Lambert, and F. Nori, Rep. Prog. Phys. **77**, 016001 (2014).
- [128] C. Robens, W. Alt, D. Meschede, C. Emary, and A. Alberti, Phys. Rev. X **5**, 011003 (2015).
- [129] G. Weihs, T. Jennewein, C. Simon, H. Weinfurter, and A. Zeilinger, Phys. Rev. Lett. **81**, 5039 (1998).
- [130] M. A. Rowe, D. Kielpinski, V. Meyer, C. A. Sackett, W. M. Itano, C. Monroe, and D. J. Wineland, Nature **409**, 791 (2001).
- [131] S. Groblacher, T. Paterek, R. Kaltenbaek, Ä. Brukner, M. Zukowski, M. Aspelmeyer, and A. Zeilinger, Nature **446**, 871 (2007).
- [132] D. N. Matsukevich, P. Maunz, D. L. Moehring, S. Olmschenk, and C. Monroe, Phys. Rev. Lett. **100** (2008).
- [133] B. S. Tsirelson, Lett. Math. Phys. **4**, 93 (1980).
- [134] J. Barrett, N. Linden, S. Massar, S. Pironio, S. Popescu, and D. Roberts, Phys. Rev. A **71**, 022101 (2005).
- [135] S. Popescu and D. Rohrlich, Phys. Lett. A **169**, 411 (1992).
- [136] T. Scholak and P. Brumer, J. Chem. Phys. **141**, 204311 (2014).
- [137] R. Grimm, M. Weidemüller, and Y. B. Ovchinnikov (Academic Press, 2000) p. 95.
- [138] J. Eschner, G. Morigi, F. Schmidt-Kaler, and R. Blatt, J. Opt. Soc. Am. B **20**, 1003 (2003).
- [139] H. Bethe and E. Salpeter, *Quantum Mechanics Of One- And Two-Electron Atoms* (Dover, 2008).
- [140] E. Fermi, Z. Phys. **59**, 680 (1930).
- [141] M. J. Seaton, Proc. Roy. Soc., Ser. A **208**, 418 (1951).
- [142] J. L. Miller, Physics today **69**, 14 (2016).
- [143] A. Garg and N. D. Mermin, Phys. Rev. D **35**, 3831 (1987).
- [144] T. Scheidl, R. Ursin, J. Kofler, S. Ramelow, X.-S. Ma, T. Herbst, L. Ratschbacher, A. Fedrizzi, N. K. Langford, T. Jennewein, and A. Zeilinger, Proceedings of the National Academy of Sciences **107**, 19708 (2010).
- [145] R. Y. Chiao, P. G. Kwia, and A. M. Steinberg, Quantum and Semi-classical Optics: Journal of the European Optical Society Part B **7**, 259 (1995).

- [146] V. Jacques, E. Wu, F. Grosshans, F. Treussart, P. Grangier, A. Aspect, and J.-F. Roch, *Science* **315**, 966 (2007).
- [147] A. G. Manning, R. I. Khakimov, R. G. Dall, and A. G. Truscott, *Nat Phys* **11**, 539 (2015).
- [148] X.-s. Ma, J. Kofler, and A. Zeilinger, *Rev. Mod. Phys.* **88**, 015005 (2016).
- [149] S. Mukamel, *Principles of nonlinear optical spectroscopy*, Oxford series in optical and imaging sciences (Oxford University Press, 1995).